Fall 1-31-2013

Quantification of neural substrates of vergence system via fMRI

Yelda Alkan
New Jersey Institute of Technology

Copyright Warning & Restrictions

The copyright law of the United States (Title 17, United States Code) governs the making of photocopies or other reproductions of copyrighted material.

Under certain conditions specified in the law, libraries and archives are authorized to furnish a photocopy or other reproduction. One of these specified conditions is that the photocopy or reproduction is not to be "used for any purpose other than private study, scholarship, or research." If a, user makes a request for, or later uses, a photocopy or reproduction for purposes in excess of "fair use" that user may be liable for copyright infringement,

This institution reserves the right to refuse to accept a copying order if, in its judgment, fulfillment of the order would involve violation of copyright law.

Please Note: The author retains the copyright while the New Jersey Institute of Technology reserves the right to distribute this thesis or dissertation

Printing note: If you do not wish to print this page, then select "Pages from: first page # to: last page #" on the print dialog screen

ABSTRACT

QUANTIFICATION OF NEURAL SUBSTRATES OF VERGENCE SYSTEM VIA FMRI

by
Yelda Alkan

Vergence eye movement is one of the oculomotor systems which allow depth perception via disconjugate movement of the eyes. Neuroimaging methods such as functional magnetic resonance imaging (fMRI) measure neural activity changes activity in the brain while subjects perform experimental tasks. A rich body of primate investigations on vergence is already established in the neurophysiology literature; on the other hand, there are a limited number of fMRI studies on neural mechanisms behind the vergence system.

The results demonstrated that vergence system shares neural sources and also shows differentiation within the boundaries of frontal eye fields (FEF) and midbrain of the brainstem in comparison to saccadic, rapid conjugate eye movements, system with application of simple tracking experiment. Functional activity within the FEF was located anterior to the saccadic functional activity ($z > 2.3$; $p < 0.03$). Functional activity within the midbrain was observed as a result of application of vergence task, but not for the saccade data set. The novel memory-guided vergence experiment also showed a relationship between posterior parahippocampal area and memory where two other experiments were implemented for comparison of memory load in this region. Significant percent change in the functional activity was observed for the posterior parahippocampal area. Furthermore, an increase in the interconnectivity was observed for vergence tasks via utilization of Granger-Causality Analysis. When prediction was involved the increase

in the number of causal interactions was statistically significant ($p < 0.05$). The comparison of the number of influences between prediction-evoked vergence task and simple tracking vergence task was also statistically significant for these two experimental paradigms, $p < 0.0001$. Another result observed in this dissertation was the application of hierarchical independent component analysis from to the fronto-parietal and cerebellar components within saccade and vergence tasks. Interestingly, cerebellar component showed delayed latency in the group level signal in comparison to fronto-parietal group level signals, which was evaluated to determine why segregation existed between the components acquired from the implementation of independent component analysis. Lastly, region of interet (ROI) based analysis in comparison to global (whole) brain analysis indicated more sensitive results on frontal, parietal, brainstem and occipital areas at both individual and group levels.

Overall, the purpose of this dissertation was to investigate neural control of vergence movements by 1-spatial mapping of vergence induced functional activity, 2-applying different signal processing methods to quantify neural correlates of the vergence system at causal functional connectivity, underlying sources and region of interests (ROI) based levels. It was concluded that quantification of vergence movements via fMRI can build a synergy with behavioral investigations and may also shed light on neural differentiation between healthy individuals and patients with neural dysfunctions and injuries by serving as a biomarker.

QUANTIFICATION OF NEURAL SUBSTRATES OF VERGENCE SYSTEM VIA FMRI

by
Yelda Alkan

A Dissertation
Submitted to the Faculty of
New Jersey Institute of Technology
and University of Medicine and Dentistry of New Jersey
in Partial Fulfillment of the Requirements for the Degree of
Doctor of Philosophy in Biomedical Engineering

Joint Program in Biomedical Engineering

January 2013

APPROVAL PAGE

QUANTIFICATION OF NEURAL SUBSTRATES OF VERGENCE SYSTEM VIA FMRI

Yelda Alkan

Dr. Tara L. Alvarez, Dissertation Advisor — Date
Associate Professor of Biomedical Engineering, NJIT

Dr. Bharat B. Biswal, Dissertation Coadvisor
Associate Professor of Biomedical Engineering, UMDNJ — Date

Dr. William C. Hunter, Committee Member — Date
Professor of Biomedical Engineering, NJIT

Dr. Mesut Sahin, Committee Member — Date
Associate Professor of Biomedical Engineering, NJIT

Dr. Eugene Tunik, Committee Member — Date
Associate Professor of Rehabilitation and Movement Sciences, UMDNJ

BIOGRAPHICAL SKETCH

Author: Yelda Alkan

Degree: Doctor of Philosophy

Date: January 2013

Undergraduate and Graduate Education:

- Doctor of Philosophy in Biomedical Engineering,
  New Jersey Institute of Technology, Newark, NJ, 2013
- Master of Science in Biomedical Engineering,
  New Jersey Institute of Technology, Newark, NJ, 2008
- Bachelor of Science in Electrical and Electronics Engineering
  Yeditepe University, Istanbul, Turkey, 2004

Major: Biomedical Engineering

Presentations and Publications:

Y. Alkan, B. B. Bharat, and T. L. Alvarez, "Differentiation between Vergence and Saccadic Functional Activity within the Human Frontal Eye Fields and Midbrain Revealed through fMRI", *PLoS One*, 6(11), 2011.

Y. Alkan, B. B. Biswal, P. A. Taylor, T. L. Alvarez, "Segregation of frontoparietal and cerebellar components within saccade and vergence networks using hierarchical independent component analysis of fMRI", *Vis Neurosci.*, 28(3):247-61, 2011.

Y. Alkan, P. A. Taylor, B. B. Biswal, T. L. Alvarez, "An FMRI Investigation of a Memory Guided vergence task: Insights to the Parahippocampal Area", *Proceedings of the IEEE 38th Annual Northeast Bioengineering Conference,* 2012.

R. Saigal, Y. Alkan, B. B. Biswal, T. L. Alvarez, "Comparison of Whole-Brain to Region-Based fMRI Analyses", *Proceedings of the IEEE 38th Annual Northeast Bioengineering Conference*, 2012.

Y. Alkan, B. B. Biswal, S. Gohel, P. A. Taylor, T. L. Alvarez, " Functional Connectivity in Vergence and Saccade Eye Movement Tasks Assessed using Granger Causality Analysis", 33rd *Annual International Conference of the IEEE EMBS Boston, Massachusetts USA*, 2011.

T. L. Alvarez, V. R. Vicci, Y. Alkan, E. H. Kim, S. Gohel, A. M. Barrett, N. Chiaravalloti, B. B. Biswal, "Vision therapy in adults with convergence insufficiency: clinical and functional magnetic resonance imaging measures", *Optom Vis Sci*.,87(12), 2010.

T. L. Alvarez, Y. Alkan, S. Gohel, B. Ward Douglas, B. B. Biswal, "Functional anatomy of predictive vergence and saccade eye movements in humans: a functional MRI investigation", *Vision Res*., 50(21):2163-75, 2010.

Y. Alkan, B. B. Biswal, T. L. Alvarez, "Visual cortical circuits revealed using fMRI and ICA". *Proceedings of the IEEE 36th Annual Northeast Bioengineering Conference*, 2010.

T. L. Alvarez, Y. Alkan, S. Gohel, B. B. Biswal, "Functional connectivity in oculomotor movements", *Proceedings of the IEEE 36th Annual Northeast Bioengineering Conference,* 2010.

Y. Alkan, B. B. Biswal, V. R. Vicci, T. L. Alvarez, "Cortical location of FEF revealed using fMRI". *Proceedings of the IEEE 36th Annual Northeast Bioengineering Conference*, 2009.

Y. Alkan, T. L. Alvarez, B. B. Biswal, V. R. Vicci, "Independent components of oculomotor learning", *Neural Engineering, 4th International IEEE/EMBS Conf* (won the student paper and travel award), 2009.

Y. Alkan, B. B. Biswal, T. L. Alvarez, "Saccadic and vergence functional activity in the pons". *Proceedings of the IEEE 35th Annual Northeast Bioengineering Conference*, 2009.

Y. Alkan, T. L. Alvarez, E. H. Kim, R. Jaswal, B. B. Biswal, S. Gohel, V. R. Vicci, "Functional MRI as a Tool to Quantify Cortical Changes from Vision Rehabilitation", *Proceedings - International Conference on Tools with 25 Artificial Intelligence, ICTAI* , art. no. 5365894, pp. 766-770, 2009.

T. L. Alvarez, Y. Alkan, E. H. Kim, R. Jaswal, D. Ludlam, P. Moinot, B. B. Biswal, V.R. Vicci, "Neuroplasticity in vision dysfunction", *Neural Engineering, 4th International IEEE/EMBS Conference*, 2009.

E. H. Kim, T. L. Alvarez, Y. Alkan, R. Jaswal, B. B. Biswal, V. R. Vicci, "Decomposition of vergence dynamics using independent component analysis" *Proceedings - International Conference on Tools with 25 Artificial Intelligence, ICTAI*, art. no. 5365894, pp. 766-770, 2009

E. H. Kim, Y. Alkan, R. Jaswal, D. Ludlam, B. B. Biswal, V. R. Vicci, T. L. Alvarez, "ICA decomposition of vergence dynamics in convergence insufficiency patients", *Proceedings of the IEEE 35th Annual Northeast Bioengineering Conference*, 2009.

J. Nguyen, Y. Alkan, B. B. Biswal, B. Gayed, S. J. Han., J. L. Semmlow, T. L. Alvarez, "An fMRI investigation in oculomotor learning through vergence eye movements", *Proceedings of the IEEE 35th Annual Northeast Bioengineering Conference*, 2009.

E. H. Kim, T. L. Alvarez, Y. Alkan, R. Jaswal, B. B. Biswal, V. R. Vicci, "Decomposition of vergence dynamics using independent component analysis", *Proceedings - International Conference on Tools with 25 Artificial Intelligence, ICTAI*, art. no. 5365894, pp. 766-770, 2009.

R. Jaswal, Y. Alkan, E. H. Kim, B. B. Biswal, V. R. Vicci, T. L. Alvarez, "Diffusion tensor imaging of neural plasticity in visual dysfunction", *Proceedings of the IEEE 35th Annual Northeast Bioengineering Conference*, 2009.

R. Jaswal, T. L. Alvarez, Y. Alkan, E. H. Kim, B. B. Biswal, "The Cerebral Vascular Enhancement Effect in Establishing Diffusion Tensor Imaging Protocols", *Proceedings - International Conference on Tools with 25 Artificial Intelligence, ICTAI*, pp.771-775, 2009.

Y. Alkan, B. B. Biswal, B. Gayed, J. L. Semmlow, S. J. Han, T. L. Alvarez, "Cortical location of saccadic oculomotor learning using fMRI", *Proceedings of the IEEE 33th Annual Northeast Bioengineering Conference*, 2007.

Y. Alkan, B. B. Biswal, S. J. Han, T. L. Alvarez, "Cortical Location of Saccadic and Vergence Oculomotor Learning Revealed using fMRI*", Proceedings of the IEEE 33th Annual Northeast Bioengineering Conference*, (won first place in the student paper competition), 2007.

Victory is for those who can say "Victory is mine". Success is for those who can begin saying "I will succeed" and say "I have succeeded" in the end.”- Mustafa Kemal ATATURK

ACKNOWLEDGMENT

I would like thank to Dr. Tara L. Alvarez for her encouragement which made me start this PhD journey and thankful for sharing her knowledge and evaluations in the field with me. I am grateful for her support and mentoring for my dissertation.

I would like to acknowledge Dr. Bharat B. Biswal for his unfailing help, encouragement, and support throughout the creation of this dissertation. I am always benefited from his wisdom and wide knowledge as a mentor and teacher. My appreciation and gratefulness will grow over years, and I will always owe a debt to him for believing in me.

I am also deeply grateful to Dr. Mesut Sahin for his generous help, support and guidance for the times that I was so close to giving up. His participation as a committee member to my dissertation was valuable. My heartfelt special thanks go to him for both being a great teacher and also for his very friendly approach to whoever needs support. I would like to also thank my committee members, Dr. William C. Hunter and Dr. Eugene Tunik for their professional advisement and supportive feedbacks for my dissertation. They both were very helpful and made me believe that my research was important.

I could not also have managed this dissertation without the cheerful and ready assistance of Suril Gohel, Paul A. Taylor and Xin Di. I appreciate and thank them for their prompt, thoughtful support and their beloved, trustworthy friendship.

Thank you to the faculty members of Biomedical Engineering Department and students of the Vision and Neural Engineering Laboratory of New Jersey Institute of Technology (NJIT) for their supportive approaches which made me feel I am not alone.

I am thankful to Gokhan Ordek, Soha Saleh and Jonathan Groth for being very good friends. Your friendship and your support are always very precious to me. You never bargained with me for your help and were ready to assist me at any time. I would like to also gratefully thank Ulku Oflaz, Aslihan Oflaz, and Nizamettin Avci for being my second family. They were always with me to help, support, encourage and care when I needed them the most.

My beautiful family, I can neither express my appreciation nor show with words how thankful I am. I can only say love each of you by heart and thank you being with me for every step of my life and being a very precious light in dark times with love, care, and patience.

TABLE OF CONTENTS

TABLE OF CONTENTS
(Continued)

TABLE OF CONTENTS
(Continued)

TABLE OF CONTENTS
(Continued)

Chapter **Page**

TABLE OF CONTENTS
(Continued)

LIST OF TABLES

LIST OF FIGURES

LIST OF FIGURES
(Continued)

LIST OF FIGURES
(Continued)

CHAPTER 1

PROJECT GOALS

Motor learning is critical to the survival of a species and changes throughout life via neuroplasticity. Saccades and smooth pursuit are classified as conjugate movements where the eyes move in tandem. Vergence is the inward (convergence) and outward (divergence) rotation of the eyes to view objects at different spatial depths. While the neural correlates of saccadic eye movements are established, few studies have quantified the functional activity of vergence eye movements using fMRI. Thus, quantification of the neural components of vergence system in comparison with saccadic system is highly needed in the field of vision.

The first purpose of this dissertation is to map the neural substrates of vergence system and compare it to the saccadic system to elucidate the spatial commonality and differentiation between these systems via application of different image and signal processing methods using general linear model (GLM), independent component analysis (ICA), Granger causality analysis (GCA), and region of interest (ROI) based brain analysis in comparison to global (whole) brain analysis on fMRI data.

Hence, quantification of vergence movements via fMRI will shed light on behavioral eye movement investigations and may serve as a biomarker for identification of neural differentiation between healthy subjects and patients with neural dysfunctions and injuries.

1.1 Specific Aims

The first purpose of this dissertation is to investigate whether the neural substrates involved in initiating vergence and saccade eye movements share neural resources. It is hypothesized that differentiation will be observed within the frontal eye fields and midbrain regions. Secondly, the posterior parahippocampal area (PPHA) was investigated for memory-guided vergence experiment and compared with the other experiments where less cognitive involvement was required. Granger causality analysis was implemented as an alternative signal processing method on selected ROIs from fMRI data to understand whether the number of influences among selected ROIs changes depending on the experimental paradigm applied. Additionally, underlying sources of fMRI data and the characteristics of the source signals obtained via both spatial and temporal ICA methods was investigated for a single subject and group level analyses. Region of interest (ROI) based analysis versus Global (whole) brain analysis was applied on the key regions for vergence system such as the frontal area, parietal, occipital, and brainstem regions (ROIs) to assess whether more persistent functional activation in means of correlation and spatial extent occured in addition to discovering region based connectivity. The following methods were used to test hypotheses:

1. Mapping of the neural substrates of vergence eye movements was compared to saccades to elucidate the spatial commonality and differentiation between these systems where the stimulus was presented in a block design in which the “off”stimulus was a sustained fixation and the “on” stimulus was random tracking for vergence or saccadic eye movements.

2. To investigate functional activity changes in posterior parahippocampal area for vergence eye movements via application of three different experiments: fixation versus random tracking and predictable tracking versus random tracking and memory-guided vergence paradigms. A novel experimental task, memory-guided vergence paradigm, started with random tracking of binocular disparity cues and was followed by predictable tracking pattern of the targets, and at the last phase LED targets turned off and vergence

eye movements expected from participants to the remembered locations of the cues which were memorized in predictable phase. It was also hypothesized that significant spatial extent of functional activity of posterior parahippocampal area would be observed for memory guided oculomotor task. This suggests when involvement of working memory is required, posterior parahippocampal area functions as one of the crucial regions for a memory task.

3. To study the number and direction of influences among ROIs using a Granger Causality Analysis (GCA), a statistical technique used to identify whether an ROI is significantly influencing or "connected" to another ROI for vergence ocular movements. Directionality among selected ROIs for vergence ocular movements with experimental designs of fixation versus random tracking and predictable tracking versus random tracking was compared.

4. Cortical and subcortical networks behind saccade and vergence eye movements were investigated by implementing a hierarchical ICA to examine the similarities and differences between networks and regions of interest (ROIs) via six types of oculomotor experiments.

5. To investigate sensitivity of the methods used for analysis of fMRI data global (whole) brain versus region of interest (ROI) based analysis vergence neural network was compared. In this specific aim, it is claimed that region of interest (ROI) based brain analysis would show greater sensitivity than the global (whole) brain analysis. It was also hypothesized that ROI based brain analysis would show persistent functional activity in some other cortical and subcortical areas corresponding with source ROI which can be evaluated as neuronal connectivity among these regions.

CHAPTER 2

BACKGROUND

How does the brain work? This is one of the fundamental questions that the science world has been looking for an answer to for centuries. The visual system and its components, like oculomotor movements are adopted as a track that helps us to understand the mechanism of the brain. This section of the dissertation will provide detailed information on the anatomy of the eye, oculomotor movements, the neurology behind saccadic and vergence eye movements and functional magnetic resonance imaging (fMRI) as an imaging modality.

2.1 The Anatomy of the Eye

The clear image of the external environment is provided by the structures of the eye. The eye is a fluid filled sphere is formed by three main tissue layers, named as the sclera, uvea, and retina. The outermost layer, the sclera, is the white fibrous part of the eye. It has two components, the limbus and the cornea. The limbus is the part that is between the cornea and the sclera. The cornea is the part of the eye which is transparent, and is the region where light enters the eye [1].

The uvea, or uveal tract, is located between the sclera and the retina. The uveal tract is composed of three main structures; the choroid, the ciliary body, the iris. The choroid is a capillary bed that nourishes the photoreceptors of the retina. The ciliary body encircles the lens. The interaction between the ciliary body and the lens provides focus on

both near and distant objects. The iris of the uveal tract is the colored part of the eye which functions like a controller of the amount of the light that enters the pupil [1, 2].

The retina, as the innermost layer of the eye is the essential contributer to the vision. Clear images of our environment come from projections onto the retina. The outer nuclear, outer plexiform layer and ganglion cell layer are layers of the retina. The retina encompasses 120 million neurons. The fovea of the retina is the area where the best vision occurs because of its neuronal and vascular circuitry. The fovea has photoreceptors which are named as rods and cones. An outer segment, including the photosensitive substance, an inner segment, a cell body, and a synaptic terminal are the four parts of the photoreceptors [1, 2].

Rods and cones and their functions are different. Rods are highly sensitive to light and are used for night vision. Cones have low sensitivity to light, hence are used for day vision. Cones have high temporal resolution, short integration time, less photopigment and lower amplification, whereas rods have low temporal resolution, long integration time, more photopigment, and higher amplification [3]. Other neruons of the retina are bipolar cells, ganglion cells, horizontal cells and amacrine cells which are involved in processing visual input from the retina to the brain [2].

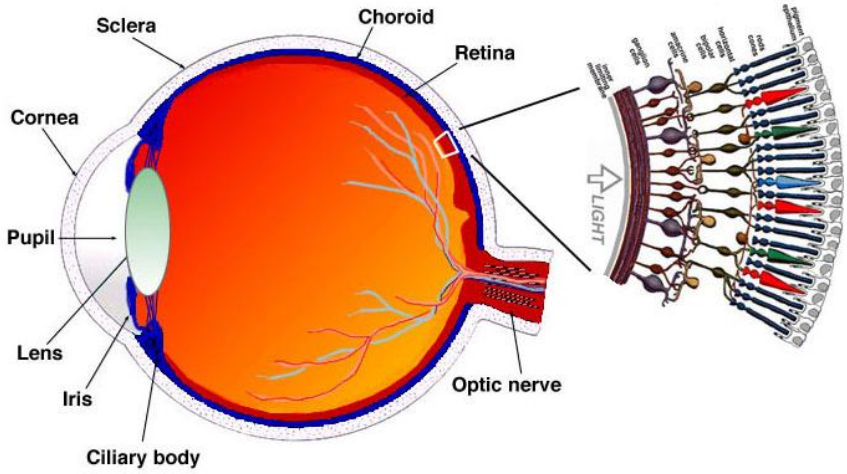

Figure 2.1 Schematic enlargement of the eye and its components [4].

2.2 The Visual Pathway

The image from the external environment is projected onto the retina. The visual system is very complex, and includes involvement of the cortical and subcortical areas. Felleman and Van Essen reported a hierarchical layout of brain areas in macaque that possibly has a role in the visual stream which is shown in Figure 2.2 [5]. The axons of the ganglion cells form the optic nerves; optic tracts, and optic chiasm are also other important components of the flow of visual information. The optic nerve has fibers from only the eye, while, the optic tract has fiber from both eyes. Fibers of each eye cross at the optic chiasm. Thus, fibers of the left half of the retina project to the left optic tracts, and convey information regarding the right visual field. Fibers from the right half of each retina project in the right optic tracts, carrying information regarding the left visual field. The fibers of the optic nerve penetrate the three subcortical areas: the pretectum, the superior colliculus, and the lateral geniculate nucleus (LGN). The pretectum is located in the midbrain and controls the pupillary reflexes. For example, saccadic eye movements are controlled by the superior colliculus. LGN is another subcorrtical area where its axons

terminate at the primary visual cortex (V1) of the occipital lobe, also known as Brodmann Area 17 (BA 17) [1, 3].

Figure 2.2 Cortical and subcortical areas involved in the visual stream with its hierarchical design [5].

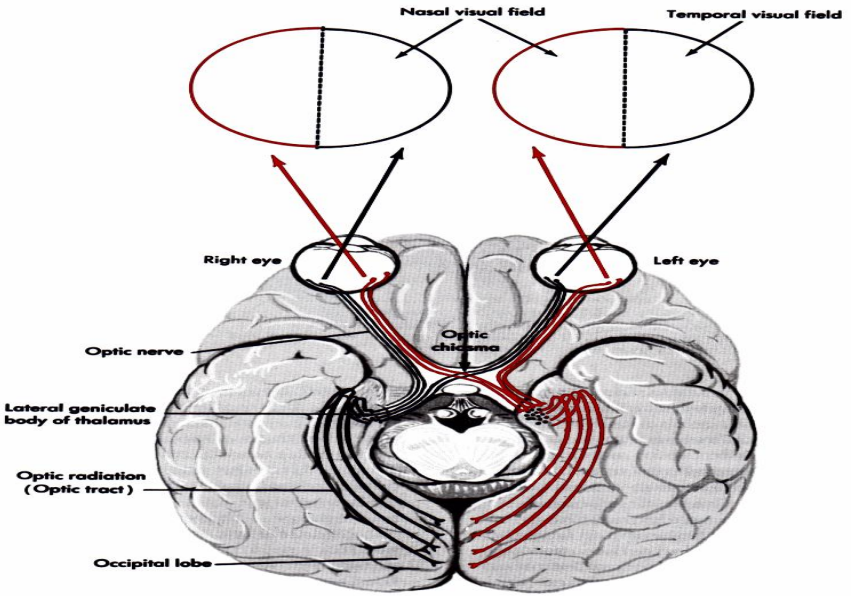

Figure 2.3 The visual pathway [6].

2.3 The Extraocular Muscles of the Eye and Ocular (Eye) Movements

The control of eye movements involves six pairs of eye muscles: the lateral and medial rectus muscles, the superior and inferior rectus muscles, and the superior and inferior oblique muscles. These muscles move the eyes in their axes: horizontal, vertical, and torsional. Horizontal movement can be defined with abduction which rotates the eye away from the nose, and the adduction which rotates the eye toward the nose. The medial and lateral rectus muscles are involved in the control of the eyes on the horizontal axes. The movement of the eye for the vertical axes uses superior and inferior rectus muscles and also might require the involvement of the oblique muscles. Elevation and depression are two terms used for when these muscles rotate the eye up and down on the vertical axes, respectively. The torsional axes recruit the oblique muscles for the purpose of intorsion (rotating top of the eye toward the nose) and extorsion (rotating the top of the eye away from the nose) movements [1, 3].

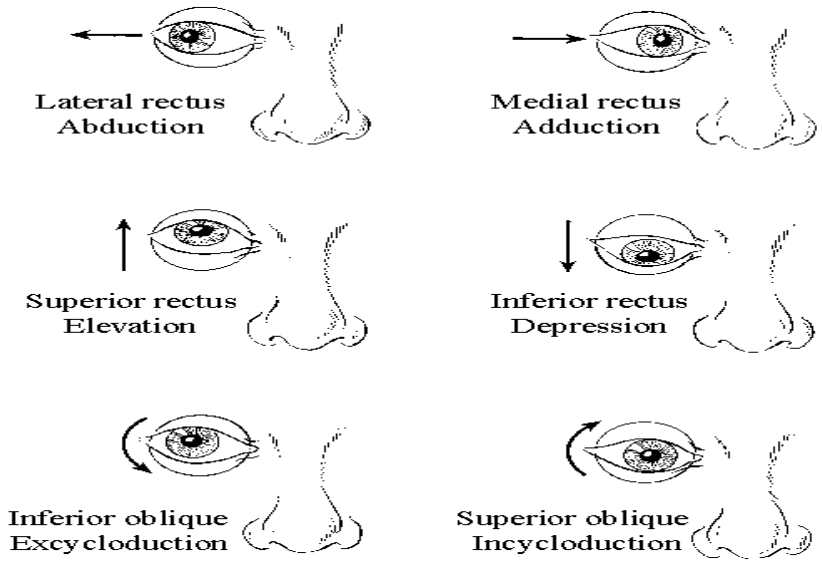

Figure 2.4 The muscles of the eye [7].

There are five groups of eye movements with a categorization of gaze stabilization and gaze shifting mechanism. Gaze stabilization mechanisms can be listed as vestibulo-ocular systems and optokinetic systems in which one focuses the eye on a target from the external world, while compensating head movements [1]. Gaze shifting mechanisms include smooth pursuit, saccadic and vergence eye movements. Smooth pursuit eye movements provide clear vision of the moving objects that is in our environment by tracking them [8]. Saccadic movements are those which move the eye quickly to objects of interest [3]. Opposite to the conjugate (horizontal) saccadic and smooth pursuit eye movements, vergence movements are disconjugate. The sense of different depths of the targets requires involvement of the vergence system. Convergence is a type of vergence movement where one uses for looking for near targets. Divergence is used when looking for far targets. The perception or sense of the different depths of the targets is accomplished by the differences of the retinal position (retinal disparity) during vergence movements [3].

2.4 The Neural Correlates of Saccadic and Vergence Eye Movements

Horizontal saccadic movements are generated in the paramedian pontine reticular formation (PPRF) of the brainstem. In addition to the PPRF, there are other cortical areas involved in the control of saccadic eye movements [1]. For example, the frontal eye field (FEF) controls the superior colliculus via exciting the saccadic related neurons; on the other hand, commands for triggering of inhibitory signals from subtantia nigra [3]. The supplementary eye field (SEF) is important for initiation of successful saccades [9]. The dorsolateral prefrontal cortex (DLPFC), as a region of decision making is responsible for inhibition of unwanted saccades [3, 9]. Furthermore, the parietal eye field (PEF) is also essential for triggering reflexive saccades and, is also involved in visually guided saccades [9].

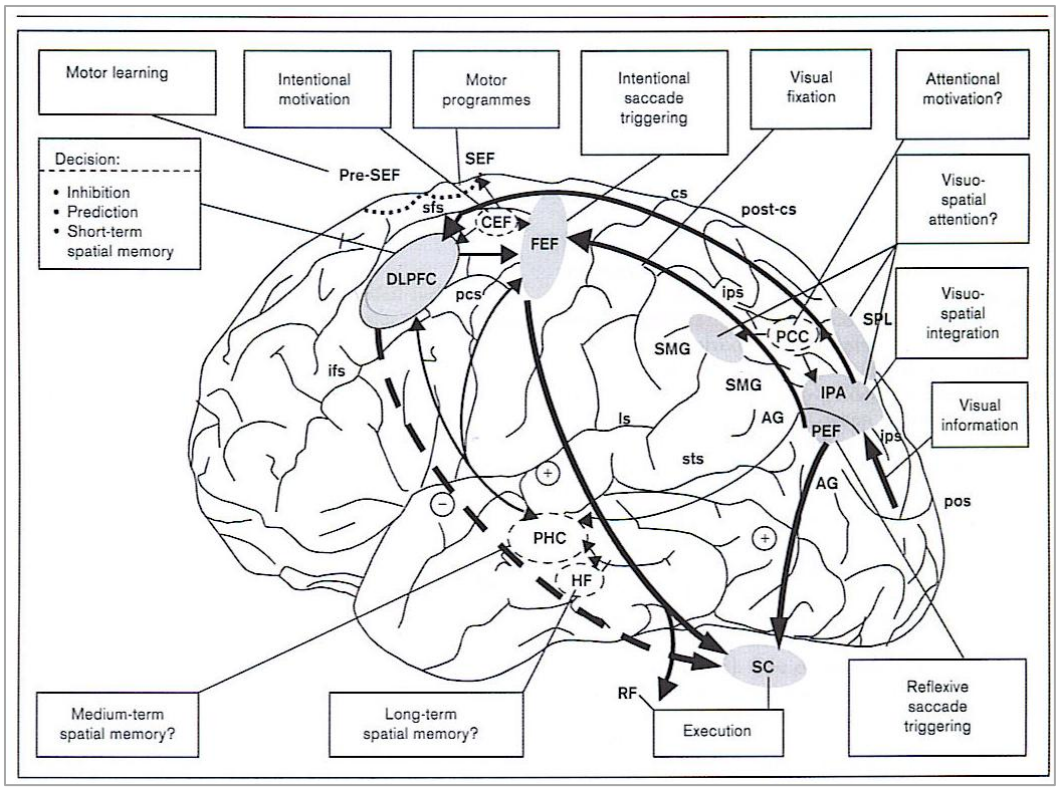

Figure 2.5 The pathway and cortical regions involved in saccadic control [10].

The cortical and subcortical areas involved in vergence eye movements for primates indicate recruitment of the primary visual cortex (BA 17) [11], the frontal eye field [12-14], the posterior parietal area [15, 16], the midbrain [17-19], the oculomotor vermis [20-22], the posterior interposed nuclues [23, 24] and the flocculus [25] of the cerebellum.

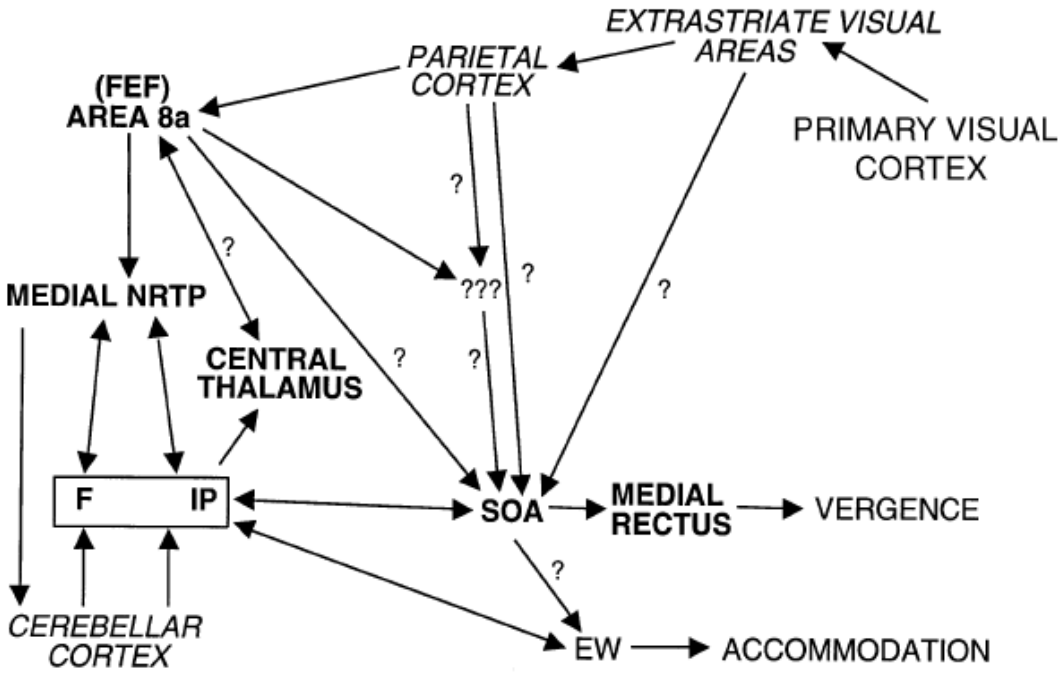

Figure 2.6 Neural pathways involved in the control of vergence eye movements. Areas that are known to contain cells related to vergence eye movements are bolded. The areas that appear to contain cells related to vergence eye movements remain to be identified and are indicated by question marks. Abbreviations: EW, nucleus of Edinger-Westphal; F, fastigial nucleus; FEF, frontal eye fields; IP, posterior interposed nucleus; NRTP, nucleus reticularis tegmenti pontis; SOA, supraoculomotor area [26].

In contrast to primate investigations, there are fewer human studies that have been done to understand vergence system. Mizushima and Seki reported vergence deficit on a patient who had a hemorrhage in the midbrain [27]. Rambold and colleagues also showed how the vergence system is affected when there is an existence of lesion in the pontine area of the brainstem [28-30]. Furthermore, the functional magnetic resonance imaging

(fMRI) study by our group points to the differentiation within FEF and the midbrain for vergence, as compared with saccades which will be discussed in detail later in this dissertation [31, 32]. Additionally, two other human investigations show diparity tuned cells in the visual cortical areas [33, 34].

2.5 What is Functional Magnetic Resonance Imaging (fMRI)?

The concept of blood oxygenation level dependent (BOLD) was started by Ogawa and colleagues. During their study, they scanned anesthetized rodents to observe blood oxygenation where the amount of the oxygen level was changed. In an experimental trial, rodents first inhaled one hundred percent of oxygen and they found the lines of blood vessels were not clear. This was due to the hemoglobin in the blood being highly oxygenated, which made the hemoglobin diamagnetic means not appear in the magnetic field. When the rodents breathed normal air, which contains twenty-one percent of oxygen, or when they reduced the oxygen to zero percent, the lines of the blood vessels were clear. Furthermore, Ogawa and colleagues confirmed by their study where test tubes with oxygenated blood appeared as homogeneous black circles, whereas the spin echo image of the deoxygenated blood was distorted because of their paramagnetic characteristic. This caused inhomogeneity on the induced field while changing the resonance frequency of the water molecules [35].

Another significant study surrounding fMRI technique was done by Kwong and colleagues. During this investigation, they observed changes in the hemodynamic responses for different task. They observed an “off” and “on” trend in the signal intensity. Alterations in blood dynamics occurred when subjects viewed the images as a visual target and the primary visual cortex was activated. Conversely, under complete darkness,

the neuronal activity in this region decreased [36]. Briefly, more oxygen is used for the active regions corresponding to neural activity. The level of oxygenated hemoglobin increases, causing a decrease in the level of deoxygenated hemoglobin. The ratio between oxygenated and deoxygenated hemoglobin reaches its peak, and creates a related response to the task, then decays back to its baseline levels. Hence, the aim of the fMRI is to detect functioning of the brain depending on the blood dynamics in real time.

2.6 Analyzing fMRI Data

In this dissertation, block design (boxcar model) was considered in visual experiments to describe neural activity during the task and zero during rest. Figure 2.7 shows an example.

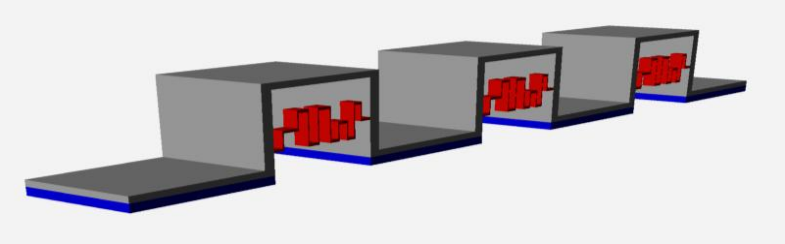

Figure 2.7 Example for experimental block design.

General Linear Modeling (GLM), Independent Component Analysis (ICA), and Granger Causality Analysis (GCA) was used to analyze the fMRI data collected to define spatial maps, temporal characteristics and causal relationships for the region of interests. GLM can be defined as a linear statistical regression analysis that provides information regarding the active regions of the brain during an experimental paradigm. ICA is a multivariate statistical technique widely known for the application on the cocktail-party problem. The concept of ICA is simple. Imagine two people's talk to a group of people, there will be multiple signals from speaker 1, speaker 2, and the noise that might come

from the listeners. Therefore, ICA can be used to remove noise component and reconstruct the underlying source signals that come from speakers. GLM is much more common than the ICA approaches, ICA of fMRI data has potential [37-39] to acquire both spatial and temporal information relevant to the experiment while removing the human and machine based artifacts. GCA is another multivariate statistical technique that assesses the direction of causality across the region of interests for the tasks that are implemented. The idea of Granger Causality can simply explained as if event X causes event Y, then the knowledge of past parameters of X can be used to predict the current parameter of Y. ROI-based analysis was tested on an fMRI data with comparison to global (whole) brain analysis. This method will be discussed in detail later.

Implementation of these methods on this fMRI datum will be explained in detail in later sections of the dissertation. Hence, each method will be used to define active regions, sources of the signals acquired, and causal interactions across regions for the visual tasks that are applied.

CHAPTER 3

DIFFERENTIATION BETWEEN VERGENCE AND SACCADIC FUNCTIONAL ACTIVITY WITHIN THE HUMAN FRONTAL EYE FIELDS AND MIDBRAIN REVEALED THROUGH fMRI (SPECIFIC AIM 1)

Purpose: Eye movement research has traditionally studied solely saccade and/or vergence eye movements by isolating these systems within a laboratory setting. While the neural correlates of saccadic eye movements are established, few studies quantified the functional activity of vergence eye movements using fMRI. This study mapped the neural substrates of vergence eye movements and compared them to saccades to elucidate the spatial commonality and differentiation between these systems.

Methodology: The stimulus was presented in a block design where the "off" stimulus was a sustained fixation and the "on" stimulus was random vergence or saccadic eye movements. Data were collected with a 3T scanner. A general linear model (GLM) was used in conjunction with cluster size to determine significantly active regions. A paired t-test of the GLM beta weight coefficients was computed between the saccade and vergence functional activities to test the hypothesis that vergence and saccadic stimulation would have spatial differentiation in addition to shared neural substrates.

Results: Segregated functional activation was observed within the frontal eye fields where a portion of the functional activity from the vergence task was located anterior to the saccadic functional activity ($z > 2.3$; $p < 0.03$). An area within the midbrain was significantly correlated with the experimental design for the vergence but not the saccade data set. Similar functional activation was observed within the following

regions of interest: the supplementary eye field, dorsolateral prefrontal cortex, ventral lateral prefrontal cortex, lateral intraparietal area, cuneus, precuneus, anterior and posterior cingulates, and cerebellar vermis. The functional activity from these regions was not different between the vergence and saccade data sets assessed by analyzing the beta weights of the paired t-test ($p < 0.2$).

Conclusion: Functional MRI can elucidate the differences between the vergence and saccade neural substrates within the frontal eye fields and midbrain.

3.1 Introduction

During natural viewing conditions we use a combination of version (saccade and smooth pursuit) and vergence (convergence and divergence) eye movements [8]. As mentioned in the Chapter 2, saccades and smooth pursuit are conjugate movements where the eyes move in tandem, on the other hand, vergence is the inward (convergence) and outward (divergence) rotation of the eyes to view objects at different spatial depths. With the increased presence of smart phones and tablets, our society has become more dependent on small interface devices. In addition, the use of 3D stereoscopic displays for computers, which stimulates vergence, is becoming common for vocational and recreational activities. Hence, the combination of vergence and saccadic movements especially for near viewing applications are prevalent within our activities of daily living. Currently clinicians are reporting an increase in visual symptoms associated with sustained near viewing tasks where vergence is utilized [40-42]. However, fewer studies have been conducted on vergence compared to saccadic eye movements [43]. Thus, a detailed functional MRI study quantifying the neural substrates of vergence movements in comparison with saccadic movements is warranted.

In the last five years alone, numerous reviews have summarized the state of the art in saccadic research describing: eye movement behavior in humans [44]; single cell electrophysiology research on primates [45]; case reports of humans with lesions [46] and functional imaging studies [47]. Many primate studies have investigated the cellular responses from saccadic stimuli [8, 45]. Yet, many of those studies did not include a dynamic vergence stimulus such as a step change in disparity. Hence, it is unclear whether the cells that encode for saccades are also tuned for disparity – the input stimulus for vergence.

There are a few investigations that have specifically sought to study the cortical location of the disparity vergence signal in primates where cells have been identified that modulate their activity for vergence but not for saccadic stimuli. Gamlin and Yoon [14] report activity from cells that modulate their behavior with saccadic stimuli within the anterior bank of the arcuate sulcus which is defined as part of the frontal eye fields [14, 48]. Gamlin and Yoon report distinct cells located anterior to the saccadic cells that modulate their activity with vergence stimuli but not with saccadic stimuli [14]. Within the subcortical regions, distinct cells that encode for vergence but not for saccadic / smooth pursuit movements have also been identified within the midbrain, specifically within the mesencephalic reticular formation and dorsal lateral to the oculomotor nucleus [15, 18, 49-52].

Behavioral eye movement data support interactions between vergence and saccadic eye movements [53-57]. Studies report that peak vergence velocity is greater when it is accompanied by a saccadic movement [53, 58] and that saccadic peak velocity is slower when it is accompanied by a vergence movement [59]. Several studies support

that the parietal lobe modulates its activity for saccadic [60-62] and disparity (the input to vergence) [63, 64] stimulation. The cerebellum has also been implicated in error processing for motor learning for both saccadic [65-67] and vergence [20-22] movements.

Based upon the aforementioned data from both cellular and behavioral studies of the saccadic and vergence systems, specific aim 1 of this dissertation claims that the neural substrates involved in initiating vergence and saccade eye movements will have shared neural resources within the parietal and cerebellar regions. It is also further hypothesized that differentiation will be observed within the frontal eye fields and midbrain regions. The aim of this study is to compare the vergence and saccade neural resources using the blood oxygenation level dependent signal from fMRI to systematically study the spatial differences and commonality between the neural substrates used to elicit saccade and vergence eye movements.

3.2 Methodology

3.2.1 Subjects

The New Jersey Institute of Technology (NJIT) and University of Medicine and Dentistry of New Jersey (UMDNJ) Institution Review Board (IRB) approved this study. All subjects signed written informed consent forms approved by the NJIT and UMDNJ IRB in accordance with the Declaration of Helsinki.

Eight subjects participated in this study (5 female and 3 male with a mean age of 26±4 years). Each subject's near point of convergence (NPC) was measured by having an examiner slowly bring the tip of a pen towards the subject along his midline [68]. When

the subject could no longer maintain fusion, the distance from the subject's orbit to the pen tip was recorded in cm as the NPC. The NPC was measured twice and averaged. All subjects had a normal near point of convergence (NPC) of less than 6 cm. Binocular vision was assessed by the Randot Stereopsis Test (Bernell Corp., South Bend, IN, USA). All subjects had normal binocular vision defined as better than 70 seconds of arc. Six of the subjects were emmetropes and two were corrected to normal refraction where the average prescription among these myopes was -1D. These two subjects wore their corrective refraction during the experiment. All subjects were right handed. None of the subjects had a history of brain injury or other neurological disorders. Subjects participated in an eye movement experiment prior to functional scanning. Each subject's eye movements were recorded to ensure the subject understood the task. All subjects were able to perform the task requested.

3.2.2 Materials and Apparatus

Images were acquired using a 3.0 Tesla Siemens Allegra MRI scanner with a standard head coil (Erlangen, Germany). Visual stimuli were a set of non-ferrous light emitting diode (LED) targets that formed a line 5 cm in height by 2 mm in width located at three positions.

Eye movements were recorded using an infrared (λ = 950 nm) limbus tracking system manufactured by Skalar Iris (model 6500, Delft, Netherlands). All of the eye movements were within the linear range of the system (±25°). The left-eye and right-eye responses were calibrated, recorded and saved separately for offline analysis. A custom MATLAB^{TM} (Waltham, MA, USA) program was used for offline eye movement data

analysis. Blinks were identified by the saturation of signal. Blinks were manually omitted from the eye movement traces.

3.2.3 Imaging Instrumentation and Procedure

The subject was positioned supine on the gantry of the scanner with his head along the midline of the coil. All participants were instructed to limit head motion. Foam padding was used to restrict additional movement and motion correction software described below was utilized to ensure head motion did not influence the results. Ear plugs were used to reduce scanner noise by up to 30 dB while still allowing the participant to hear instructions from the operators to ensure communication during the scan. In all experiments, the radio frequency power deposition and field-switching rate were kept below levels specified by the U.S. Food and Drug Administration (FDA)

The subcortical regions were of interest in this study; hence all subjects were positioned so that images could be attained of the whole brain. All functional scans used a T2* weighted echo planar imaging (EPI) sequence. The imaging parameters were FOV = 220 mm, 64 x 64 matrix, TR = 2000 ms, TE = 27 ms and flip angle = 90°. The whole brain was imaged in an axial configuration where 32 slices were collected and each slice was 5 mm thick. The resolution was 3.4 x 3.4 x 5 mm. There were 70 volumes acquired per scan lasting a total of 2 minutes and 20 seconds. Between scans, the subjects were asked if they were comfortable and could perform the task. Subjects confirmed they could perform each task with ease. After all functional tasks, a high resolution MPRAGE (magnetization-prepared rapid gradient-echo) data set was collected. The MPRAGE imaging parameters were: 80 slices, FOV = 220 mm, slice thickness = 2 mm, TR = 2000

msec, TE = 4.38 msec, T1 = 900 msec, flip angle = 8º and matrix = 256 x 256 which resulted in a spatial resolution of 0.9 x 0.9 x 2 mm.

3.2.4 Functional Experimental Design

The experiment followed a standard block design of fixation (no eye movement) for the "off" phase compared to random eye movements for the "on" phase using saccadic or vergence step stimuli. Each visual step stimulus was presented for a random duration of time between 0.5 to 3.0 seconds. Approximately 20 visual step stimuli were presented within each eye movement phase. The subject could not anticipate the timing of the visual stimulus. Subjects confirmed they were able to comfortably view the visual stimuli during the imaging session. For all experiments, only one target was illuminated at a time. The saccadic visual stimulus is shown in Figure 3.1. The scanner room was darkened where the subject only saw the visual stimulus. A saccadic magnitude of 10° from midline was chosen because saccades less than 15° from midline do not evoke head motion [69]. The saccadic experiment began with fixation on the middle LED for 20 seconds, shown in Figure 3.1 image B1. Next, subjects would track targets that would randomly appear in three locations: 0° (midline); 10° into the left visual field; or 10° into the right visual field, Figure 3.1 image B2. Subjects performed tracking of saccadic step stimuli lasting for the duration of 20 seconds. This sequence was repeated for 3.5 cycles.

For vergence stimulation, subjects viewed the same LED apparatus used during the saccadic experiment, but the orientation was changed to be aligned with the subject's midline and the spacing between visual targets was adjusted to stimulate 2°, 3° and 4° of combined sustained convergence demand as shown in Figure 3.1 image A2. Experiments also took place in a darkened room where the subject only saw the visual stimulus. There

were three vergence fixation points, 2°, 3° and 4° centered along the subject's midline to produce symmetrical vergence step stimuli. The maximum vergence step stimulus was a 2° disparity change which was chosen due to the physical constraints of the imaging center and to decrease the occurrence of saccades within the symmetrical vergence response [70-72]. For the random phase, the time when the next target was displayed was randomized between 0.5 to 3 seconds in duration.

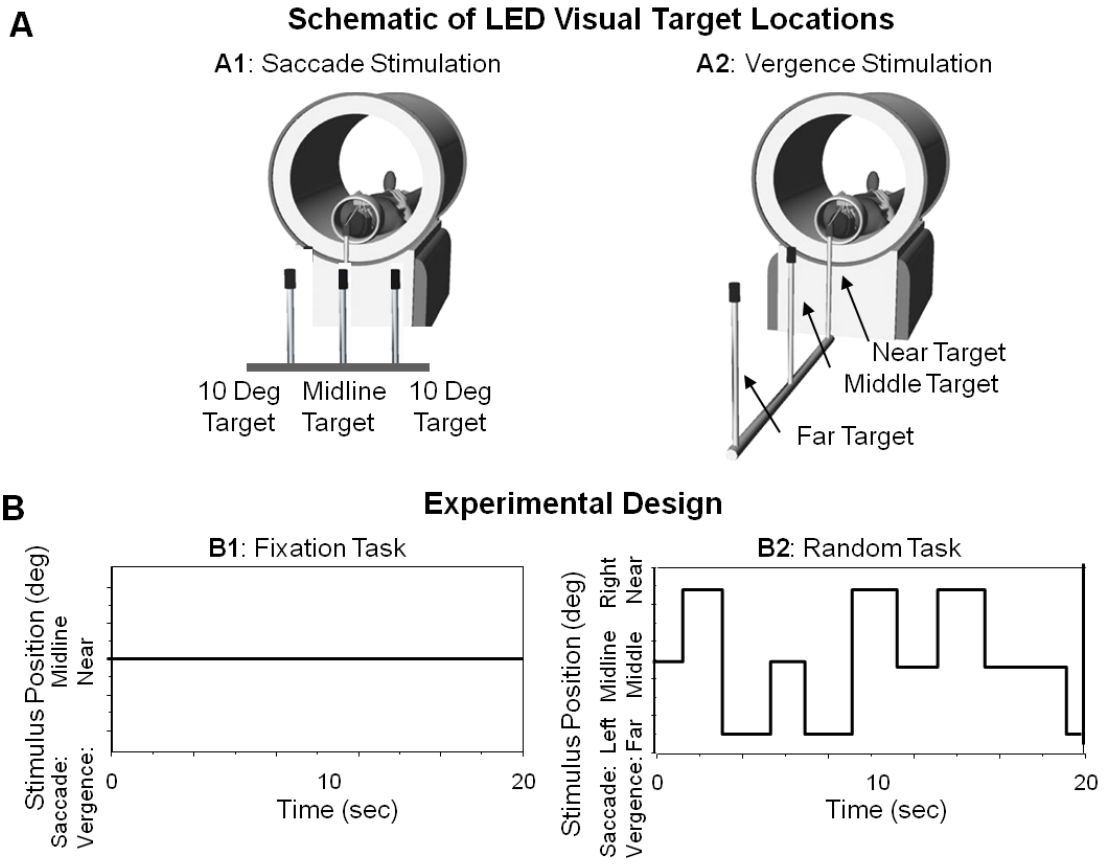

Figure 3.1 Experimental set-up and design. The schematic of the custom fMRI compatible light emitting diodes (LEDs) for the saccade (image A1) and vergence (image A2) experiments. Subjects would sustain fixation (plot B1) on either the midline target during the saccade experiment or near target during the vergence experiment for 20 seconds and then track the illuminated LEDs in a random pattern for 20 seconds (plot B2). A block design protocol is used where the "off" stimulus is sustained fixation and the "on" stimulus is the random eye movement tracking.

A total of three saccade and three vergence experimental trials were collected in case head motion was a problem which was not the case within this data set.

3.2.5 Data Analysis

3.2.5.1 Individual Subject Analysis using a Data Driven Reference Vector. Data were analyzed with AFNI (Analysis of Functional NeuroImages) software [73]. All the scans were first registered and motion corrected. A minimum least-square image registration method available in AFNI was utilized to detect and correct for the presence of any motion-induced changes on the 3D image space. Six parameters were monitored to determine whether head motion was a problem within our data set. Three parameters indicated the movement within each plane (anterior to posterior, right to left, and inferior to superior, calculated in mm) and three parameters indicated the amount of rotation about the three orthogonal axes (yaw, pitch and roll, calculated in degrees). A recent comparison of several software packages found that the AFNI image registration algorithm was both reliable and fast in comparison with other software [74]. The least-square image registration method employed in this study used the fourth image in each data set as a reference and the motion parameters were estimated for the time-series set. After motion correction, individual anatomical and functional brain maps were transformed into the standardized Talairach-Tournoux coordinate space [75].

The hemodynamic response can vary due to age [76, 77], trauma [78, 79], fatigue [80] and/or physiological variations [81]. Due to the variations in the hemodynamic response function, a data driven independent component analysis was used to obtain a reference vector corresponding to the experimental stimulus [31, 82-90]. Probabilistic independent component analysis available through the MELODIC (Multivariate

Exploratory Linear Optimized Decomposition into Independent Components) software from FSL was used to calculate the independent signal sources [91] for each subject. The signal source that had the greatest Pearson correlation coefficient with the experimental block design was the reference vector used to correlate each voxel within our data set during an individual subject analysis. A representative example of typical source vectors from subject S4 for the saccade and vergence experiment are shown in Figure 3.2.

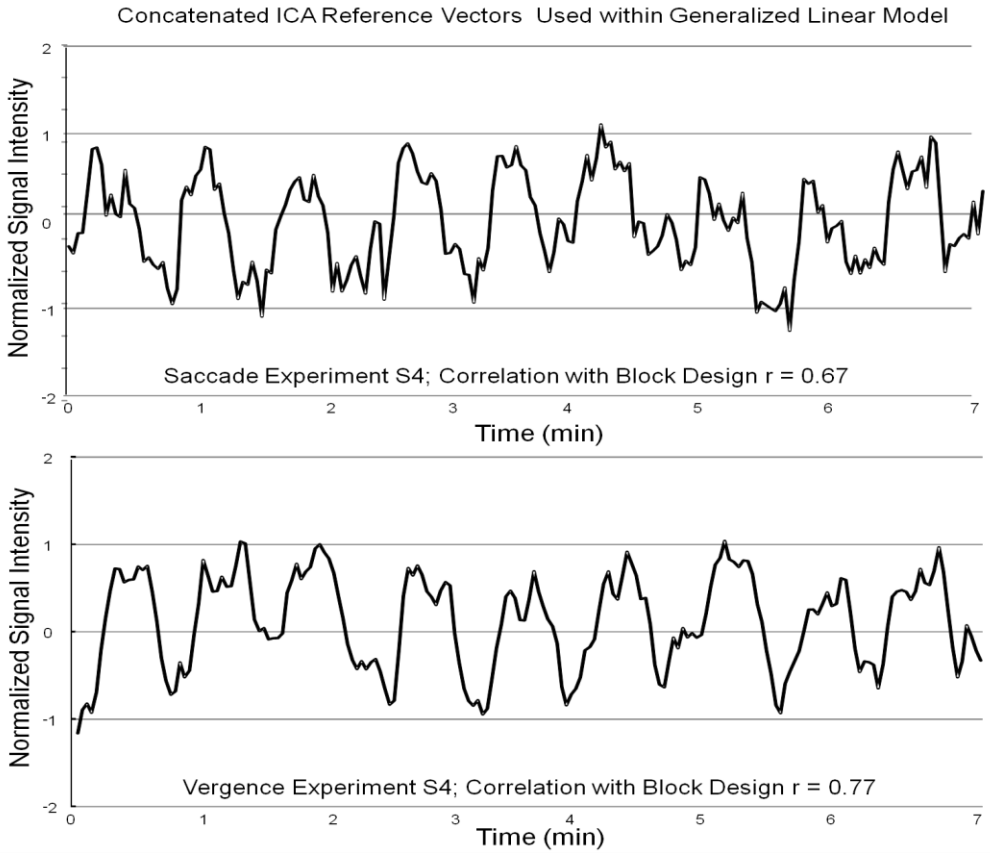

Figure 3.2 Typical reference vector from one subject (S4) from the saccadic data set (upper plot) and the vergence data set (lower plot). The source signals have a high Pearson correlation coefficient with the experimental block design (r = 0.67 for the saccade experiment and r = 0.77 for the vergence experiment).

The fMRI blood oxygenation level dependent (BOLD) signal analyzed using a general linear model (GLM) method has been reported to be correlated to direct neuronal measurements [92, 93]. Hence, the fMRI time series data within this study were analyzed

with a GLM where each voxel of the entire brain was correlated with a hemodynamic model calculated using independent component analysis for each individual subject described above. Using the GLM analysis, only data that attained a minimum threshold of functional activity corresponding to a z-score of 2.0 (two tail p = 0.05) were further analyzed.

3.2.5.2 Group Analysis. Both individual and group analyses were performed. To facilitate comparison between the vergence and saccade data sets the individual subject spatial maps were averaged. All data were first analyzed individually to observe the regions of interest (ROIs) significantly activated during the experiments. The ROIs are described below. Only ROIs that were functionally activated in all eight subjects are reported within this study.

3.2.5.3 Regions of Interests. The functional activity for the saccadic network is well established and is reviewed in several papers [8, 10, 45]. Hence, we hypothesized that our fixation versus random saccade eye movement experiment would provoke activation within the frontal eye fields (FEF), the supplementary eye field (SEF), the dorsolateral prefrontal cortex (DLPFC), the parietal eye fields (PEF), the anterior and posterior cingulate cortex and the cerebellum during the saccadic experiment. Functional MRI studies have shown that the saccade related area of FEF is localized in the upper portion of the anterior wall of the precentral sulcus [94]. It is described in a recent review paper as being in the vicinity of the precentral sulcus and/or in the depth of the caudalmost part of the superior frontal sulcus [48]. The human SEF is located on the medial surface of the superior frontal gyrus, in the upper part of the paracentral sulcus [95]. The dorsolateral prefrontal cortex is located within Brodmann Areas (BA) 46 and 9

[96]. The parietal eye field is located in the lateral intraparietal area [10]. The anterior and posterior cingulate cortexes are located in Brodmann Areas (BA) 24 and 23 respectively [10]. These regions were initially investigated as well as other areas within the brain. The individual time series from regions shown within the results are filtered with a first order Butterworth filter using a cutoff frequency of 0.1 Hz, implemented in MATLAB™.

3.2.5.4 Statistical Analysis. The combination of the individual voxel probability threshold and the cluster size threshold (11 voxels rounded to a volume of 650 mm3 for our data set) yielded the equivalent of a whole-brain corrected for multiple comparison significance level of $\alpha < 0.001$. The cluster size was determined using the AFNI AlphaSim program [97]. This program estimates the overall significance level by determining the probability of false detection through Monte Carlo simulation. Through individual voxel probability thresholding and minimum cluster size thresholding, the probability of false detection is determined from the frequency count of cluster sizes. The program is based on the assumption that the underlying population of voxel intensity has a normal distribution. Simulation used 10,000 Monte Carlo iterations, assumed a cluster connection of the nearest neighbor, voxel dimension of 3.4×3.4×5 mm and sought a significance level of 0.001. Hence, a cluster size of 650 mm3 or greater corresponded to $p < 0.001$ corrected for multiple comparisons. The functional data are displayed as a z-score shown in the figure scale bar. Individual maps of t-statistics were smoothed with a Gaussian kernel of 6 mm full-width and half-maximum to account for inter-individual anatomical variation [98-100]. In here, it is hypothesized that the vergence and saccade circuits will show some spatial differentiation. Specifically, the vergence FEF will be

adjacent and directly anterior to the functional activity of the saccadic FEF as is reported in single cell recordings in primates [14]. The null hypothesis would be that no difference in the signal amplitude would be observed between the vergence and saccade data sets. Hence, to determine whether significant spatial differences existed between the saccade and vergence data sets, the beta weights from the general linear model were compared with a paired t-test of the eight individual subjects in a voxel-wise basis to create a statistical significance spatial map. Data were thresholded for an absolute T-value greater than 2.3 (two-tailed p-value = 0.05). The statistical difference spatial maps are displayed using the scaled T-value as the color overlay upon standardized anatomical images to show the spatial location of significantly different areas of activation.

Using the paired t-test spatial maps, it is observed which ROIs were significantly different between the vergence and saccade datasets. For the ROIs where significant spatial differences were observed, the results are reported using the individual subject data. All other regions of interest that were not significantly different between the vergence and saccade dataset are reported using group data.

Functional spatial maps are displayed using the Computerized Anatomical Reconstruction and Editing Tool (Caret) Kit [101].

3.2.5.5 Representation of Time Series Signal. The time series from the functional images are displayed as the percent of signal change from the baseline. The baseline was calculated as the average of the five data points with the smallest magnitude.

3.3 Results

Six motion related parameters were computed and corrected for each subject during each of the scans. The largest average degree of rotation was 0.1° ± 0.1 and 0.2° ± 0.1 in the pitch direction for the saccade and vergence data sets respectively. The largest average amount of movement within a plane was 0.3 ± 0.2 mm and 0.3 ± 0.3 mm in the inferior to superior plane for the saccade and vergence data sets respectively. This motion was much less than one voxel. Hence, head motion was not problematic within these data sets. Thus, all data were utilized for this analysis.

Typical eye movements and the corresponding functional activity from the frontal eye fields are shown in Figure 3.3. Data are displayed with the experimental block design. Eye Movements are plotted as position (deg) as a function of time (sec). Saccadic eye movements reach the next target sooner than the vergence eye movements. Therefore, the peak velocities between these movements are different. The temporal and dynamic differences are hypothesized to be generated by differences in neural substrates because both movements are generated using the same biomechanics, the lateral and medical recti muscles.

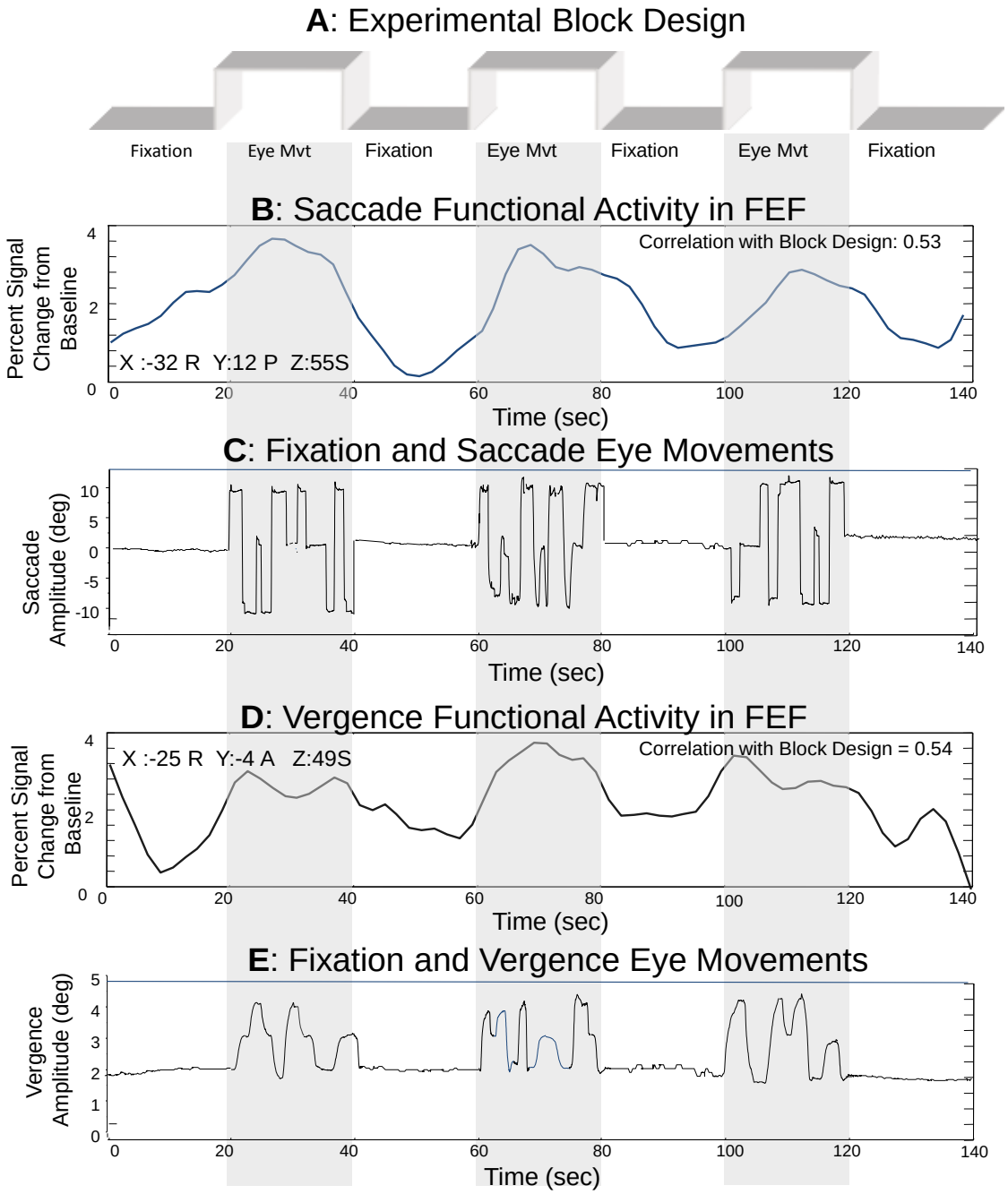

Figure 3.3 Experimental block design of 3.5 cycles alternating between fixation and eye movements (Plot A). Fixation and saccadic eye movements to targets 10 degrees into the left or right visual field or along midline plotted as position (deg) as a function of time (sec) (Plot B). Functional activity within FEF during saccadic stimulation plotted as percent signal change from baseline as a function of time (sec) (Plot C). Fixation and vergence eye movements to targets 2, 3, or 4 degrees along midline plotted as position (deg) as a function of time (sec) (Plot D). Functional activity within FEF during vergence stimulation plotted as percent signal change from baseline as a function of time (sec) (Plot E).

Data were first analyzed individually to determine how many of the eight subjects showed activation for a given anatomical location. Only areas that showed significant activation for all subjects are included in the results. The averaged group functional activity from the eight subjects performing the fixation versus a random saccadic oculomotor task is shown in Figures 3.4 and 3.5, left portion of the figures. Figures 3.4 and 3.5 show an axial slice displaying the anatomy of functional activity. Figure 3.4 also shows semi-inflated views of the lateral hemispheric surfaces and the cerebellum. Table 3.1 lists the peak activation with Talairach-Tournoux coordinates for a given anatomical location of the averaged subject data set with the corresponding z-score and Brodmann Area (BA) from the saccadic task. For the saccadic functional activation induced from the fixation versus random eye tracking oculomotor visual tasks, activity is observed in the vicinity of the superior frontal sulcus (denoted with a blue arrow Figure 3.5) and precentral sulcus (denoted with a green arrow Figure 3.5), also defined as the frontal eye fields [48]. Functional activity is also observed in the medial frontal gyrus, referred to as the supplementary eye field; the dorsolateral prefrontal cortex; the ventral lateral prefrontal cortex; the intraparietal sulcus, referred to as the parietal eye field or Brodmann Area 40 [10]; the cuneus; the precuneus; the anterior and posterior cingulates; and the cerebellar vermis. Similar areas were activated within the vergence data as shown in Figures 3.4 and 3.5 as well as Table 3.2.

Although the functional activation from saccadic and vergence visual stimuli had many shared neural resources, there was an observed differentiation within the frontal eye fields, Figures 3.5 and 3.6 and Table 3.1 compared to Table 3.2. Specifically, group peak activation for the fixation versus vergence eye movement task was anterior

quantified as Talairach-Tournoux coordinates 32L, 6A, 49S and 24R, 2A, 50S (Table 3.2), to average peak bilateral activation of the saccadic task quantified as Talairach-Tournoux coordinates 36L, 9P, 50S and 30R, 5P, 48S (Table 3.1). The individual subject peak activation is summarized in Table 3.3 where we also observed on an individual basis that the peak activations in the frontal eye fields were anterior to the activation within the saccade data. Then a voxel-wise paired t-test is conducted using the beta weights from the general linear model to determine whether the cortical activation was significantly more anterior. Results are shown in Figure 3.5.

Figure 3.5A shows the functional activity from the fixation versus the random saccadic eye movement task as well as the fixation versus the random vergence eye movement task where the FEF (white arrows), the precentral sulcus (green arrows) and the superior frontal sulcus (blue arrows) are labeled. The functional activity for vergence is anterior to a similar saccadic task. Figure 3.5B shows the statistical spatial maps of the saccade minus vergence paired t-test data sets (defined as the positive values) and statistical spatial maps of the vergence minus saccade paired t-test data sets (defined as the negative values). Significant spatial differentiation was observed. It is then sought to evaluate the correlation of the underlying time series with the experimental block design.

One subject's time series signals from the frontal eye field for one trial (2 min 20 sec) are assessed in Figure 3.6. The time series with the maximum correlation with the block design (a square wave of "off" and "on" stimuli for 3.5 cycles) has a Pearson correlation coefficient of r = 0.64. This signal is from Talairach- Tournoux location 33R, 11P, 56S within the frontal eye field (FEF) from the saccade data set. The time series with the maximum correlation with the block design from the frontal eye field within the

vergence data set has a correlation of r = 0.54 (25R, 4A, 49S, in Talairach-Tournoux coordinates). Hence, the time series are highly correlated with the experimental task.

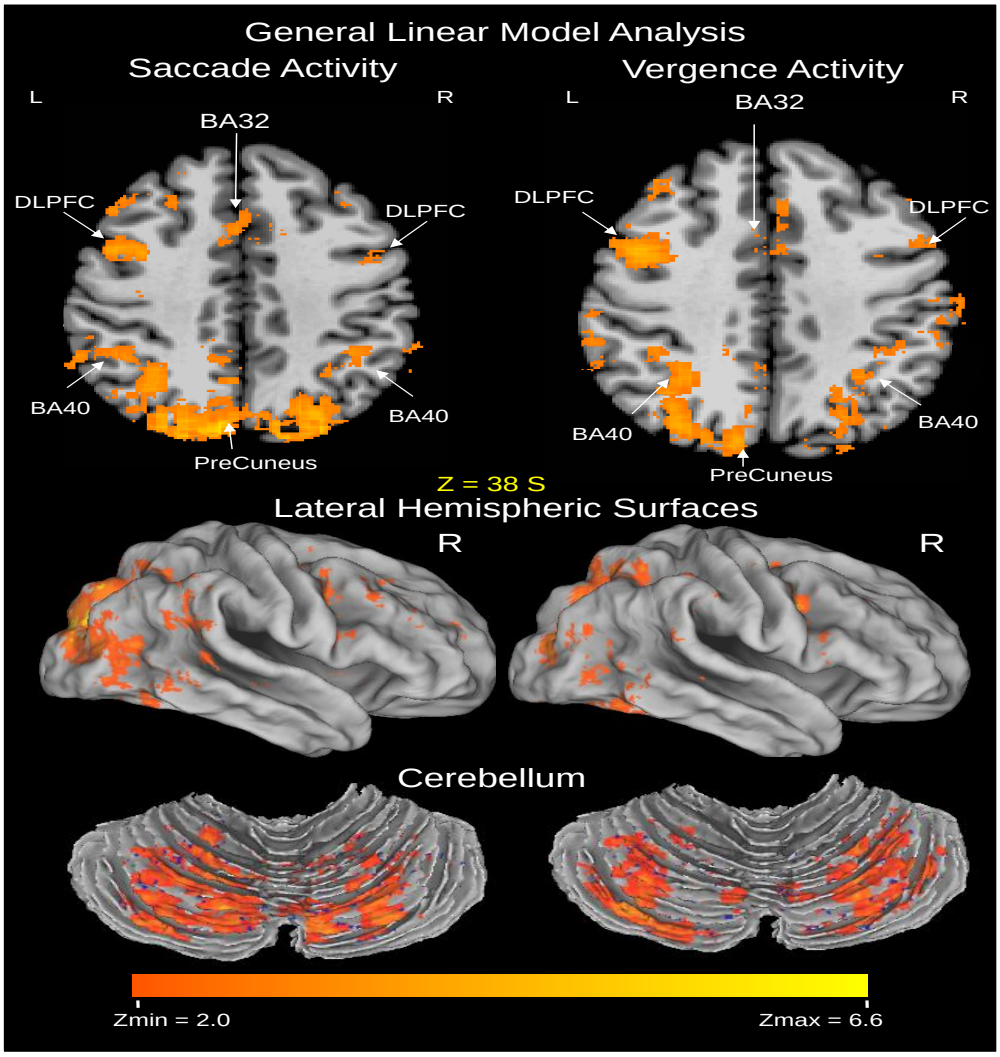

Figure 3.4 Functional activation for the group analysis of fixation versus random eye movements for the saccade (left side) and the vergence data set (right side) showing typical commonality. DLPFC = dorsolateral prefrontal cortex and BA = Brodmann Area. The number of mm above the bicommissural plane is indicated. The functional activation is denoted by the scale bar as a z-score from a minimum of 2.0 to a maximum value of 6.6. Data are overlaid onto a standardized Talairach-Tournoux normalized image. Semi-inflated images of the functional activity within the lateral hemispheric surface and cerebellum are displayed using Caret software

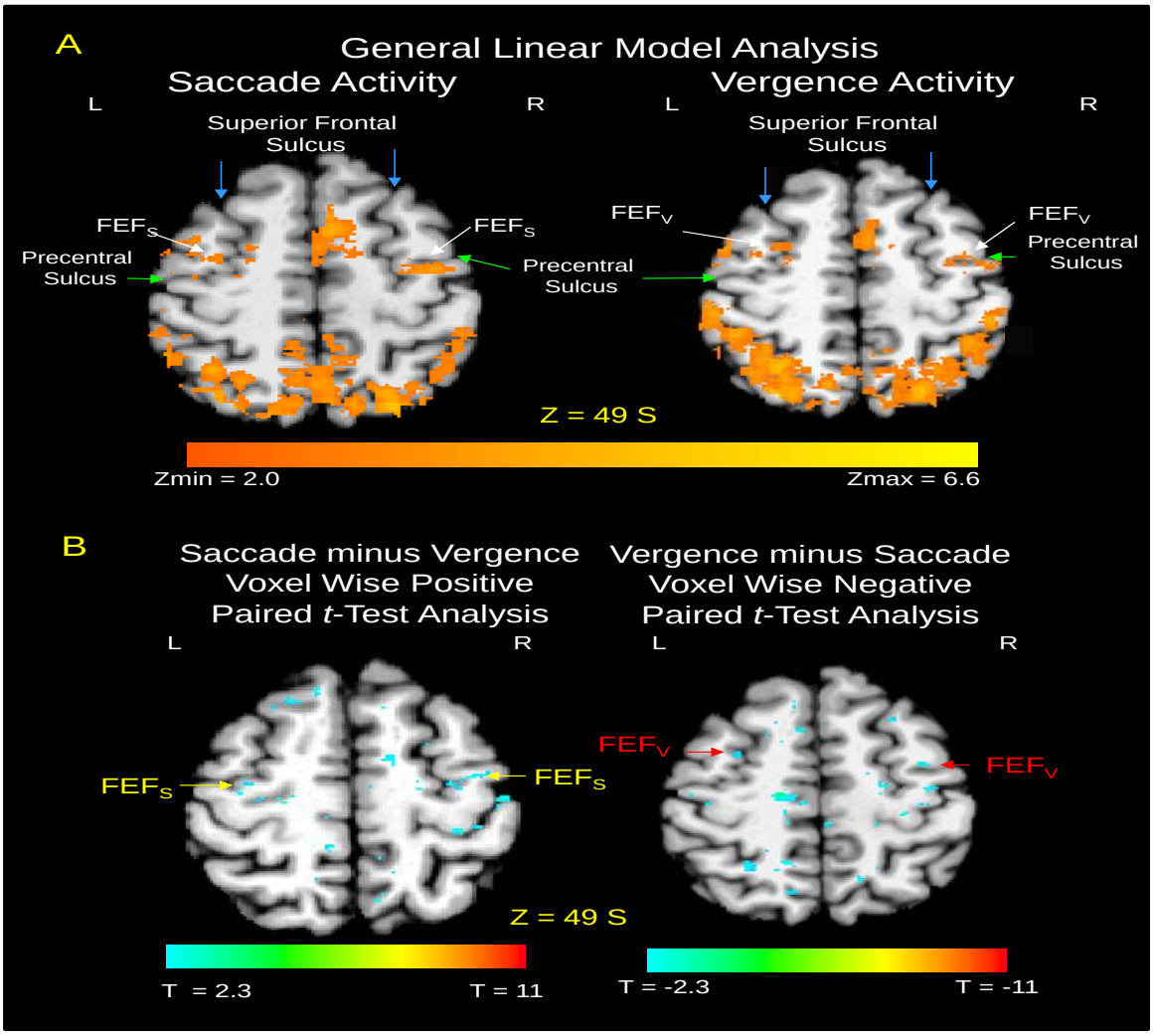

Figure 3.5 Axial images showing differentiation between the functional activity of the frontal eye fields (FEF) from saccade (left) and vergence (right) eye movements. Functional activity using the GLM analysis is shown in Figure 3.5A. The voxel wise positive and negative paired t-tests show significant differentiation between FEF for vergence and saccades, Figure 3.5B. The GLM analysis reports activity using the scale bar of a z-score from 2.0 to 6.6. The paired t-tests using the beta weights from the GLM analysis reports significant differences from T = ±2.3 to ±11 (two-tailed p-value = 0.05 to $p < 0.0001$). Functional activity and paired t-test significant differences are overlaid onto Talairach-Tournoux normalized axial structural images. The axial slice is 49 mm superior to the bicommissural plane for all images. L: left; R: right. The superior frontal sulcus is denoted with blue arrows and the precentral sulcus is denoted with green arrows in Figure 3.5A. The significant differences within FEF are denoted with red arrows for vergence (FEFv) and yellow arrows for saccades (FEFs) in Figure 3.5B.

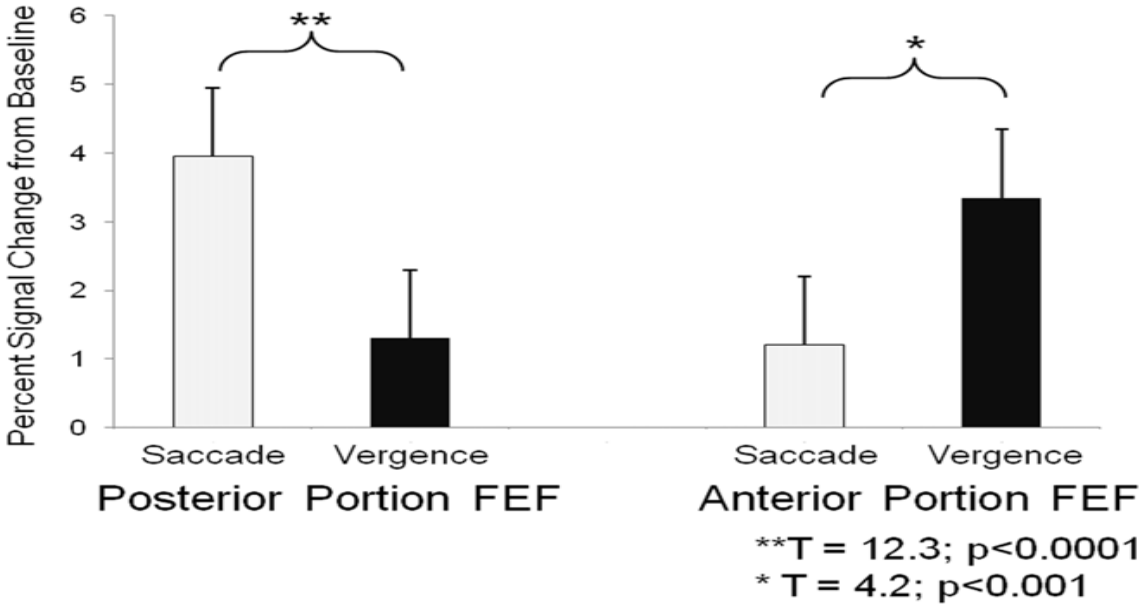

Figure 3.6 Percent signal change from baseline within the posterior (left) and anterior (right) portions of the frontal eye fields (FEF). Significantly more signal change is observed within the posterior portion of FEF in the saccade compared to the vergence data set. Significantly more signal changes is observed within the anterior portion of FEF in the vergence compared to the saccade data set.

Table 3.1 Average Peak Activation of the Fixation Versus Random Saccadic Oculomotor Task in Talairach-Tournoux coordinates with the Level of Significance Denoted as a z-Score

Region	BA	X (mm)	Y (mm)	Z (mm)	z-score
Frontal Eye Field, Superior Middle Frontal Gyrus, Precentral Gyrus	8/6	-36L	-9P	50S	3.4
	8/6	30R	-5P	48S	2.4
Supplementary Eye Field, Medial Frontal Gyrus	6	1R	-2P	53S	2.7
Dorsolateral Prefrontal Cortex	9	-33L	2A	36S	3.4
		36R	4A	34S	2.5
Anterior Cingulate/ Cingulate Gyrus	24/32	-2L	14A	38S	2.8
Inferior Ventral Lateral Prefrontal Cortex, Inferior Frontal Gyrus, precentral Gyrus	45/47	-26L	17A	1S	3.7
		41R	11A	2S	2.7
Parietal Eye Field Inferior Parietal Area	40	-33L	-53P	48S	3.6
		29R	-54P	41S	2.8
Cuneus, Lingual Gyrus	17/18	8R	-70P	12S	6.4
Precuneus	7	-5L	-73P	42S	4.4
Superior Parietal Area	7	-30L	-65P	50S	4.3
		26R	-70P	50S	4.7
Posterior Cingulate	31	1R	-67P	23S	2.6
	30	-7L	-65P	8S	5.0
		6R	-59P	8S	3.9
	29	0	-40P	18S	3.2
Cerebellar Vermis IV/V		6R	-61P	-5I	4.1

Table 3.2 Average Peak Activation of the Fixation Versus Random Vergence Oculomotor Task in Talairach-Tournoux Coordinates with the Level of Significance Denoted as a z-Score

Region	BA	X (mm)	Y (mm)	Z (mm)	z-score
Frontal Eye Field, Superior Middle Frontal Gyrus, Precentral Gyrus	8/6	-32L	6A	49S	2.3
	8/6	24R	2A	50S	2.5
Supplementary Eye Field, Medial Frontal Gyrus	6	-3L	7A	49S	2.9
Dorsolateral Prefrontal Cortex	9	-48L	10A	35S	2.6
		43R	4A	35S	4.7
Anterior Cingulate/ Cingulate Gyrus	24/32	2R	20A	38S	2.2
Inferior Ventral Lateral Prefrontal Cortex, Inferior Frontal Gyrus, precentral Gyrus	45/47	-50L	13A	5S	2.3
		53R	17A	7S	2.9
Parietal Eye Field Inferior Parietal Area	40	-26L	-54P	44S	3.5
		29R	-52P	46S	4.2
Cuneus, Lingual Gyrus	17/18	12R	-92P	-3I	4.8
Precuneus	7	11R	-79P	37S	3.5
Superior Parietal Area	7	-32L	-55P	51S	3.5
		26R	-55P	52S	4.4
Posterior Cingulate	31	1R	-66P	22S	2.5
	30	-7L	-65P	9S	3.1
		5R	-65P	7S	3.8
	29	-12L	-53P	-1I	2.1
		7R	-41P	5S	2.5
Cerebellar Vermis IV/V		-9L	-43P	2S	2.2
Midbrain		8R	-20P	-4I	2.4

Table 3.3 Individual Subject Analysis of Saccade and Vergence FEF

Subject	Saccadic Task				Vergence Task			
	X (mm)	**Y(mm)**	**Z(mm)**	**z-score**	**X(mm)**	**Y(mm)**	**Z(mm)**	**z-score**
1	-38L	-10P	49S	6.4	-30L	12A	57S	2.8
	40R	1A	48S	6.6	23R	5A	58S	3.9
2	-32L	-7P	49S	9.5	-25L	13A	51S	3.8
	36R	-6P	50S	5.7	33R	17A	49S	4.2
3	-33L	-12P	52S	6.7	-23L	12A	46S	4.0
	29R	-5P	52S	5.7	25R	16A	47S	6.6
4	-31L	-5P	53S	4.3	-27L	11A	47S	4.5
	25R	-6P	58S	3.8	37R	5A	41S	11.7
5	-31L	-10P	54S	7.4	-23L	10A	50S	3.7
	36R	-16P	54S	5.0	26R	8A	57S	5.5
6	-34L	-7P	46S	2.6	-21L	13A	50S	4.3
	32R	-2P	45S	4.8	22R	7A	54S	4.4
7	-30L	1A	47S	5.1	-30L	10A	47S	2.9
	30R	1A	52S	8.3	19R	7A	51S	3.4
8	-29L	-6P	53S	4.2	-21L	11A	40S	4.0
	34R	-7P	53S	7.4	27R	10A	38S	5.1
Average ± Standard Deviation	-32L ± 3	-7P ± 4	50S ± 3	5.8 ± 2.2	-25L ± 4	12A ± 1	49S ± 5	3.8 ± 0.6
	33R ± 5	-5P ± 5	52S± 4	5.9 ± 1.5	27R ± 6	9A ± 5	49S ± 7	5.6 ± 2.7

Differentiation was also observed subcortically within the midbrain, Figure 3.7A. Activity observed within the vergence data set (Figure 3.7A right) but not within the saccade data set (Figure 3.7A left). An individual subject analysis was conducted and the Talairach-Tournoux coordinates with the z-score of peak activation is summarized in Table 3.4. A paired t-test analysis using spatial maps was performed on the subcortical regions to determine whether these activations were significantly different between the saccade and vergence data sets, Figure 3.7B. The area within the cross hair shows that this region of interest is significantly different between the vergence and the saccadic dataset. A typical filtered time series signal of the midbrain from the vergence data set is shown in Figure 3.7C. This signal has a correlation of $r = 0.50$ with the block design (square wave) and is located at Talairach-Tournoux location 7R, 13P, 15I. The midbrain functional activity within the vergence data set is highly correlated with our experimental task. Furthermore, when comparing the same subcortical locations within the saccade and vergence data sets, significant differences between the percent signal change from baseline are observed assessed using a paired ttest Specifically, there is a greater percent signal change from baseline in the vergence data set compared to the saccade data set, ($T=3.6$, $p < 0.01$). Results are shown in Figure 3.7D.

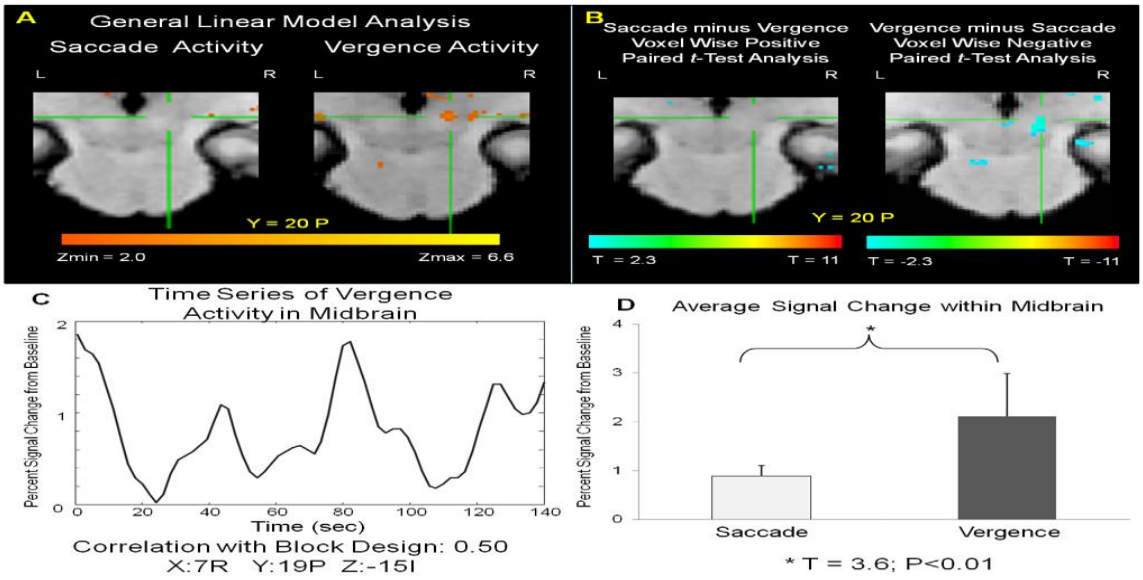

Figure 3.7 Functional activity within the midbrain using a GLM analysis (Plot A). Positive and negative paired t-test statistical spatial map showing differentiation between the midbrain for the fixation versus random saccadic and vergence tasks identified via the cross hair. A positive T value is for the saccade minus vergence data set and a negative T value is for the vergence minus saccade data set (Plot B). Typical time series signal from the midbrain which has a correlation of 0.5 with the block design (square wave) (Plot C). Talairach Tournoux coordinates are: 7 R, 19 P and 15 I. Comparison of the percent signal change from baseline of the same time series signals from the saccade and vergence data sets within the midbrain (Plot D).

Table 3.4 Individual Subject Analysis of the Midbrain from the Vergence Data Set

Subject	Fixation vs. Random Vergence Task			
	X (mm)	**Y (mm)**	**Z (mm)**	**z-score**
1	6R	-24P	-10I	4.8
2	10R	-19P	-12I	2.6
3	12R	-24P	-6I	4.7
4	5R	-27P	3S	4.0
5	5R	-13P	-8I	4.2
6	8R	-22P	-5I	2.9
7	6R	-19P	-7I	3.5
8	6R	-10P	3S	3.8
Average ± Std	7R ± 3	-20P ± 6	-5I ± 6	3.8 ± 0.8

Table 3.5 highlights some specific, significant differences observed within the paired t-tests spatial maps shown in Figure 3.5 (identified via yellow arrows for the saccade data and red arrows for the vergence data) and Figure 3.7 (identified via the cross hairs). Table 3.5 summarizes the z-score of a specific Talairach-Tournoux location of activation within the frontal eye fields for saccades and vergence and the midbrain for the vergence data set. These specific Talairach-Tournoux locations highlight significant differences between the saccade and vergence data sets quantified via a two tailed positive or negative T value greater than 2.3.

Table 3.5 Saccade Minus Vergence Data Sets / Positive Paired T-Test and Vergence Minus Saccade Data Sets / Negative Paired t-Test Statistics Showing Differentiation between FEF and Midbrain in Comparing Fixation Versus Random Saccade and Vergence Tasks

Region	**Talairach -Tournoux Stereotactic Coordinates**			**z-score in Saccade Data set**	**z-score in Vergence Data set**	**Paired *t*- test T value**
	X (mm)	Y (mm)	Z (mm)			
FEF (Activity in Saccade data set)	-36L	-9P	50S	3.4	<1	2.7
	30R	-5P	48S	2.4	<1	2.4
FEF (Activity in Vergence data set)	-32L	6A	49S	<1	2.3	-2.3
	24R	2A	50S	<1	2.5	-2.3
Midbrain (Activity in Vergence Data set)	8R	-20P	-5I	<1	2.6	-4.3

3.4 Discussion

3.4.1 Significant Spatial Difference between Saccade and Vergence Data Sets

The activation within the frontal eye fields (FEF) showed significant spatial differences between the saccade and vergence data sets where the vergence activation was located directly anterior to the saccadic activation. The location of the FEF is located in the vicinity of the intersection of the precentral sulcus and the superior frontal sulcus [48, 102-105]. One human functional imaging study of vergence eye movements used positron emission tomography (PET) but did not observe any significant signals within the frontal lobe, which they attribute to a limitation of the PET instrumentation [106].

There are four non-human primate single cell electrophysiology studies that investigated the influence of disparity in FEF using symmetrical step stimuli [14], near and far targets [107], and smooth sinusoidal tracking stimuli [12, 108]. The first study of symmetrical steps is the most relevant to our present investigation because the visual stimuli are the same. When studying symmetrical vergence step stimuli in non-human primates, Gamlin and Yoon (2000) report differentiation within the FEF. Cells that encode for symmetrical vergence stimuli were located adjacent and anterior to cells that encoded for saccadic stimuli [14]. Most of these vergence cells (28 out of 34) did not significantly change their activity during conjugate (saccade or smooth pursuit) eye movements. They also tested monocular vision to determine whether the cells modulated their activity correlated with a motor signal rather than a sensory retinal disparity input. Their data support that these cells are “more closely related to the movement than to the retinal disparity of the target that elicited it” [14]. This study of functional activity in humans using fMRI support similar findings that the vergence activity to symmetrical

vergence steps within the FEF was located adjacent and significantly anterior to functional activity evoked using fixation versus random saccadic eye movements.

The other non-human electrophysiology studies of FEF are not as directly related to our present study. One reports that approximately two-thirds of the cells that traditionally modulate their activity during saccadic movements are broadly tuned for near or far disparity signals and hence these cells do carry information about depth [107]. The last two studies investigated smoothly moving targets in depth (smooth vergence movement) and within the frontal plane (smooth pursuit movement). Reviewing the two studies, the results showed that 63% to 66% of the neurons studied within the caudal portion of FEF encoded for both smooth pursuit and smooth vergence tracking signals, 21% to 25% encoded only smooth pursuit signals and 17% to 9% responded only during smooth vergence tracking [12, 108]. These three studies on FEF all tested different stimuli compared to the symmetrical step studied within our present investigation.

The midbrain within the brain stem has also been identified as a region that encodes specifically for vergence and projects directly to the oculomotor neurons [15, 50]. Three types of cells have been identified: vergence tonic cells (also called positioning encoding cells), vergence burst cells (also called velocity encoding cells), and burst-tonic cells. One study states “conjugate and vergence signals are generated independently and are combined at the extraocular motoneurons” [52]. This data support differentiation within the midbrain where functional activity was observed in the vergence data set but not in a similar location for the saccade data set. Some cellular differentiation between the saccade and vergence systems is expected. Patients with

internuclear ophthalmoplegia have a loss of saccadic or adduction movements but vergence or abduction movements are preserved [56, 109].

3.4.2 Shared Neural Sources between Saccade and Vergence Data Sets

Several behavioral studies discuss the nonlinear interaction between the saccadic and vergence systems [53-57]. Vision and Neural Engineering Laboratory of NJIT and other investigators have published that even when symmetrical vergence stimuli are presented to a subject, many of the responses contain saccades [70-72]. Similarly, studies have shown that with saccadic movement, a transient divergent and then convergent movement is observed [110, 111]. Therefore, it would be expected that the vergence and saccade oculomotor systems would share some neural resources. These results support many shared neural areas in terms of similar amplitudes and spatial extent of functional activity. Specifically, similar activity within the supplementary eye fields when comparing the vergence and saccade data sets was seen. For saccades, the SEF has been identified as an area involved in gain control [112], attention [113], and in the production of an error signal [103]. Activation was observed in SEF for both the fixation versus random eye movement tasks utilizing vergence or saccade responses which may be from high-level processes, as supported in other studies that may potentially influence both systems. The dorsolateral prefrontal cortex has been described as a brain region that supports attention, planning, spatial orientation and behavioral restraints [47, 114, 115]. Activation within the dorsolateral prefrontal cortex was also similar between the vergence and saccade data sets and may in part be activated from these higherlevel cognitive functions. The ventral lateral prefrontal cortex also showed similar areas of activation within this study. It has been implicated in working memory and task

switching [116, 117]. Both these cognitive functions were evoked to follow the experimental protocol within this study.

Both the anterior and posterior cingulates stimulated similar functional activity for fixation versus random eye movements utilizing saccade and vergence stimuli. Several studies of saccadic eye movements support that the anterior cingulate is involved in regulating error [118-121] where the execution of saccades within our study would also need to regulate an error signal. Similar studies for vergence are not available. The posterior cingulate cortex (PCC) has been suggested to be involved in visuospatial encoding and attention while studying saccadic movements from primates [122-124]. The saccadic and vergence activation within the PCC of this study may also in part be due to visuospatial encoding and attention.

Several studies support that the parietal lobe is involved in visual attention when studying saccadic eye movements [60-62]. Two recent papers studying hand reaching in depth support the hypothesis that a disparity signal is encoded within the parietal area [63, 64]. Functional imaging vision studies of humans support a disparity signal is present in the parietal lobe [31, 106, 125, 126] as do single cell recordings from primates [15, 16]. The present study supports that the parietal lobe is functionally active during both saccadic and vergence eye movements.

The cerebellum also showed similar activation behaviors between the saccadic and vergence data sets. Many studies from just the last two years support the concept that the cerebellum is involved in saccadic eye movements and is responsible for processing error that is used for motor learning [65-67]. The cerebellar vermis also participates in vergence eye movements as reported by dysfunctional vergence eye movements in

patients with lesions [127] and primate studies [20-22]. This data support the hypothesis that the cerebellum is involved in voluntary saccadic and vergence eye movements.

3.5 Conclusion

This study used a block design of fixation compared to a random eye movement task composed of steps to study the vergence system in comparison with the saccade system. Results show several shared neural resources between the vergence and saccade systems, specifically within the supplementary eye field, dorsolateral prefrontal cortex, ventral lateral prefrontal cortex, intraparietal area, cuneus, precuneus, the anterior and posterior cingulates, and cerebellar vermis. The results of specific aim 1 support that significant spatial differentiation exists within the frontal eye fields.

CHAPTER 4

THE ROLE OF THE POSTERIOR PARAHIPPOCAMPAL AREA IN A MEMORY-GUIDED VERGENCE TASK: AN fMRI STUDY (SPECIFIC AIM 3)

Purpose: Primate and human case investigations have emphasized the significant role of the parahippocampal area in working memory. To the best of our knowledge, there is no existing study that has implemented a memory-guided vergence task to validate the role of the parahippocampal area in memory function. This fMRI study aims: 1- to quantify the increases in the functional activity of the posterior parahippocampal area (PPHA) for three different experimental paradigms; and 2- to compare the relative correlation of the BOLD activity within the PPHA during the memory-guided vergence task (where specifically working memory is utilized) to the two other vergence experiments.

Methodology: There were three experimental paradigms utilized: random tracking versus fixation, predictable tracking versus random tracking, and performance of a memory-guided vergence task. MRI data were collected with a 3T scanner. A general linear model (GLM) was used to determine significantly active regions throughout the brain for each of the three vergence experiments. Further analysis focused on the PPHA by calculating the significance levels of the observed BOLD activity, quantifying BOLD signal percent change and the spatial extent of observed increases in functional activity in this area during each experimental paradigm.

Results: Functional activity of the PPHA was significantly increased for the memory-guided vergence experiment compared to two other visual task paradigms. The functional activity on the PPHA is statistically significant where F=3.53 for the left side

with coordinates -22L, -42P, -6I where $p < 0.05$ and $F=4.56$ for right side with coordinates 37R, -42P, -12I where $p<0.02$. Additionally, the Pearson correlation value was greater for the memory-guided vergence task for time course collected from the PPHA where $r = 0.65$. Average signal percent change was also quantified for both the PPHA for each vergence tasks. There was a significant percent change in the average signal from the voxels in the PPHA, [$F (2, 13) = 9.28$, $p < 0.005$]. Lastly, percent change of the functional activity was also quantified for the PPHA among experiments, [$F (2, 13) = 5.9$, $p<0.02$].

Conclusion: Significant increases in the functional activity of the PPHA were observed for memory-guided vergence task. To the best of our knowledge, this is the first fMRI study suggests that when utilization of working memory is required, the PPHA functions as one of the crucial regions for a vergence eye movement dependent memory task.

4.1 Introduction

Short term memory, also called working memory, is a cognitive function that maintains information that had been stored before but is unavailable in the current condition. The concept of working memory had been first introduced by Baddeley and Hitch, 1974 [128]. In their theory, working memory comprises three distinct control mechanisms on the conveyed information. The first component was the phonological rehearsal loop, which is involved in processing of verbal material; the second one was the visuospatial sketchpad which encodes visual and spatial information; and the third one was the central

executive, which functions as an attentional control system when planning, reasoning and comprehending [128-130].

The saccadic oculomotor system is a useful experimental model for studying working memory because it provides isolation and acquisition of information regarding visual cues while maintaining the information with an executive response [131]. Saccades are rapid version movements, commonly used during reading. The memory-guided saccade paradigm by Hikosaka and Wurtz [132] is an experimental stimulus paradigm whereby the subject is required to remember the location of saccadic targets. Memory-guided saccades have been extensively studied in animals [133], in people with neurological conditions [134] and in healthy controls [131, 135-137].

Based on the literature research there has been no investigation of memory-guided vergence eye movements using fMRI. In here, an experimental design is introduced with LED cues of 2°, 3° and 4° with combined sustained convergence demand and flashed "on" for both random tracking sequence in which the subject cannot predict the timing sequence or when the next target would be illuminated and the predictable tracking sequence in which the subject could potentially anticipate which target may be illuminated where the subjects were instructed to anticipate the next target. Then the last phase in which LEDs are completely "off" are initiated where it is needed to use the working memory for remembering sequence of illuminated targets that had been memorized in previous predictable phase.

The discovery of the working memory system and the elucidation of the roles of its neural components started with nonhuman models and continued with functional neuroimaging; these studies strongly emphasized the important roles of the posterior

parietal cortex (PPC), prefrontal cortex (PFC), frontal and supplementary eye fields [138-154].

Working memory literature also highlights the parahippocampal area as an underlying neural substrate. Encoding (or integrating) and maintenance (or enduring representations) of information and locations of objects in working memory are linked to the parahippocampal area [155, 156]. Studies done by Bohbot et al. indicated that the parahippocampal area was critical for the performance of a spatial memory tasks [157-159]. Lesion studies by Bohbot and colleagues reported that subjects with right parahippocampal lesion had more memory deficits [158, 160]. Additionally, another study by Prince and colleagues reported that the left parahippocampus is more sensitive for operations where encoding and retrieval is required whereas right parahippocampal area is more effective in encoding than in retrieval [161]. Object-based spatial coding in a virtual environment of 3D images also underscores the role of the left parahippocampal area. Schmidt and his colleagues showed that encoding and retrieval of changes in the point of views (PoV) is highly correlated with the activity of the left parahippocampal area which can be viewed as evidence for the significant contributions of this region to the spatial scene memory and object centered (allocentric) coding [162].

Thus, the purpose of this study is to use fMRI to quantify the amount of functional activity observed in the PPHA for memory-guided vergence movements (working memory is required to remember the predictable locations of the illuminated LED binocular depth targets). Here, it is hypothesized that the memory-guided vergence movements will require more involvement of the PPHA via, as evinced by an increasing the percentage of functional activity (measured with fMRI) when it is compared to the

two other experimental paradigms which were random versus fixation and prediction versus random.

4.2 Methodology

4.2.1 Subjects

The New Jersey Institute of Technology (NJIT) and University of Medicine and Dentistry of New Jersey (UMDNJ) Institution Review Board (IRB) approved this study. All subjects signed written informed consent forms approved by the NJIT and UMDNJ IRB in accordance with the Declaration of Helsinki. Six subjects participated in this study (2 female and 4 male with a mean age of 26 ± 4 years). Each subject's near point of convergence (NPC) was measured by having an examiner slowly bring the tip of a pen towards the subject along her/his midline [68]. When the subject could no longer maintain fusion, the distance from the subject's orbit to the pen tip was recorded in cm as the NPC. The NPC was measured twice and averaged. All subjects had a normal near point of convergence (NPC) of less than 6 cm. Binocular vision was assessed by the Randot Stereopsis Test (Bernell Corp., South Bend, IN, USA). All subjects had normal binocular vision defined as better than 70 seconds of arc.

4.2.2 Materials and Apparatus

Images were acquired using a 3.0 Tesla Siemens Allegra MRI scanner with a standard head coil (Erlangen, Germany). Visual stimuli were a set of non-ferrous light emitting diode (LED) targets that formed a line 5 cm in height by 2 mm in width located at three positions.

4.2.3 Imaging Instrumentation and Procedure

All functional scans used a T2* weighted echo planar imaging (EPI) sequence. The imaging parameters were field of view (FOV) = 220 mm, 64 x 64 matrix, time of repetition (TR) = 2000 ms, time of echo (TE) = 27 ms and flip angle = 90°. The whole brain was imaged in an axial configuration where 32 slices were collected and each slice was 5 mm thick. The resolution was 3.4 x 3.4 x 5 mm. After all functional tasks, a high resolution MPRAGE (magnetization-prepared rapid gradient-echo) data set was collected. The MPRAGE imaging parameters were: 80 slices, FOV = 220 mm, slice thickness = 2 mm, TR = 2000 msec, TE = 4.38 msec, T1 = 900 msec, flip angle = 8 º and matrix = 256 x 256 which resulted in a spatial resolution of 0.9 x 0.9 x 2 mm.

The subject was positioned supine on the gantry of the scanner with his head along the midline of the coil. All participants were instructed to limit head motion. Foam padding was used to restrict additional movement and motion correction software described below was utilized to ensure head motion did not influence the results. Ear plugs were used to reduce scanner noise by up to 30 dB while still allowing the participant to hear instructions from the operators to ensure communication during the scan. In all experiments, the radio frequency power deposition and field-switching rate were kept below levels specified by the U.S. Food and Drug Administration (FDA).

4.2.4 Functional Experimental Design

Vergence stimulation with LED cues was used during scanning. Orientation aligned with the subject's midline and the spacing between visual targets was adjusted to stimulate 2°, 3° and 4° of combined sustained convergence demand as shown in Figure 4.1 image A.

Experiments took place in a darkened room where the subject only saw the visual stimulus. 2°, 3° and 4° were fixation points centered along the subject's midline (as detailed above) before to produce symmetrical vergence stimuli. The maximum vergence stimulus was 2° disparity change which was chosen due to the physical constraints of the imaging center and to decrease the co-occurrence of saccades with the symmetrical vergence response [70-72].

Three types of experiments were performed. Full descriptions of two of the experimental paradigms (fixation versus random tracking and predictable tracking versus random tracking) can be found in previous sections of this dissertation [31, 32]. The third task paradigm, memory-guided vergence, started with random tracking of binocular disparity cues and was followed by predictable tracking pattern of the targets, and at the last phase LED targets turned off and vergence eye movements expected from participants to the remembered locations of the cues which had been memorized in the predictable phase. The block design and the patterns of the stimulus position can be observed in Figure 4.1, image B. The duration of each phase was 20 seconds for memory guided vergence experiment. A total of three vergence experimental trials were collected for each type of experiments in case head motion was a problem which was not the case within this data set. All experiments are listed in Table 4.1.

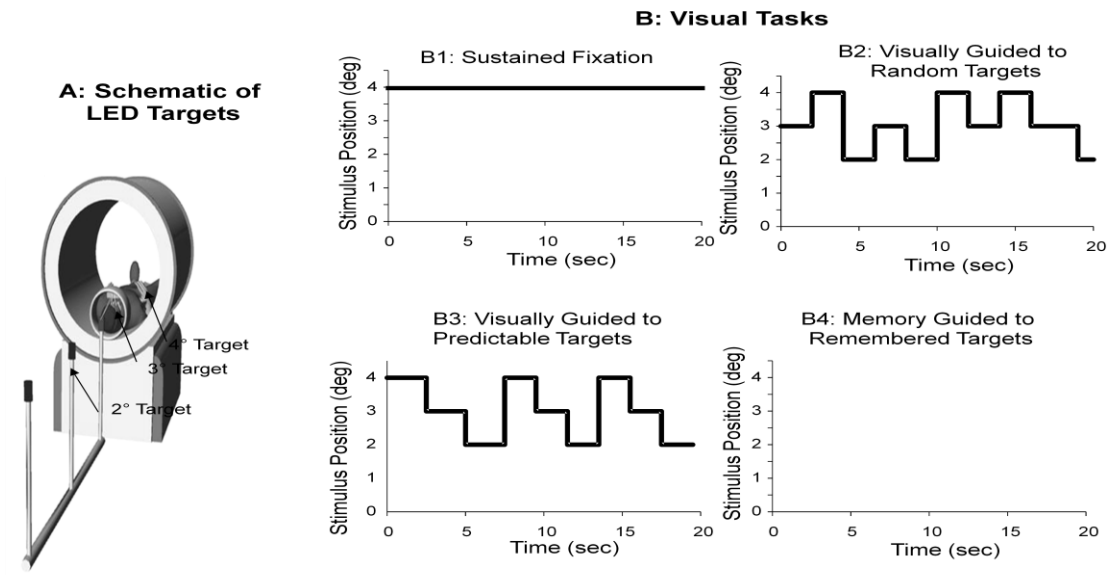

Figure 4.1 Experimental set-up and design. The schematic of the custom fMRI compatible light emitting diodes (LEDs) for the memory-guided vergence experimental paradigm. Subjects would started with random tracking on either the midline target during the experiment for 20 seconds and then predictable tracking initiated for 20 seconds (plot B2), last phase was when LEDs were off, vergence movements expected to the memorized target locations.

Table 4.1 A Schematic of Experimental Paradigms Applied

Experiment Number	Eye Movement Type	Visual Stimulus Target Type	Experimental Pattern
1	Vergence	LED targets	Sustained Fixation vs. Random Tracking (B1 vs. B2)
2	Vergence	LED targets	Predictable Tracking vs. Random Tracking (B2 vs B3)
3	Vergence	LED targets	Random Tracking vs. Predictable Tracking vs. Off (B2 vs B3 vs B4)

4.2.5 Data Analysis

4.2.5.1 Individual Subject Analysis using a Data Driven Reference Vector. As previously discussed in Chapter 3 in detail, data were analyzed with AFNI (Analysis of Functional NeuroImages) software [73]. All the scans were first registered, secondly, motion corrected, then the standardized Talairach-Tournoux coordinate space

transformation is applied to the individual anatomical and functional brain maps [75]. Probabilistic ICA available through the MELODIC (Multivariate Exploratory Linear Optimized Decomposition into Independent Components) software from FSL was used to calculate the independent signal sources [91]. The signal source that had the greatest Pearson correlation coefficient with the experimental block design was used a reference vector used to correlate each voxel within our data set during an individual subject analysis. Representative examples of typical source vectors for each conducted vergence experiment are shown in Figure 4.2. Using a general linear model (GLM) method, each voxel of the entire brain was correlated with a hemodynamic model calculated using independent component analysis, only data that attained a minimum threshold of functional activity corresponding to a z-score of 2.0 (two tail p = 0.05) were further analyzed.

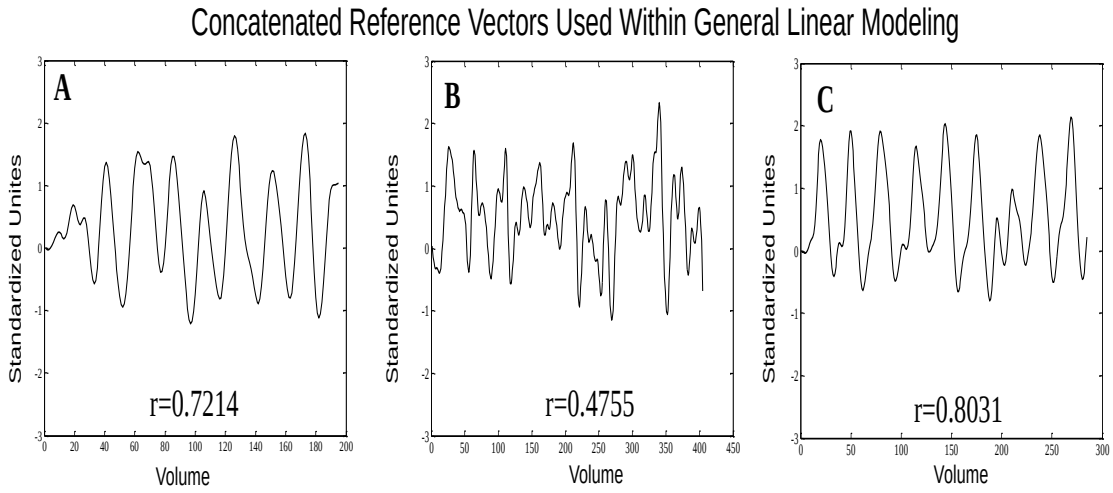

Figure 4.2 Typical reference vectors from one subject from each conducted experiments The source signals have a high Pearson correlation coefficient for A (exp#1-Table 4.1) r = 0.7214; B (exp#2-Table 4.1) r = 0.4755; C (exp#3-Table 4.1) r = 0.8031.

4.2.5.2 Group Analysis. In addition to individual analysis, group analyses were performed as well. To facilitate comparison between the conducted experiments the

individual subject spatial maps were averaged together in standard space. Similar regions had been reported in our previous studies, except PPHA [31, 32].

4.2.5.3 Regions of Interest. In specific aim 1 (Chapter 3), it is reported that shared neural substrates within the frontal eye fields (FEF), the supplementary eye field (SEF), the dorsolateral prefrontal cortex (DLPFC), ventral lateral prefrontal cortex, lateral intraparietal area, cuneus, precuneus, anterior and posterior cingulates, cerebellar vermis with the comparison to the saccadic system and the spatial differentiation observed within the frontal eye fields and midbrain regions only for the vergence system [32]. While activity within these regions of interest (ROIs) is analyzed in this current study, however, here the main ROI was parahippocampal area because of the known but previously unstudied involvement of memory-guided vergence experiment. The parahippocampal cortex is part of medial temporal lobe with the border to the collateral sulcus, and located posterior to the entorhinal and perirhinal cortex [157]. The functional activity observed on this region and its bilateral spatial extent were further investigated corresponding with our new experimental paradigm while comparing to our other conducted experiments.

4.2.5.4 Statistical Analysis. As covered in Chapter 3, the combination of the individual voxel probability threshold and the cluster size threshold (11 voxels rounded to a volume of 650 mm3 for our data set) yielded the equivalent of a whole-brain corrected for multiple comparison significance level of $\alpha < 0.001$. The cluster size was determined using the AFNI AlphaSim program [97]. The simulation used 10,000 Monte Carlo iterations, assumed a cluster connection of the nearest neighbor, voxel dimension of 3.4 x 3.4 x 5 mm and sought a significance level of 0.001. Hence, a cluster size of 650 mm3 or

greater corresponded to $p < 0.001$ corrected for multiple comparisons. The functional data are displayed as a z-score shown in the figure scale bar. Individual maps of t-statistics were smoothed with a Gaussian kernel of 6 mm full-width and half-maximum to account for inter-individual anatomical variation [98-100].

The 3DANOVA function [163] was applied to test the statistical significance of any changes observed in the spatial extent change in the PPHA across the three different experiments. One subject's time series signals from the PPHA had been assessed for conducted experiments via obtaining their Pearson correlation values with the experimental block design. In addition, the signal percent change averaged across voxels in the PPHA was calculated for each experimental task. Twelve signals from same coordinates for each subject for each experiment were collected. Calculation of signal percent change was done by the steps as listed here; 1- collecting time series for each subject from PPHA for each experimental paradigm, 2- sorting the values of the time series from lower to higher, 3) taking the mean of time series, 4- calculating mean of the first five and last five values belong timeseries, 5- calculating the difference between first five and last five, 6- dividing of the difference to the mean of the time series, 7- averaging of values obtained from step 6 , 8- multiplying by 100 to get the final value. Furthermore, the PPHA region in this study was defined by the mask created by Kennedy and colleagues [164] in order to calculate percent change of functional activity through experiments by a custom MATLAB^{TM} code for the PPHA. The number of voxels in this mask was eighty-nine. The PPHA mask can be seen in Figure 4.3. One- way repeated measures ANOVA by using STATVIEW (5th version, SAS Institute Inc, 1998, Cary, NC, USA) is implemented on the values of both signal percent change and the values

acquired from calculation of percent change of functional activity from the common PPHA mask applied.

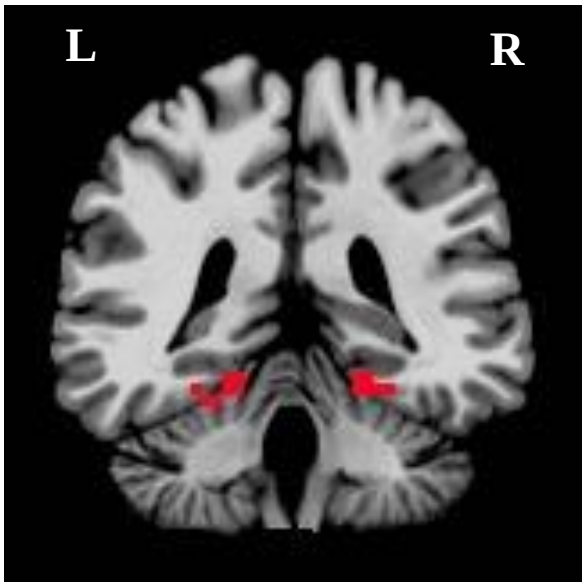

Figure 4.3 Posterior Parahippocampal area (PPHA) mask created by Kennedy and colleagues [164].

4.3 Results

Data were initially analyzed individually to determine how many of the six subjects showed activation in a given anatomical location. Only areas that showed significant activation for all subjects are included in the results. The averaged and thresholded group functional activity obtained from the PPHA for the six subjects performing fixation versus random tracking, prediction versus random tracking and memory-guided vergence oculomotor tasks are shown in Figure 4.4. Figure 4.4 shows from lower to higher coronal slices displaying the anatomy of persistent functional activity on the PPHA. Table 4.2 lists the peak activation (z-score value) with Talairach-Tournoux coordinates and Brodmann Area (BA) for a given anatomical location of the averaged subject data set for the fixation versus random tracking experiment; Tables 4.3 and 4.4 show analogous data

for the prediction versus random tracking and memory-guided vergence oculomotor tasks, respectively. Functional activity for non-PPHA areas [31, 32] such as the frontal eye fields, supplementary eye fields, inferior ventral lateral prefrontal cortex, parietal eye field, cuneus, precuneus, superior parietal area, posterior cingulate, cerebellar vermis, midbrain for the different group of subjects was already reported. Therefore, no further analysis was conducted on these areas except reporting their z-score and BA coordinates.

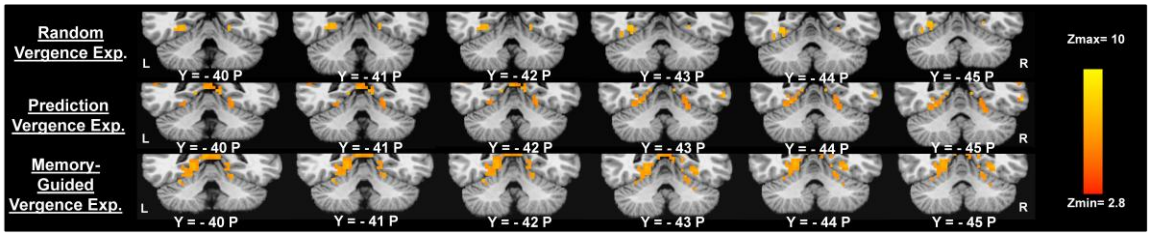

Figure 4.4 Coronal images showing functional activity of the PPHA from lower to higher slices for each our experiments that had been applied. Data are overlaid onto a standardized Talairach-Tournoux normalized image.

Table 4.2 Average Peak Activation of the Fixation Versus Random Vergence Oculomotor Task in Talairach-Tournoux Coordinates with the Level of Significance Denoted as a z-Score. for the x Axis: Positive is Right (R) and Negative is Left (L); for the y Axis: Negative is Posterior (P) and Positive is Anterior (A); and for the z Axis: Positive is Superior (S) and Negative is Inferior (I)

Regions for Fixation versus Random Tracking Exp.	**Brodmann Area**	**X (mm)**	**Y (mm)**	**Z (mm)**	**z-score**
Frontal Eye Field, Superior Middle Frontal Gyrus, Precentral Gyrus	8/6	-43L	4A	39S	5.68
	8/6	39R	5A	40S	3.99
Supplementary Eye Field, Medial Frontal Gyrus	6	-6L	4A	48S	4.67
		5R	5A	47S	5.4
Dorsolateral Prefrontal Cortex	9	-48L	4A	32S	5.37
		43R	6A	34S	4.12
Anterior Cingulate/ Cingulate Gyrus	24/32	-7L	5A	38S	4.32
		5R	6A	40S	3.73
Inferior Ventral Lateral Prefrontal Cortex, Inferior Frontal Gyrus, precentral Gyrus	45/47	-48L	11A	3S	4.46
		43R	10A	2S	3.99
Parietal Eye Field Inferior Parietal Area	40	-33L	-56P	45S	4.6
		34R	-53P	44S	5.4
Cuneus, Lingual Gyrus	17/18	-13L	-91P	-2I	8.24
		9R	-91P	-5I	8.92
Precuneus	7	-12L	-77P	41S	4.81
		10R	-75P	43S	4.53
Superior Parietal Area	7	-34L	-50P	48S	4.87
		33R	-52P	49S	4.92
Posterior Cingulate	31	-6L	-66P	18S	4.8
		9R	-66P	18S	4.2
	30	-10L	-68P	6S	5.38
		9R	-71P	9S	5.54
	29	-11L	-55P	2S	4.97
		7R	-56P	-1I	5.24
Cerebellar Vermis IV/V		-3L	-37P	5S	4.32
Midbrain		7R	-25P	-6I	3.29
Parahippocampal area		-21L	-45P	-7I	5.75
		23R	-46P	-10I	5.66

Table 4.3 Average Peak Activation of the Random Tracking Versus Predictable Tracking Vergence Oculomotor Task in Talairach-Tournoux Coordinates with the Level of Significance Denoted as a z-Score. For the x Axis: Positive is Right (R) and Negative is Left (L); for the y Axis: Negative is Posterior (P) and Positive is Anterior (A); and for the z Axis: positive is Superior (S) and negative is Inferior (I)

Regions for Predictable versus Random Tracking Exp.	**Brodmann Area**	**X (mm)**	**Y (mm)**	**Z (mm)**	**z-score**
Frontal Eye Field, Superior Middle Frontal Gyrus, Precentral Gyrus	8/6	-39L	4A	45S	9.54
	8/6	39R	12A	39S	8.9
Supplementary Eye Field, Medial Frontal Gyrus	6	-7L	5A	48S	7.17
		5R	5A	49S	8.33
Dorsolateral Prefrontal Cortex	9	-48L	10A	33S	9.17
		42R	15A	31S	7.75
Anterior Cingulate/ Cingulate Gyrus	24/32	-5L	14A	39S	8.22
		4R	10A	39S	7.79
Inferior Ventral Lateral Prefrontal Cortex, Inferior Frontal Gyrus, precentral Gyrus	45/47	-42L	22A	6S	8.79
		42R	21A	7S	8.79
Parietal Eye Field Inferior Parietal Area	40	-34L	-45P	49S	7.21
		34R	-42P	48S	6.51
Cuneus, Lingual Gyrus	17/18	-7L	-60P	5S	8
		7R	-88P	5S	7.86
Precuneus	7	-6L	-65P	46S	7.48
		7R	-66P	46S	8.2
Superior Parietal Area	7	-34L	-61P	48S	7.29
		36R	-59P	47S	7.5
Posterior Cingulate	31	-7L	-67P	19S	6.44
		10R	-66P	21S	6.28
	30	-11L	-59P	7S	7.19
		11R	-58P	5S	7.35
	29	-5L	-50P	10S	7.06
		4R	-47P	9S	6.84
Cerebellar Vermis IV/V		-3L	-44P	3S	7.33
Midbrain		-3L	-23P	-6I	6.28
Parahippocampal area		-19L	-41P	-6I	6.51
		19R	-45P	-5I	7.37

Table 4.4 Average Peak Activation of the Memory-Guided Vergence Oculomotor Task in Talairach-Tournoux Coordinates with the Level of Significance Denoted as a z-Score. For the x Axis: Positive is Right (R) and Negative is Left (L); for the y Axis: Negative is Posterior (P) and Positive is Anterior (A); and for the z Axis: Positive is Superior (S) and Negative is Inferior (I)

Regions for Memory Guided Vergence Exp.	Brodmann Area	X (mm)	Y (mm)	Z (mm)	z-score
Frontal Eye Field, Superior Middle Frontal Gyrus, Precentral Gyrus	8/6	-39L	5A	43S	6.85
	8/6	32R	6A	46S	5.86
Supplementary Eye Field, Medial Frontal Gyrus	6	-7L	8A	47S	6.17
		5R	9A	50S	5.93
Dorsolateral Prefrontal Cortex	9	-43L	20A	32S	6.3
		39R	16A	34S	5.66
Anterior Cingulate/ Cingulate Gyrus	24/32	-7L	18A	37S	6.23
		6R	16A	40S	5.34
Inferior Ventral Lateral Prefrontal Cortex, Inferior Frontal Gyrus, precentral Gyrus	45/47	-42L	22A	0	5.93
		40R	21A	1S	5.33
Parietal Eye Field Inferior Parietal Area	40	-43L	-40P	47S	5.8
		42R	-39P	41S	5.51
Cuneus, Lingual Gyrus	17/18	-6L	-86P	-1I	9.06
		3R	-87P	1S	8.68
Precuneus	7	-14L	-63P	45S	7.29
		12R	-62P	44S	7.25
Superior Parietal Area	7	-27L	-58P	45S	5.44
		28R	-57P	49S	6.85
Posterior Cingulate	31	-8L	-68P	19S	6.85
		5R	-64L	24S	7.55
	30	-11L	-61P	10S	7.14
		8R	-64L	10S	6.17
	29	-6L	-42P	11S	5.59
		7R	-43P	9S	5.13
Cerebellar Vermis IV/V		-3L	-42P	3S	5.24
Midbrain		-5L	-24P	-6I	4.57
Parahippocampal area		-22L	-43P	-8I	6.56
		26R	-48L	-7I	6.69

ANOVA demonstrates that the functional differentiation on the PPHA is statistically significant, where F=3.53 for the left side with coordinates -22L, -42P, -6I, $p < 0.05$ and F=4.56 for the right side with coordinates 37R, -42P, -12I where $p<0.02$ shown in Figure 4.5 and Table 4.5. Table 4.5 provides information of Talairach-Tournoux coordinates and observed peak activation (z-score value) across all experiments, respectively.

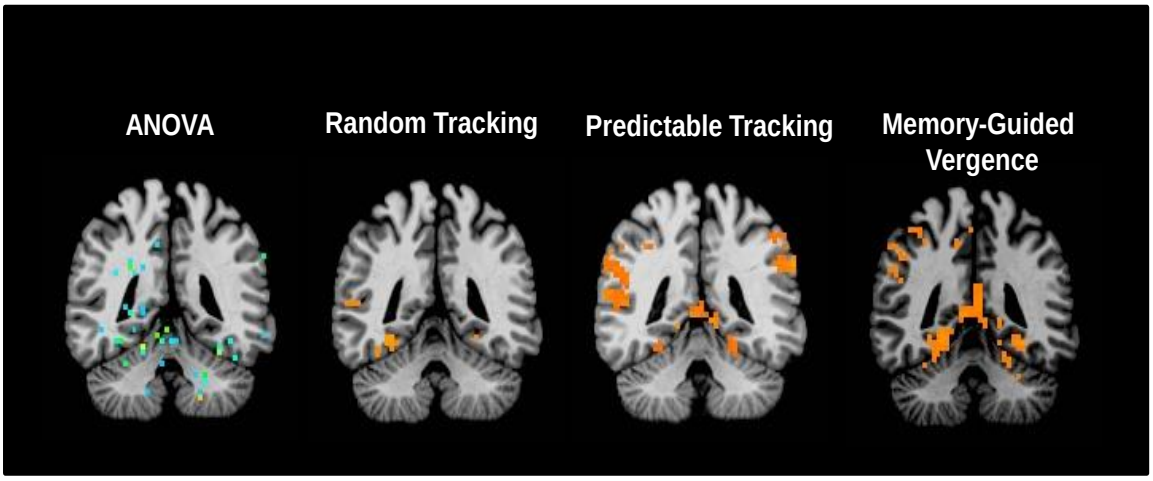

Figure 4.5 3DANOVA [163] result for our experiments which shows the observed functional activity on posterior parahippocampal area is significantly active. F=3.53 for left side with coordinates -22L, -42P, -6I, $p < 0.05$ and F=4.56 for right side with coordinates 37R, -42P, -12I where $p<0.02$.

Table 4.5 Talairach-Tournoux Coordinates with the Level of Significance Denoted as a z-Score for Anova and across All Experiments. For the x Axis: Positive is Right (R) and Negative is Left (L); for the y Axis: Negative is Posterior (P) and Positive is Anterior (A); and for the z Axis: Positive is Superior (S) and Negative is Inferior (I)

Anova and Experiments	**Talairach -Tournoux Stereotactic Coordinates**			**z-score**
	X (mm)	Y (mm)	Z (mm)	
ANOVA	-22L	-42P	-6I	3.53
	37R	-42P	-12I	4.56
Random Tracking	-22L	-43P	-5I	<1
	32R	-43P	-12I	<1
Predictable Tracking	-21L	-41P	-5I	2.38
	37R	-42P	-12I	2.4
Memory-Guided Vergence	-21L	-41P	-5I	3.95
	32R	-43P	-11I	4.3

One subject's typical time series signals from the PPHA (Talairach-Tournoux location -21 L -47 P -1I) for each conducted experimental task are shown in Figure 4.6. The Pearson correlation coefficients between the experimental block design and filtered time series of the random tracking vergence task (r = 0.1), predictable tracking vergence task (r = 0.2) and memory-guided vergence task (r = 0.65) are shown, respectively, in panels A, B and C of Figure 4.6. The time series for the memory-guided vergence experimental task are much more highly correlated with the block design than those of other two experimental paradigms.

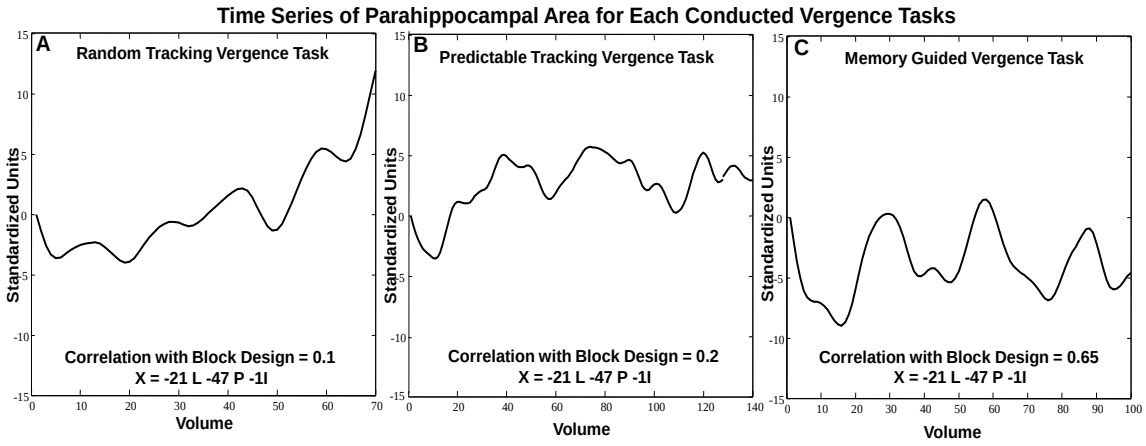

Figure 4.6 One subject's typical time series signal from the PPHA for each conducted experimental tasks are shown above. Time courses obtained are from Talairach-Tournoux location -21 L -47 P -1I within the PPHA for each experiment.

In addition, BOLD signal percent changes from baseline for the PPHA were averaged across the group for each experiment and compared. Application of the repeated measures of ANOVA shows that the PPHA has greater and statistically significant signal percent change [F (2, 13) = 9.28, $p < 0.005$] as shown in Figure 4.7.

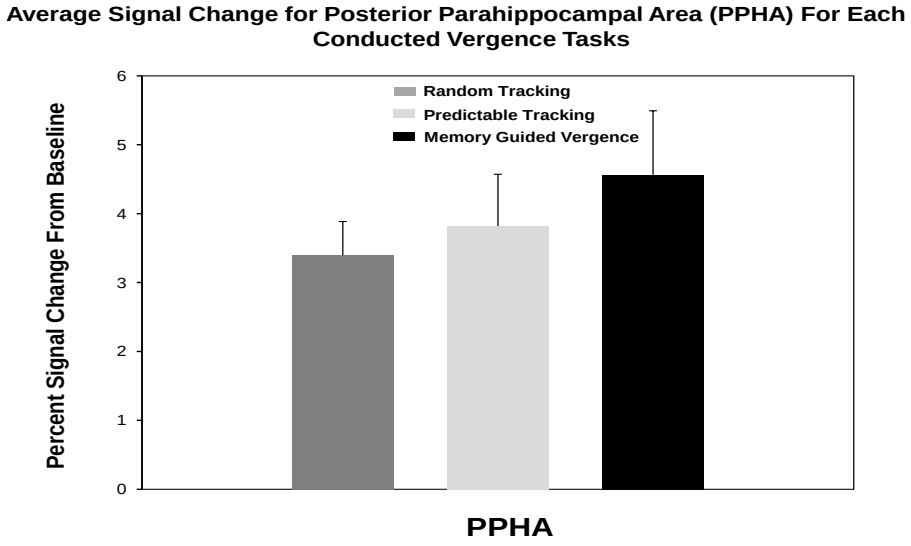

Figure 4.7 Group level average signal change obtained from collected time courses from PPHA for each applied experiments. PPHA has greater and statistically significant signal percent change [F (2, 13) = 9.28, $p < 0.005$] for conducted vergence tasks.

Finally, the PPHA mask [164] was applied to the three task data sets for each subject, as can be seen in Figure 4.3 , and the percent change of the spatial extent within the PPHA mask was calculated. Individual results were input into the repeated measures of ANOVA, which also indicated statistical difference occurs across all the experiments where [F (2, 13) = 5.9, p<0.02]. Results from the repeated measures of ANOVA are shown Figure 4.8. Additionally, Post hoc analysis showed significant difference within the group of conducted vergence experiments where p<0.03 for random tracking versus fixation and memory-guided vergence. For the future step, this investigation needs larger group of subjects for the statistical distinction between the predictable tracking versus and random tracking and memory-guided vergence experiments.

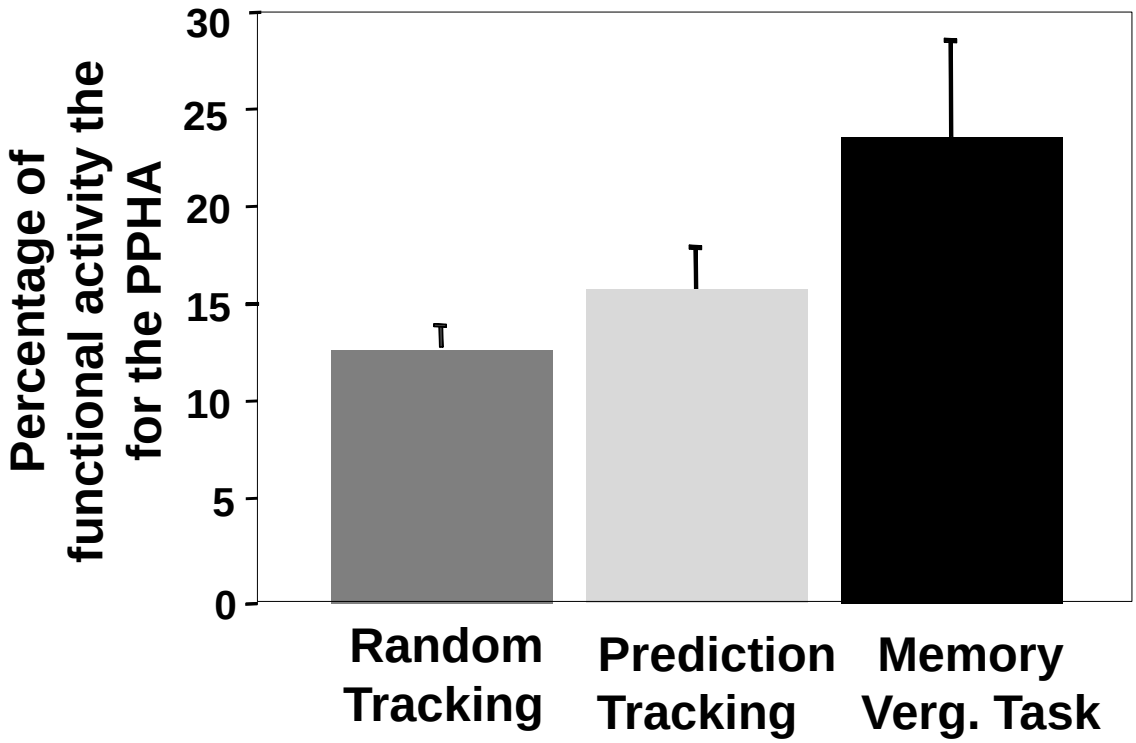

Figure 4.8 The repeated measures of ANOVA where [F (2, 13) = 5.9, p<0.02] for quantification of percent change of the functional activity for the PPHA.

4.4 Discussion

4.4.1 Overview

In this study, it has been investigated relative contributions of the PPHA when performing three different vergence experiments. Random versus fixation tracking and predictable versus random vergence tasks showed less functional activation compared to the memory-guided vergence task within the PPHA. The PPHA-based analysis had been implemented via different methods. Functional activity differences in the degree of activation in the PPHA among the three oculomotor tasks were observed using GLM. Then, comparison of time courses with the block design had been applied among vergence tasks which had been collected from same coordinates. Average signal percent change from baseline had been also calculated for PPHA, again for each our experimental paradigms. As a next step, a standard PPHA mask [164] was utilized for quantifying the relative fractions of functional activity within this ROI among vergence experiments. Finally, statistical significance of percent change of functional activity was tested by repeated measured of ANOVA was tested and Post hoc analysis across and within the vergence experiments.

4.4.2 Characteristics of Parahippocampal Area

In this investigation, as shown in results, the PPHA increases its functional involvement via enlargement of the spatial extent when the memory-guided vergence task was applied. This might be due to the cortical-parahippocampal interactions and /or neuronal characteristics of the parahippocampal area to succeed at the memory-guided oculomotor task that had been applied.

A plethora of neurophysiological investigations have shown the role of parahippocampal area involved in memory function in the levels of topographic and laminar organizations. For example, Suzuki and Amiral investigated reciprocal projections of the topographic and laminar organization between the entorhinal cortex and the perirhinal and the parahippocampal cortices [165]. One of the main finding in this primate study was to define the type of projections involved. There is a feedforward projection from perirhinal and parahippocampal cortices and a feedback projection occurs from the entorhinal cortex to the perirhinal and parahippocampal cortices. Additionally, some other investigations indicated that sensory information is also relayed from and to hippocampal formation by the entorhinal, perirhinal and parahippocampal cortices in monkeys [166-169]. In combination with results of this present study, this suggests that in humans as well; the PPHA might play a role of relay center to convey information regarding applied memory-guided task.

Sato and colleagues explored visual response properties of neurons in the parahippocampal area of the monkey brain. They found that the features of these neurons can be classified as conveying motion signals, eye-position dependent activity. They indicated in their study neurons on parahippocampal cortex was involved in spatial and object processing, on the other hand, they also linked the results of this study, considering parahippocampal cortex as polymodal area which receives sensory information from other visual, auditory, and somatosensory regions. Another study by Blatt and colleagues supports that in a primate study also by showing existence of visual responsive neurons, auditory responsive neurons or bimodal auditory/visual-responsive neurons, and somatosensory-responsive neurons at the subregions of parahippocampal gyrus which

they also defined parahippocampal gyrus as a polymodal area where memory related unimodal or multimodal sensory information occurs [165, 170-173]. Depending on the aforementioned primate studies, observed functional activity in PPHA across all the vergence experiments might be related to the types of neurons that the PPHA includes. Further investigations and more subjects are needed to characterize and/or define properties of neurons in the PPHA.

4.4.3 Object Processing and Parahippocampal Area

The significant increases in the spatial extent of the functional activation in parahippocampal area observed in the memory-guided oculomotor task compared to the other vergence tasks might be associated with encoding, maintaining and retrieving of information regarding visual stimulus. The spatial extension and quantification of significance level of functional activity for a memory-guided vergence task can lead to explore the role of parahippocampal area beside to prefrontal, frontal and parietal regional activations observed in this present study and other investigations [137, 138, 174-178]. Luck and colleagues observed activation of right parahippocampal gyrus for encoding and maintenance of bound information in working memory. This fMRI study shows that parahippocampal gyrus as a subregion of medial temporal lobe contributes to the integration of information in working memory [155]. Oh and colleagues investigated via fMRI whether there exists any classification of neural activity on cortical regions observed with respect to processing of visual representations in working memory or not. They found that the control of selection of visual information in working memory recruits parahippocampal gyrus beside to the frontal, visual association, and subcortical regions [179]. A PET study by Owen and colleagues showed that regional cerebral blood flow

increases in the right parahippocampal gyrus when subjects retrieving of information related to location of an object. They suggest that parahippocampal area might be a locus where spatial and contexture features of a visual stimulus are fused to form representations in the working memory [180].

4.5 Conclusion

This study used three different oculomotor experimental paradigms; random tracking versus fixation, predictable tracking versus random tracking and memory guided vergence task. Results show the PPHA is highly recruited for memory guided vergence task compared to our other experimental paradigms. These results support that working memory is evoked by a memory guided oculomotor task requires involvement of parahippocampal area via increasing spatial extent of functional activity.

CHAPTER 5

THE IMPACT OF HIGHER COGNITIVE DEMAND ON INTERCONNECTIVITY ASSESSED USING VERGENCE TASKS AND GRANGER CAUSALITY ANALYSIS (SPECIFIC AIM 3)

Purpose: In this present investigation, aforamentioned fMRI studies that had been conducted on vergence system using standard general linear modeling (GLM) and independent component analysis (ICA) will be extended by utilizing Granger causality analysis (GCA). With this latter method, interregional interactions among selected regions of interest (ROIs) and how much these interactions changes depending on the task, including a cognitive function like prediction will be addressed.

Methodology: Two experimental paradigms of vergence eye movements were used: random tracking versus fixation and predictable tracking versus random tracking. MRI data were collected with a 3T scanner. Significantly active regions for two vergence experiments were first determined by GLM. The strength and directionality of interactions among relevant ROIs was then investigated with GCA, a statistical technique used for estimating the degree to which the time series of one ROI significantly influences or is "connected" to another. Statistical pair-wise Student t-tests were performed on each ROI causal interaction pair, using a subject level Granger Causality Matrix (GCM) for comparison of vergence tasks. Binomial significance testing was also applied in order to compare the number of influences between the visual tasks.

Results: Statistically significant ($p < 0.05$) mean causality activation maps showed a greater number of causal interactions occuring when prediction was evoked in the

visual task. Additionally, differences of causal directionality between ROIs for both visual tasks were shown via pair-wise Student t-test. Binomial significance tests on the number of influences between experimental paradigms also suggest that there is a statistical significance between the experimental paradigms, $p < 0.0001$.

Conclusion: Anticipatory behavior in predictable tracking vergence movement requires more cognitive demand than simple random tracking vergence. This increase in demand not only affects characteristics of the eye movement responses but also induces variations in the number of Granger causal connections.

5.1 Introduction

Vision processing is a complex task comprising interactions of several brain areas. Vergence eye movements are recruited for accurate and quick visual information. As mentioned previously, primate studuies show that the cortical regions like frontal eye fields (FEF) and lateral intraparietal cortex of the parietal area [14, 15] and subcortical areas of the brain like midbrain of the brainstem and oculomotor nucleus of the cerebellum [18, 49-52] are some regions that have distinct disparity tuning cells. Moreover, fMRI investigations supported primate studies by showing the neural substrates of vergence are localized within the frontal eye fields and midbrain.

fMRI investigations are useful in estimating what cortical and/or subcortical areas of the brain are active during the performance of tasks. Conventional general linear model (GLM) analysis [38, 181, 182] and independent component analysis (ICA) [37, 39, 183, 184] have been shown to be robust statistical methods for studying connectivity within brain regions within fMRI data. However, while these methods have been widely applied to select regions of co-activation within fMRI studies, they are unable to show

directionality between the interacting regions, which is needed for fuller understanding of brain connectivity during these tasks.

For this kind of investigation, it is possible to use Granger Causality Analysis (GCA) [185]. GCA is a multivariate, data-driven and time-dependent statistical technique which has been used to assess directional connectivity between selected regions of interest (ROIs) across the brain [186, 187]. For example, GCA has been implemented in studies of visuospatial imagery [188], visuospatial judgment [189, 190], brain-behavior relationships [191, 192], motor response tasks [193, 194], cognitive set-shifting [195].

In this study, GCA is used as a tool to detect causal relationships for visual experimental designs. The goal of the research presented here is to shed light on the dynamical Granger causal relationships for simple tracking and a more cognitively demanding visual tasks, in order to 1) compute the directionality of influences for selected ROIs; and 2) compare differences between the number of directed influences or "(Granger-)causal connections" between vergence tasks.

5.2 Methodology

5.2.1 Subjects

The New Jersey Institute of Technology (NJIT) and University of Medicine and Dentistry of New Jersey (UMDNJ) Institution Review Board (IRB) approved this study. All subjects signed written informed consent forms approved by the NJIT and UMDNJ IRB in accordance with the Declaration of Helsinki.

Fifteen subjects participated in this study (8 female and 7 male with a mean age of 27±3 years). Fifteen subjects' near point of convergence (NPC) was measured by having

an examiner slowly bring the tip of a pen towards the subject along her/his midline [68]. When the subject could no longer maintain fusion, the distance from the subject's orbit to the pen tip was recorded in cm as the NPC. The NPC was measured twice and averaged. All subjects had a normal near point of convergence (NPC) of less than 6 cm. Binocular vision was assessed by the Randot Stereopsis Test (Bernell Corp., South Bend, IN, USA). All subjects had normal binocular vision defined as better than 70 seconds of arc.

5.2.2 Material and Apparatus

Images were acquired using a 3.0 Tesla Siemens Allegra MRI scanner with a standard head coil (Erlangen, Germany). Visual stimuli were a set of non-ferrous light emitting diode (LED) targets that formed a line 5 cm in height by 2 mm in width located at three positions.

Eye movements were recorded using an infrared (λ = 950 nm) limbus tracking system manufactured by Skalar Iris (model 6500, Delft, Netherlands). All of the eye movements were within the linear range of the system ($\pm 25^{o}$). The left-eye and right-eye responses were calibrated, recorded and saved separately for offline analysis. A custom Matlab (Waltham, MA, USA) program was used for offline eye movement data analysis. Blinks were identified by the saturation of signal and manually omitted from the eye movement traces.

5.2.3 Imaging Instrumentation and Procedure

The subject was positioned supine on the gantry of the scanner with his/her head along the midline of the coil. All participants were instructed to limit head motion. Foam padding was used to restrict additional movement and motion correction software

described below was utilized to ensure head motion artifacts were minimal. Ear plugs were used to reduce scanner noise by up to 30 dB while still allowing the participant to hear instructions from the operators during the scan. In all experiments, the radio frequency power deposition and field-switching rate were kept below levels specified by the U.S. Food and Drug Administration (FDA).

All functional scans used a T2* weighted echo planar imaging (EPI) sequence. The imaging parameters were field of view (FOV) = 220 mm, 64 x 64 matrix, time of repetition (TR) = 2000 ms, time of echo (TE) = 27 ms and flip angle = 90°. The whole brain was imaged in an axial configuration where 32 slices were collected and each slice was 5 mm thick. The resolution was 3.4 x 3.4 x 5 mm. After all functional tasks, a high resolution MPRAGE (magnetization-prepared rapid gradient-echo) data set was collected. The MPRAGE imaging parameters were: 80 slices, FOV = 220 mm, slice thickness = 2 mm, TR = 2000 msec, TE = 4.38 msec, T1 = 900 msec, flip angle = 8º and matrix = 256 x 256, which resulted in a spatial resolution of 0.9 x 0.9 x 2 mm.

5.2.4 Functional Experimental Design

Vergence stimulation with LED cues was used during scanning. Orientation aligned with the subject's midline and the spacing between visual targets was adjusted to stimulate 2°, 3° and 4° of combined, sustained convergence demand as shown in Figure 5.1-A1. Experiments took place in a darkened room where the subject only saw the visual stimulus. The maximum vergence stimulus was 2° disparity change, chosen due to the physical constraints of the imaging center and to decrease the co-occurrence of saccades with the symmetrical vergence response [70-72]. For all experiments, only one location was illuminated at a time.

Two experimental paradigms were performed: fixation versus random tracking, and then random tracking versus prediction where both have different cognitive demand, testing changes of influences among relative regions. In the first case the fixation versus random tracking vergence experiment followed a standard block design of fixation (no eye movement) for the "off" phase compared to random eye movements for the "on" phase using vergence step stimuli. Each visual step stimulus was presented for a random duration of time between 0.5 to 3.0 seconds. Approximately 20 visual step stimuli for a total duration of 140s were presented within each eye movement phase, shown in Figure. 5.1B. The subject could not anticipate the timing of the visual stimulus. Subjects confirmed they were able to comfortably view the visual stimuli during the imaging session.

In the second experiment (random versus predictable tracking) subjects would track the illuminated LED, which produced random vergence step stimuli for 40 s followed by predictable vergence eye movements for 40 s. Random and predictable phases were repeated for 3.5 cycles for a total duration of 280 s (4 min and 40 s), as shown in Figure 5.1C. The subjects were instructed to look at the visual target and blink when needed without moving their heads. The operator gave an audible cue when the predictable phase began. The subjects were instructed to anticipate the next target when they were in the predictable phase. The custom fMRI-compatible non-ferrous LEDs were adjusted and centered, as shown in Figure 5.1A. For the random phase, the subjects could not predict which of the three locations would be shown. For the predictable sequence, the targets began with the 4 degree vergence fixation followed by the 3 deg vergence fixation and then by the 2 degree target using the LEDs.

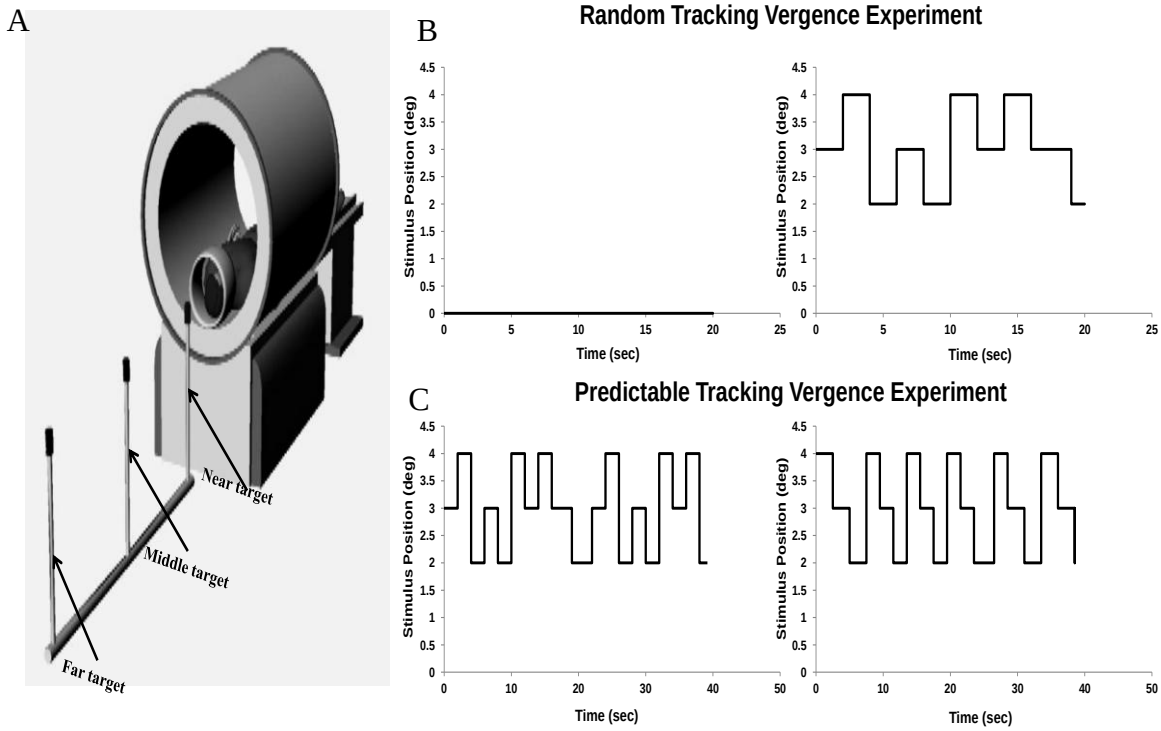

Figure 5.1 Experimental set-up and design. The schematic of the custom fMRI compatible light emitting diodes (LEDs) is shown for fixation versus random tracking and random versus predictable tracking vergence experiments.

5.2.5 Data Analysis

5.2.5.1 Individual Subject Analysis using a Data Driven Reference Vector. As it was applied and mentioned in Specific Aim 1, individual subject analysis using a Data Driven Reference Vector Data was applied by using AFNI (Analysis of Functional NeuroImages) software [73]. Registered and motion corrected scans of each individual were used to transform into anatomical and functional the standardized Talairach-Tournoux coordinate space [196]. A reference vector was chosen for each subject by using independent component analysis (ICA), blind source separation technique, to avoid hemodynamic variations across the subjects [31, 82-90]. The independent signal sources [91] for each subject was calculated with approach of probabilistic ICA embedded in the

MELODIC (Multivariate Exploratory Linear Optimized Decomposition into Independent Components) software from FSL. At the end, the fMRI time series data of each subject with each voxel of the entire brain was correlated as in the concept of General Linear Modeling (GLM). Only data has a minimum threshold of functional activity corresponding to a z-score of 2.0 (two tail $p = 0.05$) were reported and further analyzed.

5.2.5.2 Group Analysis. To facilitate comparison between the conducted experiments, the individual subject correlation spatial maps were averaged. From these averaged maps, regions of functional activity at the group level were obtained, with similar regions have been reported previously [31, 32]. Eleven ROIs were chosen based on previous primate and human investigations for further analysis by GCA [8, 14, 21, 23, 26, 27, 30, 31, 49, 64, 197-202]. For example, the frontal eye fields (FEF), the supplementary eye field (SEF), the dorsolateral prefrontal cortex (DLPFC), ventral lateral prefrontal cortex, inferior parietal area (BA40) or parietal eye field (PEF), anterior and posterior cingulates (BA 29, BA 30, BA 31), cerebellar vermis, midbrain of the brainstem were reported as neural substrates of the vergence system in a recent fMRI paper [32]. During the analysis of the random versus predictable tracking vergence experiment, the combination of the individual voxel probability threshold and the cluster size threshold (11 voxels rounded to a total volume of 650 mm3 for our data set yielded the equivalent of a whole-brain corrected for multiple comparison significance level of $\alpha < 0.001$. The cluster size was determined using the AFNI AlphaSim program [97], which estimates the overall significance level by determining the probability of false detection through Monte Carlo simulation. The functional data are displayed as a z-score shown in the Figure 5.3 scale bar.

5.2.5.3 Granger Causality Analysis. GCA is a statistical approach to evaluate influences between time series or, in application to fMRI, effective "connections" between neural regions. GCA uses F-statistics to quantify the existence of possible causal relationships between the ROI time series in terms of "lags" or "time separated values". The residual variance in the full autoregressive model can be estimated by the unrestricted equation below:

$$x(t) = c1 + \sum_{i=1}^{p} a(i)x(t-i) + \sum_{j=1}^{p} b(j)y(t-j) + u(t) \tag{5.1}$$

$x(t)$ and $y(t)$ are two different time series to be evaluated for the causality interaction; t is a given time point; *c1* is a constant over time; $a(i)$ and $b(j)$ are the linear prediction coefficients for x and y; $u(\mathrm{t})$ is the residual error of the fit; and *p* is the maximum lag length to be investigated. Using the F-test, the null hypothesis that $b(j) = 0$ for all lags j (and therefore y does not influence or Granger-cause x) is tested. An analogous test also can be applied separately to determine whether $x(t)$ Granger-causes $y(t)$ [203]. The residual variance from the above unrestricted equation is compared with the reduced autoregressive model, given by:

$$x(t) = c1 + \sum_{i=1}^{p} g(i)x(t-i) + e(t) \tag{5.2}$$

where $x(t)$ is the time series being evaluated for influence; $g(i)$ is the linear prediction coefficient for *x*; *e* is the residual or prediction error; and p is the maximum lag length [191, 203]. The F-test comparison between these two models in Equations 5.1 and 5.2 (full and reduced autoregressive, respectively) regarding residual variance is evaluated with the following:

$$F_{y,x} = \frac{\left(\sum_{i=1}^{T} e\ (i)^{2} - \sum_{i=1}^{T} u\ (i)^{2}\right) \Big/ p}{\left(\sum_{i=1}^{T} u(i)\right)^{2} \Big/ (T - 2p - 1)} \tag{5.3}$$

where T is the total number of time points and again p is the maximum length of lag [191].

In this study, the motion-corrected time series were extracted using 11 ROIs. Average time series was calculated per ROI. These averaged time series were used to derive F values and corresponding p values which defines Granger Causality matrix (GCM). Granger-causality was tested in both directions for each of the 110 ROI pairs. F values calculated for each of the 110 ROI pairs for each subject are the measure of strenght of causal interactions. Additionally, for both the experiments, average F value was calculated across all subjects for each of the 110 ROI pairs to create unthresholded group level ROI interaction maps. The 11x11 GCM is also defined using p values corresponding to 110 potential causal pairwise interactions. Subject level GCM is calculated using average time series for each of the ROI per subjects. Furthermore, group level GCM is calculated by using averaged time series across subjects (i.e., off-diagonal matrix elements). After estimation of the possible pairwise causal interactions, the GCM elements were thresholded at $p < 0.05$ (with Bonferroni correction) to calculate statistically significant causal interactions between ROIs. To derive group level differences, each subject's unthresholded GCM was p to z transformed using cumulative distribution function (CDF) and a pair-wise Student t-test was performed on this z values. The best model order, in the range of 2 to 5 [187, 191, 204, 205] to calculate GCM, was determined using the Bayesian Information Criterion (BIC) and Akaike Information Criterion for an fMRI dataset.

5.3 Results

Typical eye movement responses recorded prior to the imaging sessions are shown in Figure 5.2. The same figure shows the difference between the calibrated left and right eye movements, with Figure 5.2A showing the velocity trace, and Figure 5.2B, the position trace. The response to a random stimulus is shown as a gray line, and response to a predictable stimulus is represented as a black line. As can be seen from Figure 5.2A and 5.2B, latency is decreased and anticipatory drifts are observed in responses to predictable stimuli with the random onset delay.

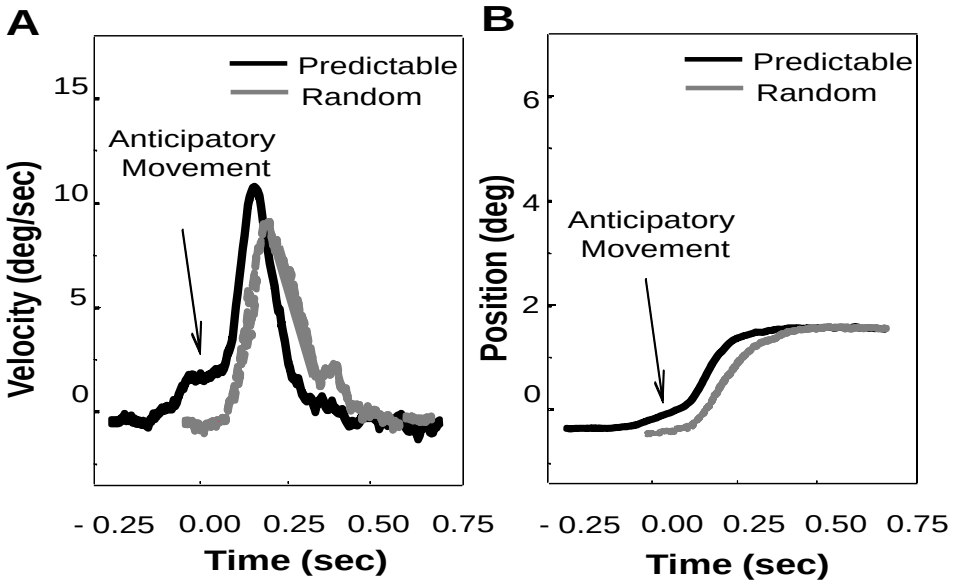

Figure 5.2 Eye movement recordings from random (gray line) and predictable step stimuli (black lines) vergence responses. Velocity (deg/sec) and position (deg) traces are plotted. Anticipatory movements are observed with the predictable responses denoted by an arrow.

fMRI data are first analyzed individually to determine how many of the fifteen subjects showed activation within a given anatomical location for each experimental paradigm. Individual data analysis was followed by the averaged subject data set for the fifteen subjects performing fixation versus random tracking and random versus

predictable tracking experiments, with the results of these analyses shown in Figure 5.3. Figure 5.3 shows axial, coronal and sagittal slices of averaged group level functional activity for ROIs such as dorsolateral prefrontal cortex (DLPFC), frontal eye field (FEF), ventrolateral prefrontal cortex (VLPFC), anterior cingulate (AC), parietal eye field (PEF), cerebellum and brainstem. Table 5.1 lists the peak activation for a given anatomical location (with Talairach-Tournoux coordinates) of the averaged subject data setwith the corresponding averaged z-score and Brodmann Area (BA) for fixation versus random tracking experiment. Table 5.2 lists the peak activation with Talairach-Tournoux coordinates for a given anatomical location of the averaged subject data set with the corresponding z-score and Brodmann Area (BA) for random versus predictable tracking experiment. Functional activity of similar areas has been reported previously in similar convergence studies [31, 32].

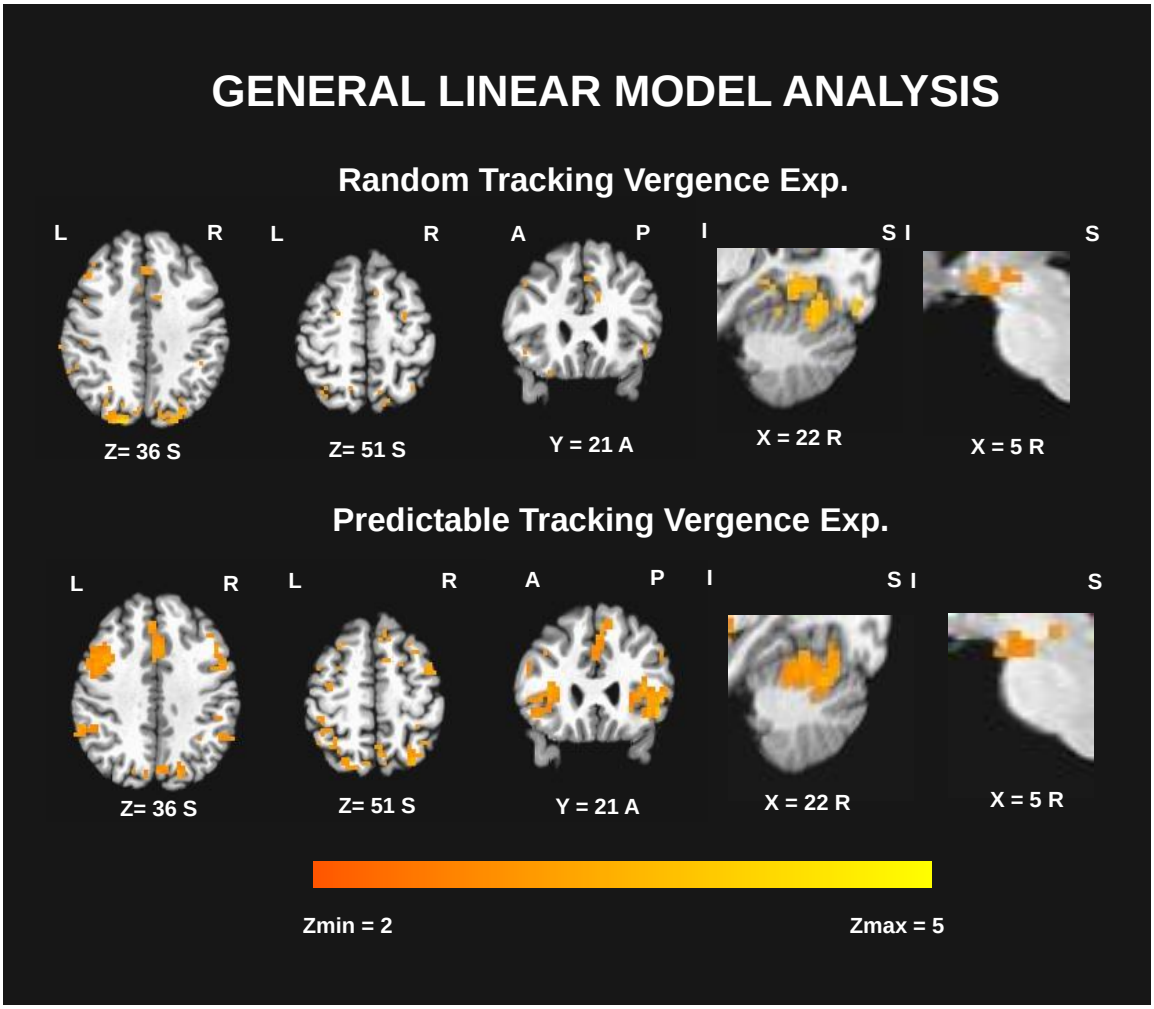

Figure 5.3 Averaged subject data set functional activity results for fixation versus random tracking vergence and random versus predictable tracking experiments. Data are overlaid onto a standardized Talairach-Tournoux normalized image.

Table 5.1 Average Peak Activation of the Fixation Versus Random Vergence Oculomotor Task in Talairach-Tournoux Coordinates with the level of Significance Denoted as a z-Score. For the x Axis: Positive is Right (R) and Negative is Left (L); for the y Axis: Negative is Posterior (P) and Positive is Anterior (A); and for the z Axis: Positive is Superior (S) and Negative is Inferior (I)

Regions for Fixation versus Random Tracking Exp.	**Brodmann Area**	**X (mm)**	**Y (mm)**	**Z (mm)**	**z-score**
Frontal Eye Field, Superior Middle Frontal Gyrus, Precentral Gyrus	8/6	-28L	6A	52S	2.12
	8/6	29R	-3P	51S	2.28
Supplementary Eye Field, Medial Frontal Gyrus	6	-2L	12A	44S	2.21
		2R	11A	43S	3.02
Dorsolateral Prefrontal Cortex	9	-48L	5A	20S	2.36
		52R	6A	24S	2.09
Anterior Cingulate/ Cingulate Gyrus	24/32	-6L	13A	36S	2.17
		10R	22A	29S	3.0
Inferior Ventral Lateral Prefrontal Cortex, Inferior Frontal Gyrus, precentral Gyrus	45/47	-46L	21A	5S	2.09
		47R	28A	5S	2.33
Parietal Eye Field Inferior Parietal Area	40	-49L	-42P	36S	2.22
		40R	-39P	36S	2.26
Posterior Cingulate	31	-4L	-73P	26S	3.44
		13R	-71P	24S	3.46
	30	-10L	-60P	8S	4.18
		8R	-67P	8S	3.33
	29	-7L	-50P	6S	3.46
		7R	-49P	3S	2.98
Cerebellar Vermis IV/V		4R	-50P	-2I	2.81
Midbrain		4R	-17P	-5I	2.06

Table 5.2 Average Peak Activation of the Random Tracking Versus Predictable Tracking Vergence Oculomotor Task in Talairach-Tournoux Coordinates with the Level of Significance Denoted as a z-Score. For the x Axis: positive is Right (R) and Negative is Left (L); for the y Axis: Negative is Posterior (P) and Positive is Anterior (A); and for the z Axis: positive is Superior (S) and Negative is Inferior (I)

Regions for Random versus Predictable Tracking Exp.	Brodmann Area	X (mm)	Y (mm)	Z (mm)	z-score
Frontal Eye Field, Superior Middle Frontal Gyrus, Precentral Gyrus	8/6	-30L	-1P	53S	3.69
	8/6	39R	-5P	51S	3.85
Supplementary Eye Field, Medial Frontal Gyrus	6	-1L	17A	38S	4.26
		1R	15A	39S	4.07
Dorsolateral Prefrontal Cortex	9	-35L	10A	39S	4.18
		53R	9A	26S	3.82
Anterior Cingulate/ Cingulate Gyrus	24/32	-1L	27A	28S	3.65
		3R	28A	29S	3.56
Inferior Ventral Lateral Prefrontal Cortex, Inferior Frontal Gyrus, precentral Gyrus	45/47	-35L	26A	5S	4.55
		44R	23A	-1I	4.97
Parietal Eye Field Inferior Parietal Area	40	-32L	-43P	47S	3.71
		48R	-38P	41S	3.89
Posterior Cingulate	31	-11L	-60P	30S	3.2
		4R	-68P	23S	3.82
	30	-15L	-55P	11S	3.38
		10R	-60P	11S	3.0
	29	-4L	-40P	20S	3.18
		4R	-44P	14S	3.2
Cerebellar Vermis IV/V		-9L	-55P	-2I	3.87
Midbrain		-5L	-16P	-10I	3.49

Figure 5.4 shows the ROI causality matrices with the mean of F values calculated across all the subjects for both random tracking (Figure 5.4A) and predictable tracking (Figure 5.4B) experiments. This result shows the strength of the interactions is less in the fixation versus random tracking experiment when it is compared to the random versus predictable tracking vergence experiment. Bonferroni corrected, mean group level maps representing statistically significant causality interactions for fixation versus random

vergence tracking experiment (Figure 5.5A, $p<0.05$), and random versus pedictable tracking vergence experiment (Figure 5.5B, $p<0.05$) and also significant differences between both experiment (Figure 5.5C, $p<0.05$) can be observed in Figure 5.5 in which black arrows represent unidirectionality and red arrows show bidirectionality. It is evident from Figure 5.5A and Figure 5.5B that the number significant causal interactions in fixation versus random tracking experiment are less than the predictable versus random tracking experiment. In order to test statistical significance of this differences a pair-wise Student t-test was performed on each ROI causal interaction pair using subject level GCM. Figure 5.5C displays significant differences observed between the two experimental paradigms ($p<0.05$).

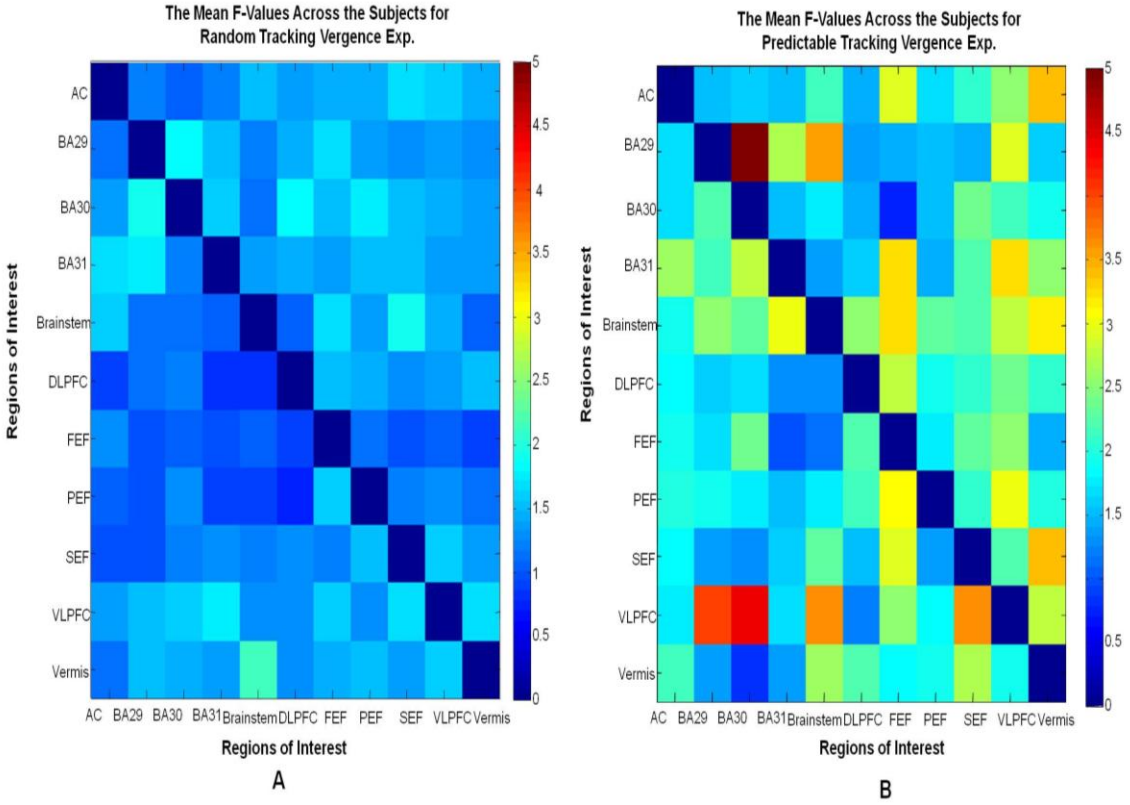

Figure 5.4 The causality matrices that includes the mean of F- values shows fixation versus random tracking vergence experiment (Figure 5.4A) has less strength of interactions when it is compared to the random tracking versus predictable tracking vergence experiment (Figure 5.4B). AC: Anterior Cingulate, BA 29: Brodmann Area 29, BA 30: Brodmann Area 31, DLPFC: Dorsalateral prefrontal cortex, FEF: Frontal eye field, PEF: Parietal eye field, SEF: Supplementary eye field, VLPFC: Ventrolateral prefrontal cortex.

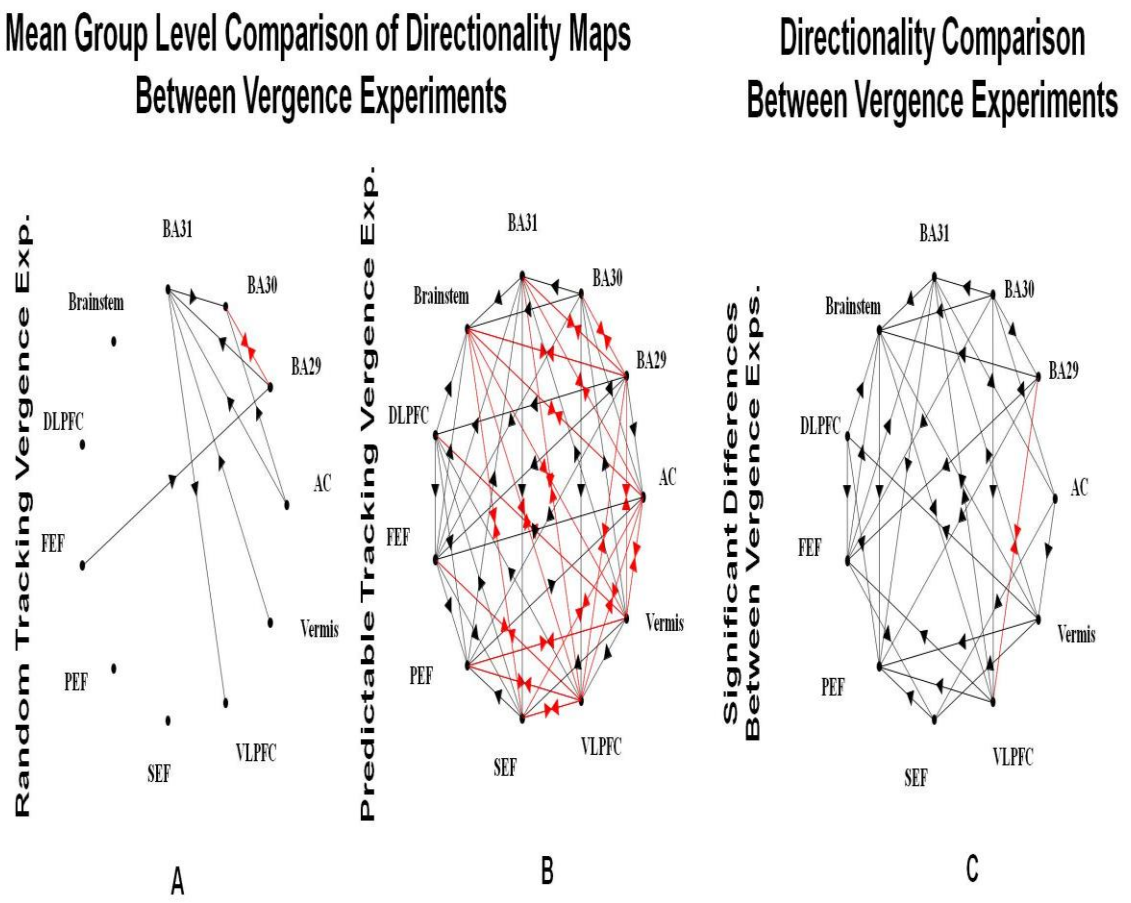

Figure 5.5 Statistically significant causal interactions, ($p < 0.05$) among ROIs for fixation versus random tracking vergence and random versus predictable tracking experiments are shown in Figure 5.5A and Figure 5.5B, respectively. Significant differences between vergence experiments are shown in Figure 5.5C. Causal interactions that are shown in black are unidirectional and the red labeled causal interactions represent bidirectionality.

Additionally, a binomial significance test ($p<0.001$) was performed on the number of significant causal interactions at subject level for both the visual experiments as can be seen in Figure 5.6. Figure 5.6 supports that when cognitive demand increases in the task applied the number of causal interactions increases.

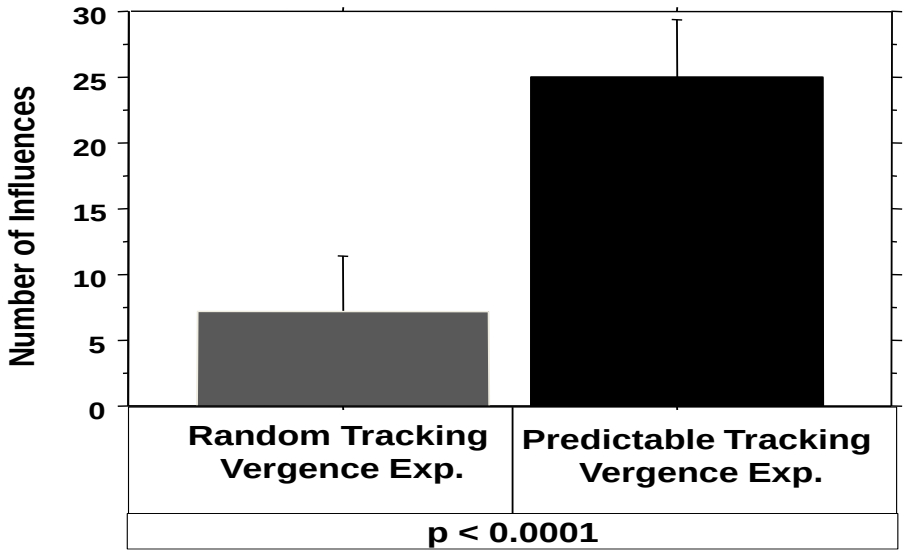

Figure 5.6 Number of GCA causal influences fixation versus random tracking vergence and random versus predictable tracking vergence experiments, $p < 0.0001$.

5.4 Discussion

5.4.1 Summary

In this fMRI study, the relation between cognitive load and the number of directed connections among relevant ROIs was investigated for the vergence movement dependent visual tasks. Differences in effective connectivity as measured using Granger causality among ROIs were compared which were significantly active during the performance of two vergence oculomotor experiments which required different cognitive demands. After GLM analysis of the functionally active regions, GCA was implemented as a further step, which provided an estimate of the direction of connectivity among the selected regions. Results indicated that there was a significantly greater number of causal interactions among selected areas of the brain for the predictable tracking vergence task than the simple random tracking vergence task. Additionally, a pair-wise Student *t*-test

was performed on causality interaction results acquired from visual tasks to show statistically significant difference between these tasks.

5.4.2 The Effects of Anticipatory Behavior in the Vergence Eye Movements

In this study, it is observed that there exists an increase in the peak velocity and decrease in the latency in the eye movementresponse for predictable stimuli versus random stimuli. Predictive behaviors on the oculomotor investigations on smooth pursuit [206, 207] saccades [208], vergence [209-212] have indicated reduced latencies and anticipatory movements before the stimulus onset. Rashbass and Westheimer showed that the use of predictive stimuli results in a decrease of latency when it is compared to the randomly appeared visual targets [209]. This finding also had been supported by other investigations [210, 211]. Krishnan and colleagues demonstrated that when predictable vergence stimulus is applied the latency is decreased [210]. Furthermore, Alvarez and colleagues reported an increase in peak velocity, decrease in latency corresponding to the stimulus in which participants would know the timing and magnitude information regarding the target seen when it is compared to the randomly tracked stimulus [211]. Additionally, Kumar claimed that when the anticipatory features are involved in the vergence eye movements where the dynamics of the vergence movements are affected by previous vergence responses can also indicate utilization of working memory [212].

5.4.3 The Brain-Behavior Relationship

Evidence from other investigations correlates variations in dynamic neural activity not only with the specific experimental tasks but also with the observed visual-spatial attention [191, 213]. Biswal and colleagues showed that variations on the extent of

cognitive demand affect brain-behavior relationships by utilizing GCA. They showed that performance at individual level differs corresponding to the cognitive demand level in the experimental tasks [191]. Buschman and Miller also suggested that the relationship of the brain areas capable of dynamic modulation depending on the current task applied. They showed that different neuronal synchrony might be adopted between frontal and parietal areas for different modes of attention [213]. Additionally, Bressler and colleagues studied the human brain and its relation to the anticipatory visual attention. According Bressler and colleagues, top-down (frontal eye field (FEF) and intraparietal sulcus (IPS) Granger causality functions as a control mechanism for increasing behavioral performance based on the vispatial attention behavioral paradigm which includes predictability of the location of the target [214]. Furthermore, Graaf and colleagues revealed fronto-parietal, thalamo-parietal interactions and different levels of information processing as the correlates of visual spatial attention network are also part of visual spatial judgments tasks. This indicates multiple communication loops converges for execution of this type of visual paradigms [189]. This literature leads us to infer firstly that there might exist task-specific connectivity. Beside that, when the cognitive demand is engaged to the experimental task, higher involvement of the areas of the brain is expected to increase the performance regarding experimental paradigm. Lastly, recruitment visual attention might occur to succeed in the prediction of the location of the target. Taken together, these approaches might explain why there is more causal interactions in our cognitively demanding vergence task than comparison to a simple tracking task.

5.4.4 Variation of BOLD Hemodynamic Responses

Several factors alter hemodynamic responses across subjects and brain regions, such as neural activity differences [215], baseline cerebral blood flow and global magnetic susceptibilities [216], vasculature differences such as vascular density [217, 218], and vascular compliance [217, 219, 220], pulse or respiration differences [221], hemotocrit concentrations [222], and aging [77]. For example, Lee and colleagues stated that larger vessels (such as visible vessels) and sulci require more blood which results in greater temporal delay when their BOLD signals are compared to vessels in the gray matter [223]. Furthermore, brain microcirculation such as arteriole dilation may be considered as another effect in which neuron-to-astrocyte signaling has crucial contributions depending on glutamate-mediated $[Ca^{2+}]_i$ fluctuations in astrocytes [224]. As a whole, the differences in the amount of causal interactions observed in this present study may also be due in part to vasculature response variations arising from across subjects and between different ROIs. Therefore, further research is required to understand regional hemodynamic response and temporal variations in the BOLD signal which are as crucial factors might influence interregional causality results of GCA.

5.5 Conclusion

This study used a block design of simple random tracking versus fixation eye movement task and predictable tracking versus random tracking eye movement experiments. Eye movement tasks that contained anticipatory behavior, which requires more cognitive involvement than the simple random tracking experiments, showed greater causal interconnectivity within specific ROIs measured with fMRI BOLD response. While, single cell recordings from primates and human case studies have reported that numerous

neural substrates participate in the generation of vergence eye movement, the connectivity between these regions is still not fully understood. Recent reviews emphasize the need for more research to understand the directionality of communication and connectivity between ROIs for vergence movements [26]. GCA has the potential to elucidate not only whether ROIs are functionally connected but also the direction of information flow. In summary, utilization of GCA on fMRI data might be complementary to other methods like GLM and ICA with exploratory approach of causal connectivity. Directionality of interactions between areas of the brain is an important feature which can be assessed by GCA application, and so this can assist in understanding not only dynamic temporal characteristics of neural responses but also dynamic responses of the brain areas to more cognitively demanding tasks.

CHAPTER 6

SEGREGATION OF FRONTOPARIETAL AND CEREBELLAR COMPONENTS WITHIN SACCADE VERGENCE NETWORKS USING HIERARCHICAL INDEPENDENT COMPONENT ANALYSIS OF FMRI (SPECIFIC AIM 4)

Purpose: Cortical and subcortical functional activity stimulated via saccade and vergence eye movements were investigated to examine the similarities and differences between networks and regions of interest (ROIs).

Methods: Blood oxygenation level-dependent (BOLD) signals from stimulus-induced functional Magnetic Resonance Imaging (MRI) experiments were analyzed studying 16 healthy subjects. Six types of oculomotor experiments were conducted using a block design to study both saccade and vergence circuits. The experiments included a simple eye movement task and a more cognitively demanding prediction task. A hierarchical independent component analysis (ICA) process began by analyzing individual subject data sets with spatial ICA to extract spatial independent components (sIC), which resulted in three ROIs. Using the time series from each of the three ROIs per subject, per oculomotor experiment, a temporal ICA was used to compute individual temporal independent components (tICs). For each of the three ROIs, the individual tICs from multiple subjects were entered into a second temporal ICA to compute group-level tICs for comparison.

Results: Two independent spatial maps were observed for each subject (one sIC showing activity in the frontoparietal regions and another sIC in the cerebellum) during

the six oculomotor tasks. Analysis of group-level tICs revealed an increased latency in the cerebellar region when compared to the frontoparietal region.

Conclusion: Shared neuronal behavior has been reported in the frontal and parietal lobes, which may in part explain the segregation of frontoparietal functional activity into one sIC. The cerebellum uses multiple time scales for motor learning. This may result in an increased latency observed in the BOLD signal of the cerebellar group-level tIC when compared to the frontal and parietal group-level tICs. The increased latency offers a possible explanation to why ICA dissects the cerebellar activity into an sIC. The hierarchical ICA process used to calculate group-level tICs can yield insight into functional connectivity within complex neural networks.

6.1 Introduction

The brain is comprised of complex communication among numerous networks. Several networks are involved in vision processing. As covered in previous sections of the dissertation, the eyes rotate so that objects of visual interest project to the fovea, the portion of the retina, which contains the greatest density of photoreceptors to yield high acuity and resolution. Eye movements (described using oculomotor control) have evolved to solve the difficult task of acquiring visual information quickly and accurately while compensating for processing delays [225].

A rich body of literature, from single-cell recordings and lesion studies on nonhuman primates to human case reports to eye movement investigations and functional imaging studies, forms our present understanding of the saccade and vergence systems [8]. Recent investigations are emerging which study the subdivisions of functional connectivity of visual processing within fMRI studies [38, 226].

FMRI measures metabolic changes and has been reported to be correlated to direct neuronal measurements [92, 93]. Variations in cerebral blood flow, blood volume, and the concentration of deoxyhemoglobin or blood oxygenation levels are the principle parameters that generate the blood oxygenation level-dependent (BOLD) signal acquired during fMRI studies [36, 227]. Most fMRI studies determine what cortical areas are active from a predetermined stimulus-induced task using a conventional GLM analysis.

The GLM assumes prior knowledge of the experimental task. This analysis is routinely used in fMRI studies and its strength is in its simplicity. In addition to showing which areas are involved in an experimental task, some limited inference about connectivity can be made with a GLM [181, 182]. Connectivity can be studied by computing which delays of the reference model yield maximum correlation dependent upon the region of interest (ROI), which can imply which site was activated first. Thus, the ROI whose maximum correlation occurred with the shortest delay would be assumed to be activated first and so forth.

However, understanding the complex interaction between sites of functional activity using simply delay shifts may not be insightful about the connectivity between sites. Functional connectivity can also be studied with data-driven methods [184, 228]. Advances in data-driven image processing algorithms such as independent component analysis (ICA) are being recommended as a means to study the connectivity or organization within networks [47, 184]. ICA is a nonlinear multivariate technique that blindly separates the source signal from the mixed data without any prior assumptions of the sources. Similar to principle component analysis (PCA), ICA attempts to maximally decorrelate the sources. On the other hand, to achieve statistical independence of sources,

information greater than the second-order statistics is needed. The most popular ICA algorithms use maximum likelihood estimation, maximization of information transfer, mutual information minimization, or maximization of non- Gaussianity [184]. ICA has routinely been used to reduce artifacts, but more recently, it is being used to study the functional connectivity within the brain [184]. In applying ICA to vision research, both a study of visual perception [38] and another investigation of saccades [226] have reported a frontoparietal component within the visual system, along with other independent components.

The goal of the research presented here is to define task-related independent components of BOLD activation during six different oculomotor experiments (a fixation versus random eye movements tracking task and a more cognitively demanding task of random versus predictive eye movements studying both saccade and vergence responses with two types of targets). The presented stimulus in each case is a standard ON/OFF block design. There are two novel aspects to this research. First, this investigation studies subdivisions within the cortical and subcortical vergence systemusing a hierarchical ICA. Second, ICA of saccade and vergence task responses has not been investigated when the cerebellum was imaged.

Spatial ICA identifies various voxel groups across the brain, whereas temporal ICA can yield insight into how the underlying BOLD response varies from one ROI to another. In this specific aim, it is expected that significant distinctions between temporal independent components (tIC) signals from ROIs in different spatial independent components (sIC) maps will be observed. These differences can be compared using “group-level” tIC signals. Potentially, temporal differences can distinguish higher level

cognitive processes. Since previous vision research experiments have identified a frontoparietal sIC during visual perception and saccadic tasks [38, 226], it is hypothesized that a frontoparietal sIC will be present during the vergence and saccade tasks performed within this study. In here also it is hypothesized that additional sIC maps may be derived from ICA. Understanding how visual task-related ROIs are potentially grouped within one sIC, and how others are segregated within different sIC, can enhance the knowledge of what neural resources are shared between systems, as well as what ROIs have greater commonality, or potentially more similar functional activity, within a neural system.

6.2 Methodology

6.2.1 Subjects

Sixteen volunteers (9F, 7M, and mean age 26±4 years between 22 and 37 years of age) participated in this study. The inclusion criterion for all subjects was normal binocular vision assessed by the Randot Stereopsis test with a fixation disparity of better than 70 s of arc. Stereopsis is the perception of depth from two slightly different projections of the world onto the retinas of the two eyes, which stimulates vergence eye movements. Normal binocular vision was also defined as a near point of convergence less than 10 cm. Near point of convergence is the distance from the subject along midline when an object is reported as diplopic. These methods are explained in detail in another one of our studies [68]. Subjects had no history of neurological injuries or dysfunctions. Fifteen of the 16 subjects were right handed. Prior to the functional scanning, eye movements were recorded to determine if the subjects understood the task and could perform these tasks

with ease. If needed, subjects wore corrective refraction during the experiment. All subjects signed a written informed consent approved by the University of Medicine and Dentistry and New Jersey Institute of Technology Institution Review Boards in accordance with the Declaration of Helsinki.

6.2.2 Materials and Apparatus

An infrared (λ = 950 nm) limbus tracking system (model 6500; Skalar Iris, Delft, The Netherlands) with ±25 deg linear range was used to record eye movements prior to the imaging session. A 12-bit digital acquisition hardware card was used (6024 E series; National Instruments, Austin, TX).

There were two types of visual stimuli used: light emitting diodes (LED) targets and a stereoscope using a projector, which are shown in Figure 6.1 Plot A. Three custom nonferrous LEDs were designed to form a line stimulus, 10 cm in height by 2 mm in width to stimulate saccade or vergence movements. Subjects could view targets with the use of a mirror through the bore of the magnet. For saccadic stimulation, the middle LED was centered along the subject's midline. Subjects would track targets that would appear in one of three locations: 1) 0 deg (midline), 2) 10 deg into the left visual field, or 3) 10 deg into the right visual field. A saccadic magnitude of 10 deg from midline was chosen because saccades less than 15 deg from midline do not evoke head motion [69]. For vergence stimulation, the three LEDs were rearranged and carefully centered along the subject's midline, drawn schematically in Figure 6.1 Plot A. There were three vergence fixation points (2, 3, and 4 degrees) to produce symmetrical vergence step stimuli. The vergence step stimulus was a 1–2 deg disparity change, which was chosen due to the physical constraints of the imaging center and in order to decrease the occurrence of

saccades within the symmetrical vergence response [70-72]. To stimulate a greater disparity change of 2– 4 deg, a stereoscope was needed.

For the stereoscope, a custom Matlab (Mathworks, Waltham, MA) program was used to generate the saccade and vergence visual stimuli. Examples of the images are drawn in Figure 6.1 Plot A. A Liquid Crystal Display (LCD) projector, located near the subject's head, was utilized with a rear projection screen (Epson, Long Beach, CA) for presentation of the stimuli. A single-line stimulus was used to stimulate saccade eye movements, and two lines were used to stimulate vergence eye movements. To stimulate vergence, red/green filter glasses (Bernell, Mishawaka, IN) were worn during the experiment. The filters were carefully matched to the wavelengths of the red and green lines shown on the computer. This created an environment such that only one eye saw the green stimulus and the other saw the red stimulus. Eye movement recordings of vergence responses confirmed that the subject could perform both the saccade and vergence oculomotor tasks. The subject would fuse the two lines, which stimulated differing amounts of retinal disparity. For the random sequence, the visual target was 4 cm in height by 2 mm in width, and for the predictable sequence, the target was 8 cm in height by 2 mm in width. The change in height gave the subject a visual cue of whether a random or predictable sequence was presented. Functional and anatomical images were collected on a 3.0 Tesla Siemens Allegra MRI magnetron with a standard head coil (Siemens, Erlangen, Germany).

6.2.3 Experimental Design

Six oculomotor experiments were conducted, as summarized in Table 6.1. Three of the experiments studied saccades (experiments 1, 3, and 5), and three investigated vergence eye movements (experiments 2, 4, and 6). Two types of visual targets were used: a series of LEDs forming a line stimulus and a stereoscope, which also used a line stimulus viewed with red/green filter glasses, shown in Figure 6.1A. Two cognitive tasks were utilized for this stimulusinduced experiment. The first task, utilizing only LED targets, studied a fixation gaze (Figure 6.1, Plot B1) versus random eye movements (Figure 6.1, Plot B2) in a standard block design (experiments 1 and 2). The second task was more cognitively demanding, using random eye movements (Figure 6.1, Plot B2) versus predictable eye movements (Figure 6.1, Plot B3), also within a standard block design. In this case, both LED targets (experiments 3 and 4) and the stereoscope (experiments 5 and 6) were used. For the saccade experiments, the setup of the LEDs and stereoscope were virtually the same, using a midline target and 10 deg targets either presented in the right or left visual field. For the vergence experiments, the LEDs stimulated a maximum of 2 deg change in disparity due to the physical limits of the imaging center compared to the stereoscope, which we programmed to have a maximum of 4 deg change in disparity.

The primary goal of this present study was to investigate the commonality among several different oculomotor tasks in order to determine whether the shared resources observed in our previous investigations between the vergence and saccade networks during simple (fixation versus random movements), and more cognitively demanding tasks (random versus predictable eye movements) [31] would be grouped together into similar spatial maps. Previous investigations (summarized briefly in the discussion) using

a conventional GLM combined with a voxel-wise paired t-test have explored the differences between data sets. In addition, our preceding studies showed many ROIs that were common between the vergence and saccade data sets [31, 32]. Hence, this present research sought to determine if the commonality previously observed between the vergence and saccade data sets, using both a simple fixation versus an eye movement task and a more cognitively demanding task involving prediction, would be segregated into common spatial maps through ICA.

The stereoscope and LED targets stimulated different amounts of accommodation, which produced differences within vergence eye movements [229-231]. This investigation may be able to identify differences and commonality between these vergence data sets. However, differentiation was not observed and potential reasons are described within the discussion. Although, since this current study sought to identify what shared resources would be segregated into similar spatial maps, the stereoscope data were analyzed and, as will be shown, consistent separation was observed.

Subjects confirmed that they were able to comfortably view the visual stimuli during the imaging session. For all experiments, only one location was illuminated at a time. The subjects were asked to perform three types of visual tasks: fixation, random eye movements, or predictable eye movements. The instructions to the subjects were to look at whichever target was illuminated, blinking as necessary but limiting all head motion. Furthermore, an audible cue was given to signal the predictable phase, during which time the subjects were instructed to anticipate the next target.

All experiments utilized a standard block design of 3.5 cycles alternating between fixation versus random or random versus predictable eye movements. Each experiment

was repeated in case motion artifacts would present a problem, though, as discussed in the Results section, no problematic motion occurred. The fixation versus random tracking experiment lasted a total of 140 s, with each phase 20 s in duration. The investigation of prediction was more cognitively demanding; hence, the duration of that experiment was longer. The random versus predictable eye movement experiment lasted a total of 280 s, with each phase 40 s in duration.

There were two types of cognitive tasks investigated: fixation versus random eye movements and random versus predictable eye movements. For fixation, the subject was asked to fixate on the midline target located at a 4 deg sustained convergence position for 20 s. This LED was the "near" target for the vergence experiments. When performing eye movements to a random target, each visual stimulus would be present for a random duration of time between 0.5 and 3.0 s. Previous research has shown that subjects were unable to anticipate the random duration of time [232]. For the saccade experiments, targets would randomly appear in one of three locations: 1) 0 deg (midline), 2) 10 deg into the left visual field, or 3) 10 deg into the right visual field; for vergence, the locations were 2, 3, or 4 deg targets when using the LEDs or 4, 6, and 8 deg targets when using the stereoscope.

The predictable saccadic stimulus would be illuminated along midline, into the right visual field (10 deg from midline), and then in the left visual field (10 deg from midline). The target would remain in each location for 2 s, as shown in Figure 6.1 Plot B3. This pattern would repeat six times. For predictable vergence stimuli using LED targets, the experiment began with illumination of the "middle" target of 3 deg, then the "far" target of 2 deg, and then the "near" target of 4 deg. Each target would be

illuminated for 2 s, and this patternwould repeat six times. A similar periodicity was used with the stereoscope, but the targets were 4, 6, and 8 deg for the "far," "middle," and "near" targets, respectively. A similar periodicity has been used in other behavioral studies to investigate the influence of prediction in vergence eyemovements [210, 211].

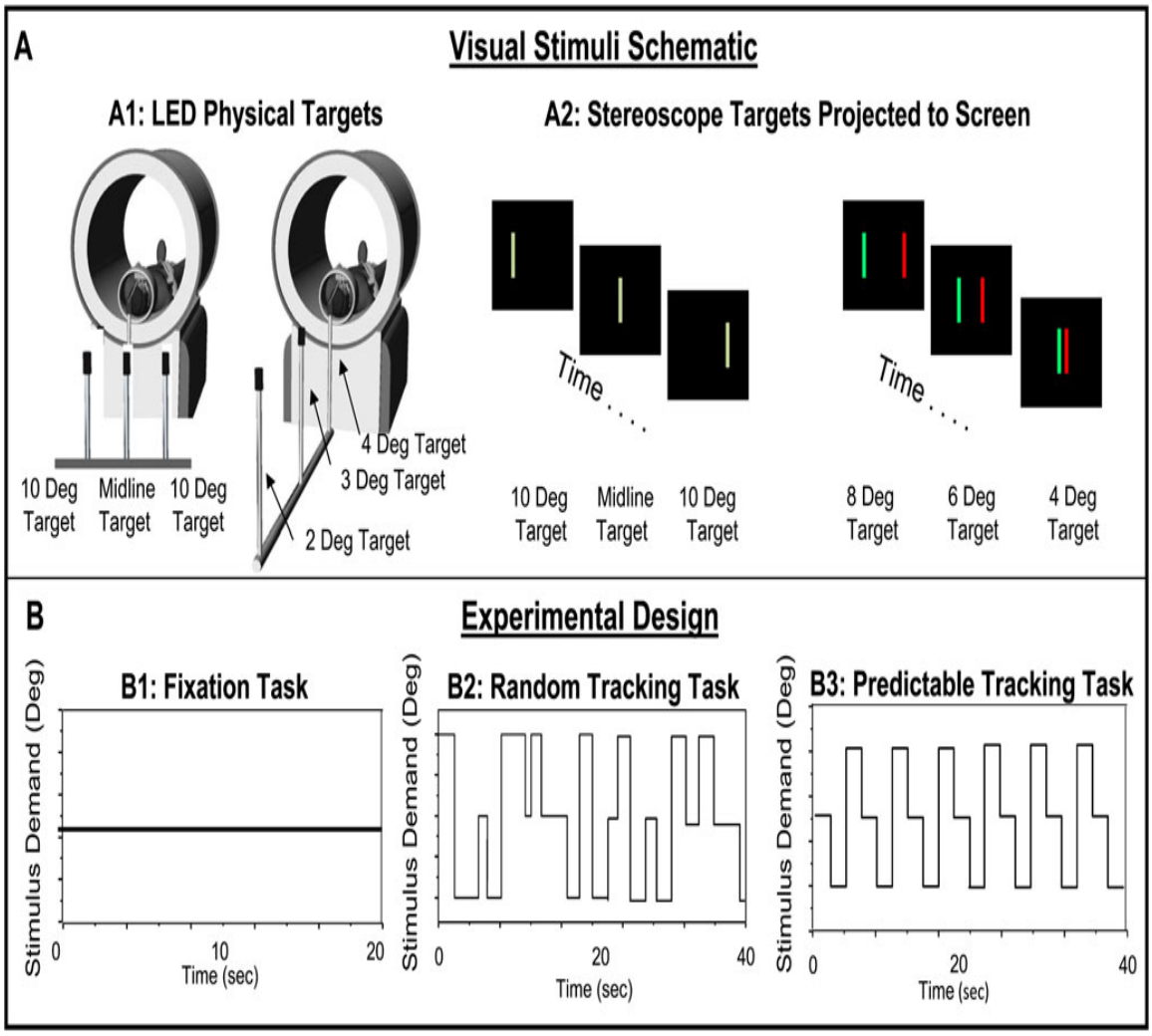

Figure 6.1 (Color online) Experimental design. Plot A1 shows the schematic of the custom LED targets for saccade and vergence experiments. Plot A2 shows the stereoscope with a single line used for saccade stimulation and a red and a green line viewed with red/green filter glasses to stimulate vergence movements. Three tasks were used in different block designs. One task was fixation (Plot B1) versus random eye movements (Plot B2) using LEDs (experiments 1 and 2). The second task was random tracking (Plot B2) versus predictable eye movements (Plot B3) using LEDs (experiments 3 and 4) and repeated with the stereoscope (experiments 5 and 6).

Table 6.1 Experimental Design Details for Saccade and Vergence Tasks

Exper. Number	Eye Movement Type	Visual Stimulus Target Type	Block Design	Figure 4.1 Exper. Design	Subject
1	Saccade	LED Targets	Fixation vs. Random	B1 vs. B2	S1 to S8
2	Vergence	LED Targets	Fixation vs. Random	B1 vs. B2	S1 to S8
3	Saccade	LED Targets	Random vs. Predictable	B2 vs. B3	S1 to S8
4	Vergence	LED Targets	Random vs. Predictable	B2 vs. B3	S1 to S8
5	Saccade	Stereoscope with Projection Screen	Random vs. Predictable	B2 vs. B3	S9 to S16
6	Vergence	Stereoscope with Projection Screen	Random vs. Predictable	B2 vs. B3	S9 to S16

6.2.4 Image Acquisition Parameters

The subject positioned himself/herself onto the gantry of the MRI instrumentation and was centered so that his/her head was located in the center of the coil. Each subject's head was stabilized using foam padding, and ear plugs were provided to protect his/her ears from machine-related noise (30 dB attenuation) while still allowing communication with the subject. The frequency power deposition and field-switching rate were below the Food and Drug Adminstration (FDA) criteria.

A quick scan was obtained and used to localize high-resolution anatomical and functional scans within the magnet. Since the cerebellum was an area of interest in this study, all subjects were positioned so that images could be attained of the whole brain. All functional scans used a T2*-weighted echo planar imaging sequence. The imaging parameters were field of view (FOV) = 220 mm, 64 x 64 matrix, Time of Repetition =

2000 ms, Time of Echo = 27 ms, and flip angle = 90 deg. The whole brain was imaged in an axial configuration where 32 slices were collected and each slice was 5 mm thick. The resolution was 3.4 x 3.4 x 5 mm for all functional imaging scans. There were 70 volumes collected (140 s) for experiments 1 and 2. There were 140 volumes (280 s) for experiments 3 through 6. Between scans, subjects were asked if they were comfortable and could perform the task. Subjects confirmed they could perform each task with ease. After all functional tasks, a high-resolution magnetization-prepared rapid gradient echo (MPRAGE) data set was collected. The MPRAGE imaging parameters were: 80 slices, FOV = 220 mm, slice thickness = 2 mm, TR = 2000 ms, TE = 4.38 ms, T1 = 900 ms, flip angle = 8 deg, and matrix = 256 x 256, which resulted in a spatial resolution of 0.9 x 0.9 3 2 mm.

6.2.5 Independent Component Analysis (ICA)

ICA is a blind source separation technique, which extracts statistically independent, underlying spatial or temporal signal sources [39, 233]. ICA assumes the data are a linear mixture of unknown sources, which can be recovered by maximizing statistical independence of components. Although not required, the ICA algorithm for fMRI data sets can begin with a common “prewhitening” technique using PCA to reduce the dimensionality of the data set [233, 234]. PCA is a second-order statistical technique, compared to ICA, which uses higher order statistics [184]. However, unlike PCA, ICA does not give any information about the relative magnitude (i.e., percentage of variance explained) of the calculated components [234].

McKeown et al., 1998 showed that ICA was capable of separating fMRI data sets into sICs which were correlated with task-related physiological changes, nontask

physiological changes, and artifacts from both human or instrumentation noise. The applications of both spatial and temporal ICA to fMRI have been validated [37, 39].

Conventional fMRI analyses utilize a GLM, which uses the same reference vector for all data sets (i.e., across all subjects). In contrast, ICA is purely a data-driven analysis. Reference vectors obtained from ICA are subject specific (due to intersubject variation such as the hemodynamic response, etc.), even if functional correlations are assumed to be similar across a group. Thus, determining a standardized method to perform a group-level analysis is not a trivial task in this case, and several methods have been employed for group-level ICA [91, 183, 228, 235-239]. In here, it has been used a hierarchical ICA process to study the commonality and differences of independent components from specific ROIs at a group, as well as at an individual level.

6.2.6 Image Processing Methodology

6.2.6.1 Registration and Motion Correction. All the scans were registered to the fourth image in the data set and motion corrected before analysis using Automated Functional NeuroImaging (AFNI) [73]. Six parameters (three for planar translation and three for rotation) were monitored to determine if head motion was a problem, and the data sets were inspected for the presence of motion-induced artifacts. Subjects had been instructed to limit head motion, and foam padding was used to further reduce movement. The motion parameters were estimated for the time series set, and for all subjects, movement was not substantial within this study.

6.2.6.2 Talairach-Tournoux Transformation and Smoothing. Individual anatomical and functional brain maps were transformed into the standardized Talairach–Tournoux

coordinate space [196]. Functional data were spatially lowpass filtered using a Gaussian kernel (6 mm full width half maximum) to account for interindividual anatomical variation [98-100].

6.2.6.3 Hierarchical ICA. A hierarchical ICA process has been used previously to study the spatiotemporal components of the BOLD fMRI signal evoked from an auditory task. Seifritz and colleagues first applied spatial independent component analysis (sICA) to individuals and then applied temporal independent component analysis (tICA) to specific ROIs identified from the sICA maps in individuals. The method of analysis in this present study began with an individual subject analysis similar to the study done by that group and was then extended to include a group-level tICA (not performed in the previous study) [240].

The hierarchical ICA process used in this study to determine the group-level temporal independent components can be divided into three steps. In the first step, "Individual Subject sICA of the Whole Brain" was used to identify task-related ROIs of high significance within individual subjects. Second, an "Individual Subject tICA per ROI" was computed for each subject, finding five tICs within specific ROIs identified in step 1. The third step was a "Group- Level tICA per ROI" in which the five tICs of each individual from step 2 were collected across the eight subjects to form a set of 40 time series (per ROI), from which a new set of five tICs were calculated to represent group-level information. The same set of steps was followed for each of the six oculomotor experiments. An overview of this analysis is shown in Figure 6.2.

In the first step of the image processing, sICA was applied to a voxel time series from the entire brain (Figure 6.2, Step 1). The standard Infomax algorithm, available

through the software toolbox Group ICA of fMRI Toolbox, was implemented [183]. The GIFT software toolbox offers two options for determining the number of components: entering a fixed number to be computed [default is 20 independent components (ICs)] or allowing PCA to determine the number of components that accounts for a specified percent of total variance.

In this study, for consistency across subjects, the former method was selected. Several studies have investigated the influence of the PCA model order choice in fMRI ICA methods, [241-243] generally recommending between 20 and 60 components depending on the fMRI data set. A different study that used a visual perception task studied 20 components. Twenty components described 99.5% of the total variance in their data set [38]. In this study, 20 sICs was chosen to account for a large percentage of total variance for individuals (.90%in each case) as well as the intersubject variability [38].

The primary purpose of the first step was to determine if common task-related functional activity was grouped together as a small number of sICs. All data were visually inspected to determine which spatial maps corresponded to the experimental block design by examining the time series associated with each sIC (through the GIFT toolbox). The results (in detail below) showed that the associated time series of two sICs followed the experimental block diagram across all six oculomotor experiments, consistently revealing activity in three common vision-related regions (the frontal and parietal lobes in one sIC and the cerebellar vermis in the second sIC). Due to the consistency of the spatial maps obtained across the six oculomotor experiments, we sought to investigate the temporal time series from the functional activity within the

spatial maps. In each of the three physiological regions from the experimentally related sICs, an ROI was defined by extracting 20 voxels centered on the location of most significant activity, as quantified by the z-scores. Thus, equal-sized and highly significant ROIs from each individual could be entered into tICA in the next step. To determine the significance of activity within each voxel of a sIC, the GIFT toolbox calculated the z-score of voxels in each data set. For each sIC, a significance threshold of z-score > 2.0 is used for display in overlays of the high-resolution anatomical image; this will be discussed in the Results section (Figure 6.4).

For the second step, ("Individual Subject tICA per ROI," as shown in Figure 6.2, Step 2), tICA was performed using the Fast ICA program [234, 244]. In order to choose an appropriate number of tICs to be calculated, we first conducted a PCA of each 20 voxel ROI to calculate how many components were required to account for 90% of the variance. Depending on the subject, between two and five components were needed; hence, computed five tICs were computed for each ROI. It was then validated that the tICA did produce at least one component, which was highly correlated with the pattern of the experimental task inducement. An example of this is given in Figure 6.3A, which shows correlation in each of the five tICs of a single ROI with the experimental block design for the eight subjects in an experiment. For each subject, an asterisk marks the component with highest correlation to the block design. An example of the time series is shown in Figure 6.3B.

The third step in our image analysis (Figure 6.2, Step 3), "Group- Level tICA per ROI," takes the collected 40 tICs from step 2 (such as those represented by the matrix in Figure 6.3A) as the input data set for another tICA. For each ROI in this step, Fast ICA

was again used to calculate five temporal components, which now represent group-level information across subjects to be used in the final analysis.

In summary, the strategy behind this hierarchical process was to specify ROIs involved in the task-activated paradigm first using sICA and then trimming each data set through the use of z-scores. Next, a multistage tICA was used to determine a time series response representing each ROI that most significantly followed the experimental design, first for individual subjects (conventional tICA) and then as a group-level tICA. The novelty of this hierarchical ICA process was in collecting the tICs of individuals produced in Step 2 to form a group-level data set as an input to another tICA for Step 3. The final tICs provided a statistically independent source set from which analysis with group-level statistical power can be made.

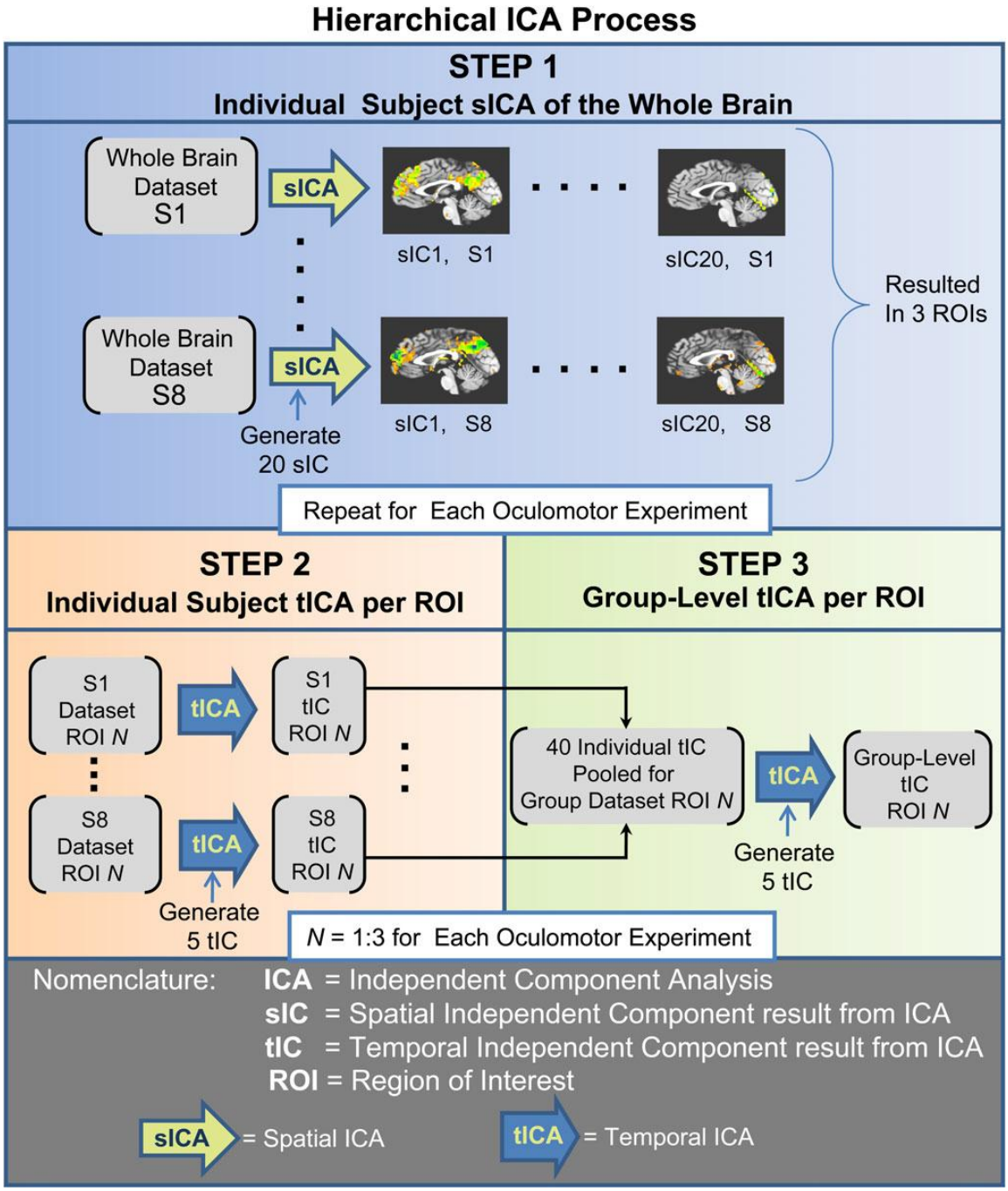

Figure 6.2 (Color online) Hierarchical ICA process (repeated for each oculomotor experiment). Step 1: "Individual Subject sICA of the Whole Brain" was first conducted on the individual data sets, producing 20 sICs from which 3 ROIs of 20 voxels each were determined by visual inspection and z-score criteria. Step 2: "Individual Subject tICA per ROI" started with each 20 voxel ROI identified in Step 1 and produced five tICs per subject per ROI. Step 3: "Group-Level tICA per ROI" collected or pooled the five tICs from all of the eight subjects per ROI from Step 2. These 40 time series were entered into another tICA to generate five group-level tICs per ROI.

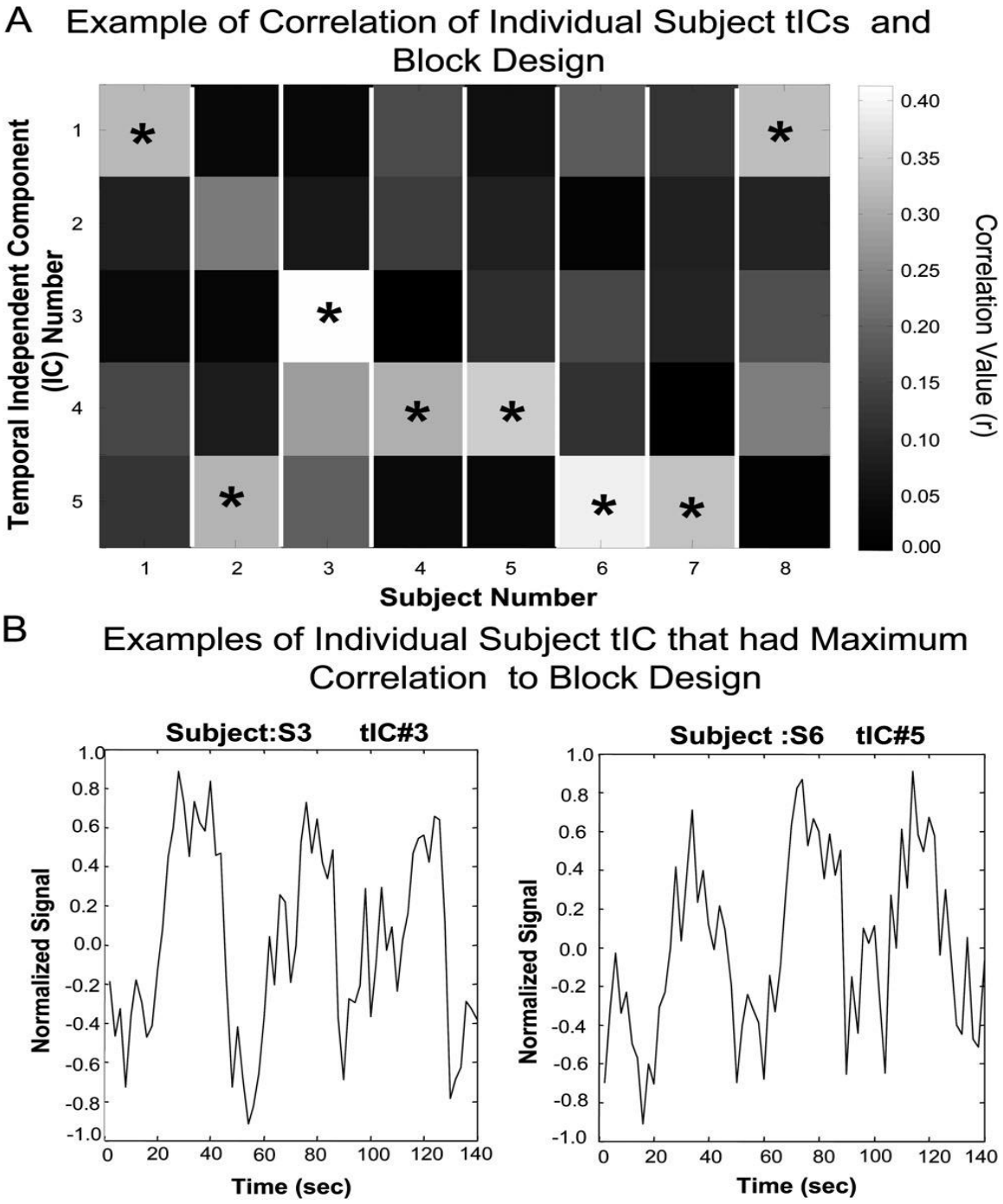

Figure 6.3 (A) Example of eight subjects' five tICs shown within each column (from one ROI of one of the oculomotor experiments) correlated with the experimental block design. The r value is denoted by the grayscale. The tIC per subject with highest correlation to the block design is marked with an "*". The 40 individual tICs are entered into the "Group-Level tICA per ROI." (B) Examples of tICs from two subjects, which had maximum correlation with the experimental block design.

6.3 Results

Before data analysis could begin, motion correction was performed as necessary. Six motion-related parameters were computed and corrected for each subject during each of the scans. The largest average degree of rotation was 0.1 deg ± 0.1 and 0.2 deg ± 0.1 in the pitch direction for the saccade and vergence data sets, respectively. The largest average amount of movement within a plane was 0.3 ± 0.2 mm and 0.3 ± 0.3 mm in the inferior to superior plane for the saccade and vergence data set, respectively. The functional data set resolution was 3.4 × 3.4 × 5 mm; hence, the average motion was much less than a voxel edge length. For this data set, headmotion was not problematic; hence, all data were utilized for this analysis.

Figure 6.4 shows a typical representation of the spatial maps of the two most common sICs, which were observed from the six different oculomotor experiments from Step 1 of the Hierarchical ICA process. The high-resolution anatomical image is shown with the functional overlay (only significant activity with a z-score > .2.0) where each experiment type is represented. After careful inspection of the data sets for the six oculomotor experiments, each subject was determined to have shown functional activity in the frontal and parietal areas in one sIC and cerebellar vermis activation in a separate sIC. These time courses associated with these individual sICs followed the experimental task design. The most significant activation (quantified via the z-score) for these two sICs predominantly resided in the midsagittal slice (Talairach Coordinate Left/ Right = 0). These two spatial components (frontoparietal and cerebellar) were consistently observed in all subjects for all six oculomotor experiments. The three ROIs (frontal, parietal, and

cerebellar areas) in these maps were then investigated with Fast ICA, as described in Steps 2 and 3 of the hierarchical ICA.

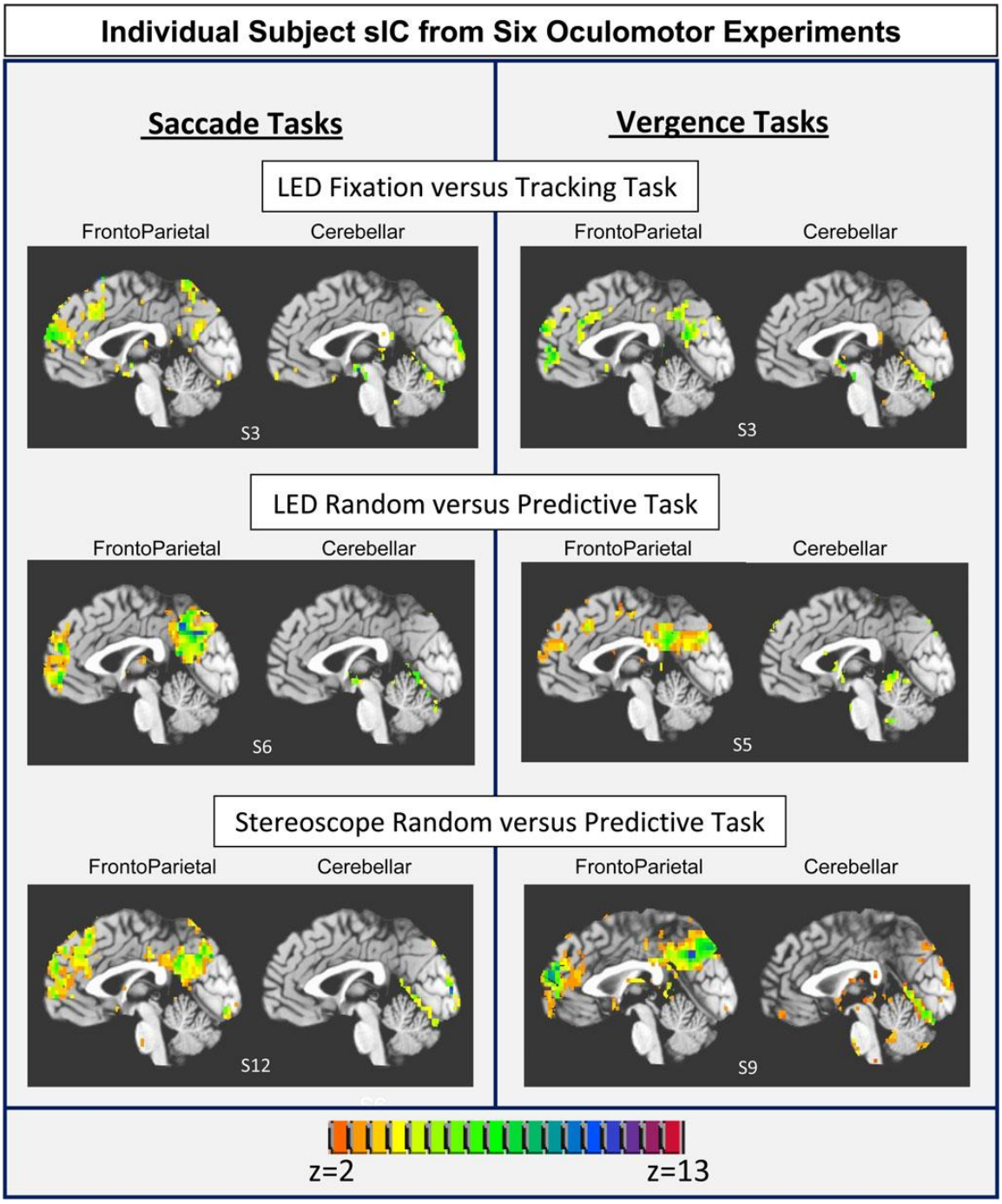

Figure 6.4 (Color online) Individual subject sICA. Typical representation of one subject's ICs for each of the six oculomotor experiments. Saccade tasks are shown on the left and vergence tasks are shown on the right. The upper row is from the fixation versus random eye movement experiments stimulated with LED targets (experiments 1 and 2). The middle and bottom row data are from the random versus predictable eye movement

experiments stimulated using LED targets (experiments 3 and 4) and the stereoscope (experiments 5 and 6), respectively.A high-resolution anatomical image is shown with functional data overlaid where only functional data with a z-score > .2.0 are displayed. For all subjects studied, one sIC contained frontoparietal activation and a separate sIC contained cerebellar activation. Data are from the midsagittal slice (Talairach–Tournoux coordinates L/R = 0 mm).

The Group-Level tICA per ROI (Step 3 from Figure.6.2) calculated a total of five tICs for the frontal, parietal, and cerebellar regions for each of the six oculomotor experiments. To identify which grouplevel tIC showed the most common behavior compared to each individual subject tIC set, a maximum correlation analysis was conducted. All five of the group-level tICs were correlated with the five individual subject tICs from each ROI in each oculomotor experiment. Since there was one set of group-level tICs and eight sets of individual subject tICs, eight maximum correlations were tabulated. Figure. 6.5 plots the mean of these maximum correlations ± 1 s.d. for each ROI and experiment using the Pearson correlation coefficient r value. The range in maximum correlations between the group-level tICs and individual subject tICs was r=0.3–0.6, with an average and s.d. of r=0.41±0.07, r=0.39± 0.05, and r=0.41±0.12 for the frontal, parietal and cerebellar components, respectively, from the six oculomotor experiments. The mean ± s.d. of maximum correlations between each group-level tIC with the experimental block design were r=0.51±0.04, r=0.45±0.08, and r=0.42±0.08 (range of r = 0.3–0.6) for the frontal, parietal, and cerebellar ROI for the six oculomotor experiments, respectively. Hence, these group-level tICs appear to be highly correlated both among the individual subject's tICs and with the experimental block design.

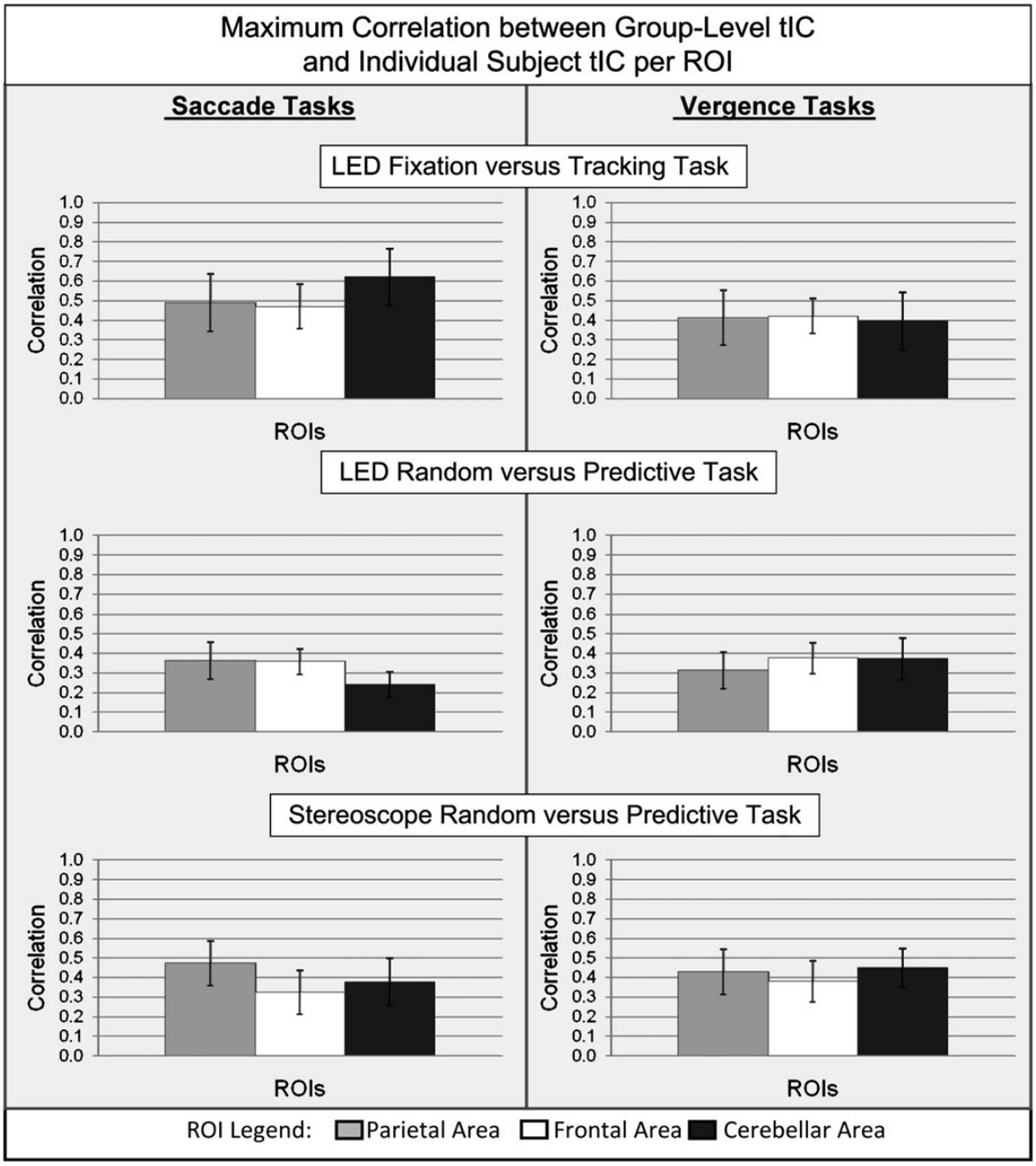

Figure 6.5 Determination of which one of the five group-level tICs from each ROI had the greatest correlation with the five individual subject tICs. The Pearson correlation coefficients (r) are plotted as the average ± 1 s.d. Data from the saccade experiments are shown on the left and from the vergence experiments are shown on the right. The upper row plots are data from the fixation versus random eye movement experiments stimulated using LED targets (experiments 1 and 2). The middle row plots are data from the random versus predictable eye movement experiments stimulated using LED targets (experiments 3 and 4). The bottom row plots are data from the random versus predictable eye movement experiments stimulated using the stereoscope (experiments 5 and 6).

Figure 6.6 plots the group-level independent components from the saccade (left plots) and vergence (right plots) fixation versus random eye movement experiments from the parietal (red lines), frontal (blue lines), and cerebellar (green lines) ROIs. One behavioral signal trend observed in these group-level tICs is that the cerebellar initial transient BOLD signal change is delayed in comparison to the initial transient BOLD signal change from the parietal and frontal regions. This could be described as a longer latency for a BOLD signal change in the cerebellum compared to that in the other regions.

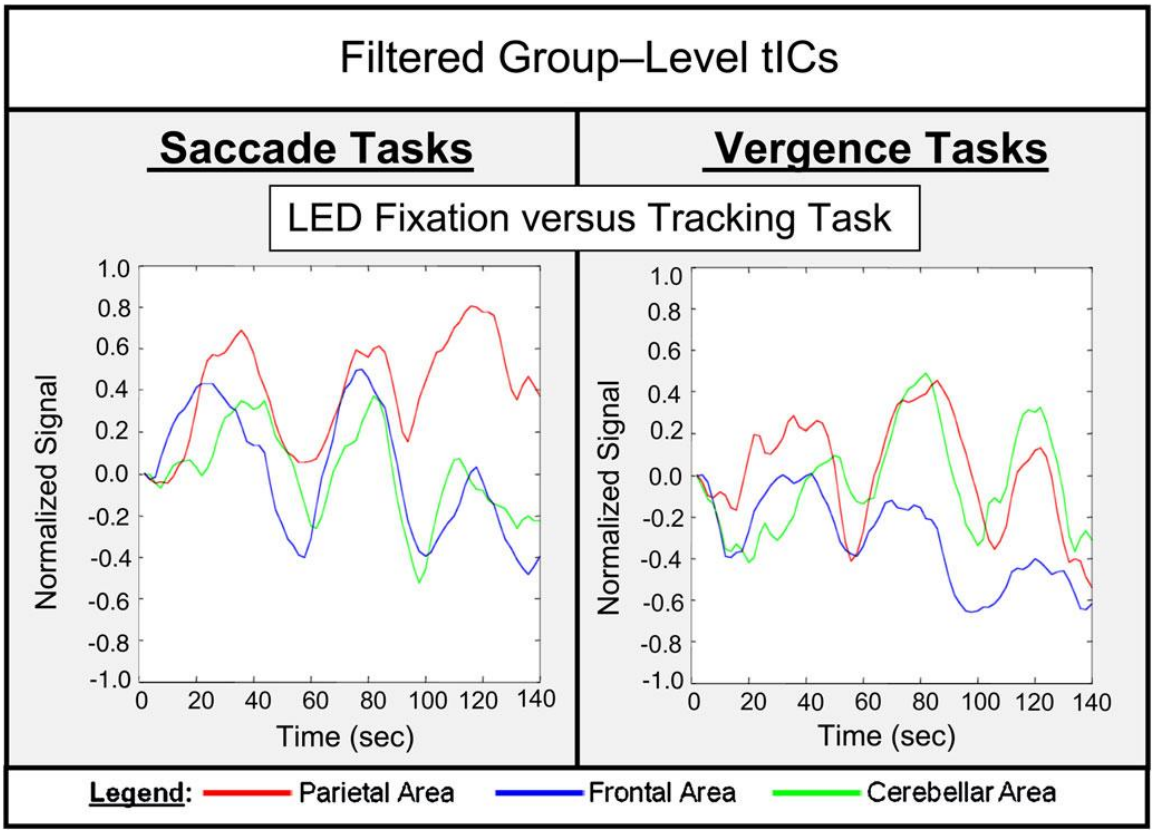

Figure 6.6 (Color online) Group-level tICs from the parietal (red lines), frontal (blue lines), and cerebellar (green lines) ROIs. The oculomotor task of fixation versus random tracking is shown with the saccade experiment in the left plot and vergence experiment in the right plot.

6.4 Discussion

6.4.1 Segregation of sICs

An important finding of this study was that for all six oculomotor experiments, one sIC contained frontoparietal functional activity and a separate sIC contained cerebellar vermis functional activity. The six experiments were composed of two types of cognitive tasks (fixation versus random eye movements and predictable versus random eye movements), studied with two types of eye movements (vergence and saccade eye movements) and two types of visual targets (LEDs and a stereoscope). This consistent segregation of frontoparietal and cerebellar sIC suggests a centrally shared neural resource is utilized within the saccade and vergence networks.

ICA has been conducted in other vision studies, which also report the existence of a frontoparietal sIC [38, 226]. Dyckman et al. (2007) studied three saccadic tasks: 1- fixation versus saccades, 2- fixation versus antisaccades (saccades to a location opposite the target), and 3- saccades versus antisaccades. The study did not image the cerebellum. They reported differentiation in two main components: one component located in the striatum and visual areas and a second in the parietal and frontal regions, with the latter delayed compared to the former. Using a similar visual stimulus of fixation versus saccade protocol, it is also reported here segregation of frontal and parietal activity in a single sIC.

Calhoun et al. [38] studied a visual perception task, which is a more cognitively demanding task than the simple oculomotor tracking studied in this study. They reported that more regions were functionally active, and more sICs following the block design were observed. Interestingly, their visual perception study reported several components

where one sIC contained frontoparietal activity and a second sIC contained cerebellar activity [38]. For the visual tasks conducted, it is also reported in here frontoparietal activity in one sIC and cerebellar activity in a separate sIC.

6.4.2 Differentiation in Group-Level tICs Between the ROIs

A hierarchical ICA is processed to study group-level tICs in order to determine differences between the components originating from the parietal and frontal ROIs compared to those in the cerebellar ROI. A delayed latency of the initial transient change is observed in the BOLD signal of the cerebellar vermis tIC as compared to the parietal and frontal tICs. These signal variations could stem from differences in the neuronal behavior of the signal, from differentiation in the hemodynamic response due to neurovascular coupling or from a combination of both resulting in differences in the shape or temporal properties of the BOLD ROI specific signals.

6.4.3 Neuronal Evidence of Shared Behavior Between The Parietal and Frontal Areas

Differences in neuronal firing rate may be due to differences in the functional connectivity and behaviors of the ROIs. A recent review by Wurtz [102] discusses a potential framework for why the brain perceives stable images when actually a series of snapshots produced by saccadic eye movements is viewed. The aspect of the review most relevant to this research is the discussion of studies in support of a retinotopic hypothesis to explain how the brain may achieve visual stability. Within the frontal and parietal lobes, neurons have been identified which have shifting receptive fields. These neurons are hypothesized to provide anticipatory activity with each saccade and to be driven by a

corollary discharge, also referred to as an efference copy [102]. Duhamel et al. [245] showed that neurons in the parietal cortex changed or "shifted" their visual sensitivity in anticipation of the upcoming saccade, a process, which is termed a shifting receptive field. Specifically, single-cell neuronal evidence from nonhuman primates shows that neurons with shifting receptive fields have been reported from the lateral intraparietal (LIP) area [149, 245-247], as well as from cells within the FEF [248-250]. There is also fMRI evidence for the presence of shifting receptive fields in the parietal area in the human brain [251] and within the frontoparietal areas [252, 253].

With regard to the results of this study, it therefore is speculated that the shared shifting receptive field behavior observed in both the LIP and FEF may in part account for segregation of the parietal and frontal functional activity, which is spatially distinct, into a single sIC observed in our individual subjects. The group-level tICs for the parietal and frontal ROIs have similar temporal and behavioral/signal shape properties as well. Analogous research is not available for vergence, but perhaps similar mechanisms are employed since vergence and saccades share many neural network resources.

6.4.4 Neuronal Evidence of Different Timescales for Correction of Error within the Cerebellum

A myriad of information exists on the study of the cerebellar activity within saccadic eye movement research. Saccades reach angular velocities of 500 deg/s for a 20 deg stimulus in humans [254] and have been modeled as a preprogrammed (also termed as a feedforward) system. Yet, the brain accurately guides the eyes to a target potentially through adaptive control [255-258]. During the last decade, many investigators studying saccadic eye movements have supported the idea that the cerebellum is utilized for motor

learning, as observed via correction of errors through a gain adaptation mechanism [65, 259-262]. The adaptive response to errors has been reported to have two or more timescales: a fast timescale that learns substantially from error but has poor retention and a slower timescale that learns little from error but has good retention [263].

In this present study, we observed a lag or increased latency in the initial transient behavior of the BOLD response in the cerebellar group-level tICs compared to the frontal and parietal group-level tICs (Figure. 6.6). As the experiment progressed, the temporal parameters between the three ROIs looked more similar. Therefore, the cerebellar tIC may have an initial lag that diminishes potentially from the reported differences in timescales of motor learning within the cerebellum.

For the six oculomotor experiments, these results consistently isolate the cerebellar activity as a single sIC, which perhaps may arise from the temporal differences observed between the cerebellar group-level tIC and the frontal/parietal group-level tICs. The functionality of the cerebellum (implicated as the region where motor learning occurs via error reduction) may also be distinct from the shared behaviors observed in the frontal/parietal ROIs (implicated to have shared resources to maintain visual stability). These distinct neuronal behaviors may result in different shapes to the BOLD signal and support in part the segregation of the cerebellar from the frontoparietal functional activity within the oculomotor network using ICA.

6.4.5 Neurovascular Coupling

Functional MRI provides an indirect neuronal measurement. This study relied upon the quantification of the local blood oxygen level-dependent contrast; hence, differences in the neurovascular coupling mechanisms could potentially affect these results [77, 264].

The BOLD signal changes are influenced by vascular factors, including vascular compliance (the tendency of arterial tissue to dilate in response to neural activity) [217, 218] and vascular density (the distribution of the capillary bed density over the cortex) [217, 219, 220]. A recent study suggests that forty-percent of the variance within the BOLD fMRI signal from the cerebellum and brainstem can be described by the cardiac and respiratory physiologic signals [221]. Hence, it may be differences in neurovascular coupling that may in part explain the segregation of frontoparietal activity in one sIC and cerebellar activity into a separate sIC.

6.4.6 Previous Studies Summarizing Differentiation Between Saccade and Vergence Data Sets

This present research studied the commonality between the vergence and saccade data sets comprised of a simple fixation versus random eye movement task and a more cognitively demanding random versus predictive task using vergence and saccade eye movements. It has been previously published detailed investigations in the differences between these data sets using the beta weights from a conventional GLM with a voxel-wise paired t-test [31, 32]. As a summary of those results here for a comparison across methodologies showed which areas of activation were common and which were different within the vergence and saccade data sets [31, 32], a GLM analysis does not reveal statistically independent spatial maps from which to investigate ROIs that may be consistently grouped together. Studying how functional activity that was observed within both the saccade and vergence data sets would be separated into different sIC, and how the temporal properties of the BOLD signal varied between sIC were the goals of this current investigation.

Previous research results by the Vision and Neural Engineering Labarotory of NJIT uncovered that more cortical areas (specifically, the inferior parietal area of Brodmann 39 and the superior ventral–lateral prefontal cortex) were functionally activated when prediction was elicited than when simple fixation versus random tracking tasks were performed (within both vergence and saccade data sets) [31]. However, during the fixation versus simple random tracking task, significant activation in the brainstem was observed, which was not apparent within the prediction data sets [31, 32]. This observation is due in part to the nature of the experimental design. For instance, the simple random tracking task data sets used fixation versus eye movements as opposed to the prediction experiments, which used eye movements throughout the experimental design. For the simple random tracking task, activation in the midbrain within the vergence data set was observed but not the saccade data set. In addition, activation in the superior colliculus was observed within the saccade data but not the vergence data. Since these areas were different between data sets, it is suspected that these regions would not appear within a common spatial map as this present study showed. This study investigates the spatial maps that were common and suggests shared neural processes between the saccade and vergence neural circuits.

In preceding studies, differentiation between the vergence and the saccade data sets was also observed within the FEF. The vergence functional activation was immediately adjacent and significantly more anterior compared to the saccade functional activation. Differentiation in FEF was observed in both the random tracking and the prediction data sets [31, 32]. Single-cell recordings from primates have also shown differentiation within FEF where vergence-encoding cells are located immediately

anterior to the cells that encode for saccade eye movements [14]. Within this present study, the observed BOLD signal from the frontal area was similar to that of the parietal area in both the vergence and saccade data sets revealed through the hierarchical ICA algorithm.

The hierarchical ICA algorithm shows that the temporal characteristics of the frontal and parietal ROIs are similar which previous studies by Vision and Neural Engineering Labarotory of NJIT did not investigate. ICA belongs to a class of data-driven analyses that can yield information about similarities between ROIs, which the more conventional general linear models do not necessarily provide.

6.4.7 Vergence Eye Movements Evoked Using a Stereoscope vs LED Targets

Eye movement studies have documented the differences between vergence eye movements with variations in disparity and accommodative stimuli [229-231]. Several types of stimuli were used within these studies to evoke vergence eye movements, which included: visual stimuli observed through a pinhole (no accommodation), a Distribution of Gaussian stimulus (negligible accommodation), stereoscope (constant accommodation), and physical LED targets located at different depths (varying accommodation). The amount of retinal disparity presented within each of these stimuli was the same. These studies showed that accommodative vergence does not influence the initial disparity vergence peak velocity. However, the accommodative vergence component begins approximately 100–200 ms after the latency seen in disparity-driven components as observed through a secondary increase in the s.d. within the velocity responses [229-231]. Hence, observed differences in vergence eye movements are dependent upon the amount of accommodation presented. In addition, single-cell

recordings have reported differentiation between accommodative and vergence responses. Within the posterior interposed nucleus of the cerebellum of rhesus monkeys, cells are modulated by disparity and/or blur stimuli eliciting accommodative and vergence responses. There was differentiation between cells where 34 of the 70 modulated activity during just vergence responses and 11 of the 70 modulated activity with accommodation stimuli. The remaining 25 of the 70 modulated their response to both accommodation and disparity movements [23].

Integrating the results from the eye movement studies and the single-cell primate research, it is hypothesized that differences between the stereoscope and LED data sets may be observed. Differences within the cerebellum were specifically searched. Statistically significant differences between the data sets generated from the stereoscope versus the LED visual stimuli were not observed. In the future, the experiments using a within subject design and a reduced FOV concentrating on the posterior interposed nucleus will be planned. It is unknown if fMRI, even with the reduced FOV, can observe this fine differentiation. Although these two vergence data sets (one evoked using a stereoscope and the other using LED targets) did not show significant differentiation, on the other hand, similar spatial maps when using sICA was observed, which lends further support of common segregation of ROIs within the vergence and saccade visual circuits.

6.5 Conclusion

This study is the first to report segregation of frontoparietal and cerebellar sICs during a fixation versus random vergence tracking experimental task and during a random versus predictable eye movement task within the saccade and vergence systems using sICA of fMRI data. This data confirm the finding of a frontoparietal sIC in a fixation versus

saccade task reported by Dyckman et al. [226]. This study supports that saccade and vergence eye movements share common functional areas that are segregated into similar sICs suggesting shared central processing between the saccade and vergence neural circuits. The data also suggest that the cerebellar tIC has a delayed latency for the initial transient change in the BOLD response compared to the frontal and parietal group-level tICs, which had more similar temporal properties. The differences in signal behaviors observed in the group-level tICs may be due in part to neuronal and/or neurovascular coupling differences, which result in temporal or signal behavioral shape differences of the tIC signal.

CHAPTER 7

REGION OF INTEREST BASED ANALYSIS COMPARISON TO GLOBAL (WHOLE) BRAIN ANALYSIS (SPECIFIC AIM 5)

Purpose: In the present investigation, it is hypothesized that region of interest (ROI) based analysis for frontal, parietal, brainstem and occipital areas shows finer sensitivity of functional activity with comparison to global (whole) brain analysis for both individual subject and group levels.

Methodology: 3T scanner is used for collection of fmri data where random tracking vergence experiment is conducted as an experimental paradigm. There are two approaches to the functional imaging data; 1-ROI based analysis for frontal, parietal, brainstem and occipital areas, and 2- global (whole) brain analysis at subject and group levels. In addition to that, maximum correlation of functional activity is quantified for each ROI with comparison to global (whole) brain analysis. Additionally, datasets are assessed by paired *t*-test. Further analysis is focused on group-level comparison between these approaches by application of hierarchical indepent component analysis (ICA).

Results: ROI based analysis shows more sensitive results than the global (whole) brain analysis for functional imaging data. Improvement of maximum correlation for ROI based approach for frontal ($p < 0.04$), parietal ($p < 0.0001$), brainstem ($p < 0.02$), and occipital regions ($p < 0.05$) at the statistically significant level. Paired *t*- test robusts the results observed by showing differences for the ROIs chosen. Group-level analysis by implementing hierarchical ICA supports what has been obtained at the individual level.

Conclusion: ROI based analysis can provide more sensitive outcomes at both individual and group levels. This approach can be implemented to analyze cortical and also subcortical regions like brainstem for finer quantification of their involvement to the task-related experimental paradigms.

7.1 Introduction

The world surrounded around people is in three dimensional (streoscopy) where vergence system is one of the main tracks of conveying of visual information. Stereoscopic vision helps one to have depth of perception for the objects in the external world. As covered in previous chapters, this visual system is highly complicated requiring frontal [14, 32, 106], parietal [63, 64], occipital [126, 197], and subcortical such as midbrain of brainstem [15, 19, 50] areas.

As mentioned in previous chapter, correlates of metabolic and direct neuronal changes can be detected by fMRI [92, 93]. General linear model (GLM) as a statistical method determines what cortical and subcortical areas are functionally active to the task-related experimental paradigm. Independent Component Analysis (ICA) is also implemented as a data-driven method to define functional connectivity [47, 184]. ICA and its implementation in the field of vision [38, 226] showed successful results to define functional organizations within complex networks. Moreover, Vision and Neural Engineering Laboratory of NJIT showed that hierarchical ICA at the group level can be used to segregate brain connectivity such as frontoparietal and cerebellar components for both saccadic and vergence networks [87].

The methods emphasized above do not focus on region of interests (ROIs) rather than that approach in these techniques is for global (whole) brain. These methods are

implemented to map task-related activity via defining clusters of activated voxels for the entire brain. ROI based analysis can be very powerful for further analysis of particular regions of interest (ROIs) for reasons which are discussed in a brief review paper by Poldrack [265]. In this review paper, the advantages of ROI based analysis listed as 1- exploring the pattern of signals in a particular ROIs across different conditions like functional activation and lack of functional activation such as reducing the effects of outliers, 2- providing statistical control like decrease of Type I error because of studying a set of ROIs instead of entire brain, 3- examining the functional activity of a ROI to detect their sensitivity for some other experimental cases [265]. Additionally, Castonon and colleagues showed that ROI based analysis is a candidate of stronger method which can provide more sensitive results to delineate the effects of conducted experimental paradigms in comparison to the standard methods [266].

ROI based approach has wide range of applications; for example, Dinstein and colleagues used ROI based technique to define the central role of intraparietal sulcus (aIPS) for motor control and movement perception [267]. Moreover, the importance of this method is also supported by Schwarzlose and colleagues [268]. They showed that fMRI ROI based approach can be used to explore distribution of category and location information within object-selective regions in visual cortex. Hence, ROI based analysis can be a useful analysis method to understand the role of the ROI for the task that has been conducted.

The main purpose of this investigation is to apply ROI based analysis on frontal, parieatal, brainstem and occipital areas in comparison to global (whole) brain analysis for the random tracking vergence experiment. In here, it is hypothesized that ROI based

analysis derives more sensitive results at both individual and group levels in comparison to global (whole) brain analysis.

7.2 Methodology

7.2.1 Subjects

Fifteen subjects participated in this investigation (8 female and 7 male with an age of 27 ± 3 years). As mentioned in previous chapters, near point of convergence (NPC) was measured by bringing the tip of a pen towards the subject along her/his midline [68]. All subjects had NPC value of less than 6 cm. Randot Stereopsis Test was used to assess participant's binocular vision. All subjects had normal stereoptic vision.

This investigation had approval by the New Jersey Insitute of Technology (NJIT) and University of Medicine and Dentistry of New Jersey (UMDNJ) Institution Review Board (IRB). Consent forms were signed by all subjects.

7.2.2 Materials and Apparatus

Images were acquired using a 3.0 Tesla Siemens Allegra MRI scanner with a standard head coil (Erlangen, Germany). Visual stimuli were a set of non-ferrous light emitting diode (LED) targets that formed a line 5 cm in height by 2 mm in width located at three positions.

7.2.3 Imaging Instrumentation and Procedure

Functional imaging instrumentation and the procedure was similar to the previous chapters (see chapters above). The subject was positioned supine on the gantry of the scanner with his/her head along the midline of the coil. All participants were instructed to limit head motion. Foam padding was used to restrict additional movement and motion

correction software described below was utilized to ensure head motion artifacts were minimal. Ear plugs were used to reduce scanner noise by up to 30 dB while still allowing the participant to hear instructions from the operators during the scan. In all experiments, the radio frequency power deposition and field-switching rate were kept below levels specified by the U.S. Food and Drug Administration (FDA).

All functional scans used a T2* weighted echo planar imaging (EPI) sequence. The imaging parameters were field of view (FOV) = 220 mm, 64 x 64 matrix, time of repetition (TR) = 2000 ms, time of echo (TE) = 27 ms and flip angle = 90°. The whole brain was imaged in an axial configuration where 32 slices were collected and each slice was 5 mm thick. The resolution was 3.4 x 3.4 x 5 mm. After all functional tasks, a high resolution MPRAGE (magnetization-prepared rapid gradient-echo) data set was collected. The MPRAGE imaging parameters were: 80 slices, FOV = 220 mm, slice thickness = 2 mm, TR = 2000 msec, TE = 4.38 msec, T1 = 900 msec, flip angle = 8º and matrix = 256 x 256, which resulted in a spatial resolution of 0.9 x 0.9 x 2 mm.

7.2.4 Functional Experimental Design

LED cues were used during scanning. 2°, 3° and 4° of combined visual targets were oriented aligned with the subject's midline as shown in Figure 7.1A. Experiment was conducted in complete darkness. Only one visual target was illuminated at a time. Fixation versus random tracking vergence experiment was the experimental paradigm. Standard block design was used with combination of "off" and "on" phases. During "off" phase, there was no visual stimulus. Subjects were asked to look at the closest visual target during this phase. "On" phase where vergence step stimuli was illuminated in a random duration of time between 0.5 to 3.0 seconds. Figure 7.1B shows the phases of the

experiment. The subject could not anticipate the timing of the visual stimulus. Total duration of the experiment was 140 seconds.

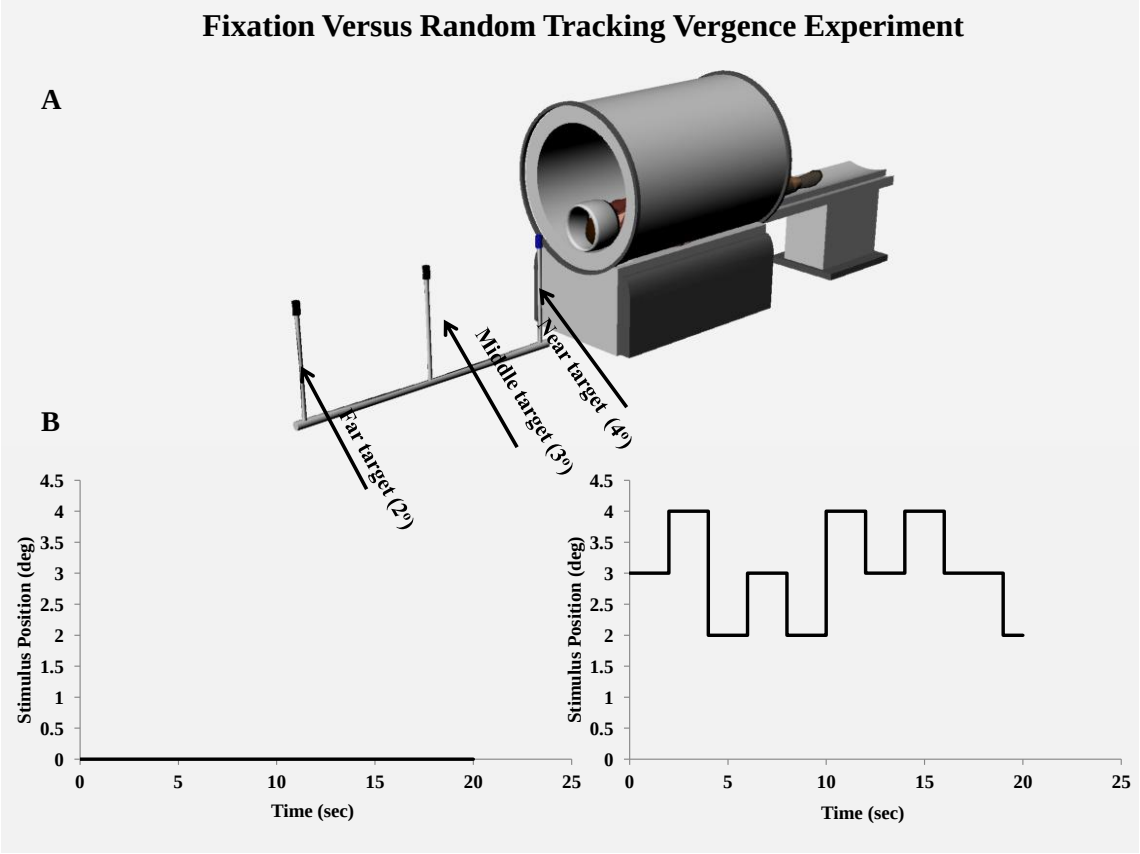

Figure 7.1 Experimental set-up and design. The schematic of the custom fMRI compatible light emitting diodes (LEDs) for fixation versus random tracking experimental paradigm with "off" and "on" phases.

7.2.5 Data Analysis

7.2.5.1 Individual Subject Analysis using a Data Driven Reference Vector. Data were analyzed with AFNI (Analysis of Functional Images) [73]. In this investigation, there were two types two types of analysis; 1- Region of Interest (ROI) based, 2- Global (whole) brain analysis. Pre-processing steps for both the approaches were kept consistent with each other. Frontal, parietal, brainstem and occipital areas were defined region of interests for the ROI based brain analysis. The roles of these areas were covered in detail

in previous chapters of the dissertation. For example, Vision and Neural Engineering Laboratory (VNEL) of NJIT reported areas within frontal, parietal, brainstem and occipital regional boundaries as neural substrates of the vergence system [32]. Castonon and colleagues showed in their study, defining subject-specific ROI with ROI based brain analysis can offer increased sensitivity [266]. Hence, for each ROI, subject-based masks were drawn as shown in Figure 7.2. Midsagittal view was taken as a reference slice and masking was continued for three upper and lower slices corresponding to the midsagittal slice.

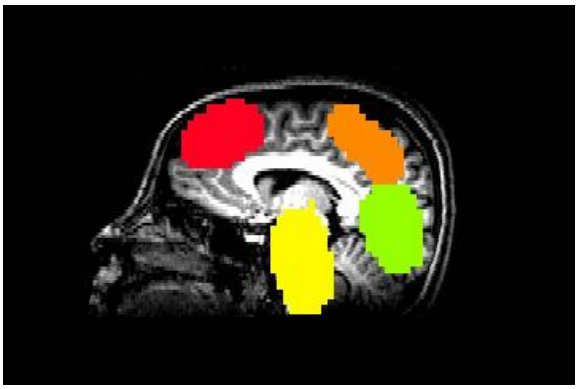

Figure 7.2 Example of ROI masks from a subject.

Time series from each of the voxels from the ROI masks were extracted and used in ICA algorithm. Probabilistic ICA in the Multivariate Explaratory Linear Optimized Decomposition into Independent Components (MELODIC) software from FSL was used to calculate each subject's hemodynamic reference vectors only from the ROI. ROI based hemodynamic reference vectors were chosen based on the criteria of the highest Pearson correlation coefficient with the experimental block design. A general linear model (GLM) regression analysis was used to correlate each chosen ROI's hemodynamic reference vectors with the entire brain. This regression provided to obtain functional activity maps

from each ROI for each individual subject. Individual subject ROI based brain analysis is summarized in Figure 7.3A.

Global (whole) brain analysis steps were similar to the ROI based brain analysis excluding the step of masking corresponding to the ROI. Hemodynamic reference vector obtained from ICA available through the MELODIC software was chosen as similar to the ROI based brain analysis. Hemodynamic reference vector has the greatest Pearson correlation value with the block design used in GLM regression analysis. Functional activity maps were created for each individual subject via GLM like in ROI based brain analysis.

After completion of these steps, maximum and mean correlation values were derived from each ROI masks for each individual subject. Furthermore, same masks were used on the global (whole) brain individual subject's data sets to compare maximum and mean of the correlation values.

7.2.5.2 Group Level Analysis. A hierarchical ICA process [87] has been used for group level brain analysis. The hierarchical ICA analysis utilized to determine group-level hemodynamic reference vectors. First step was to pool each individual subject's chosen hemodynamic reference vectors. Next step was implementation of the FastICA as standard Infomax algorithms available through the sofware toolbox GroupICA of fMRI Toolbox [183]. For each ROI and global (whole) brain analysis, fifteen hemodynamic reference vectors origins from each subject for both approaches were pooled to calculate five hemodynamic reference vectors. One out of five hemodynamic reference vectors was chosen according to the highest Pearson correlation with the block design to represent group-level information across the subjects. Hierarchical ICA and its application were

discussed in detail in Chapter 6 of this dissertation. Finally, group-level functional activity maps were created via GLM regression of these group-level hemodynamic reference vectors. Figure 7.3B briefly summarizes the steps applied. As in indivudual subject analysis, same steps were conducted for ROI based brain analysis and global (whole) brain analysis at group level.

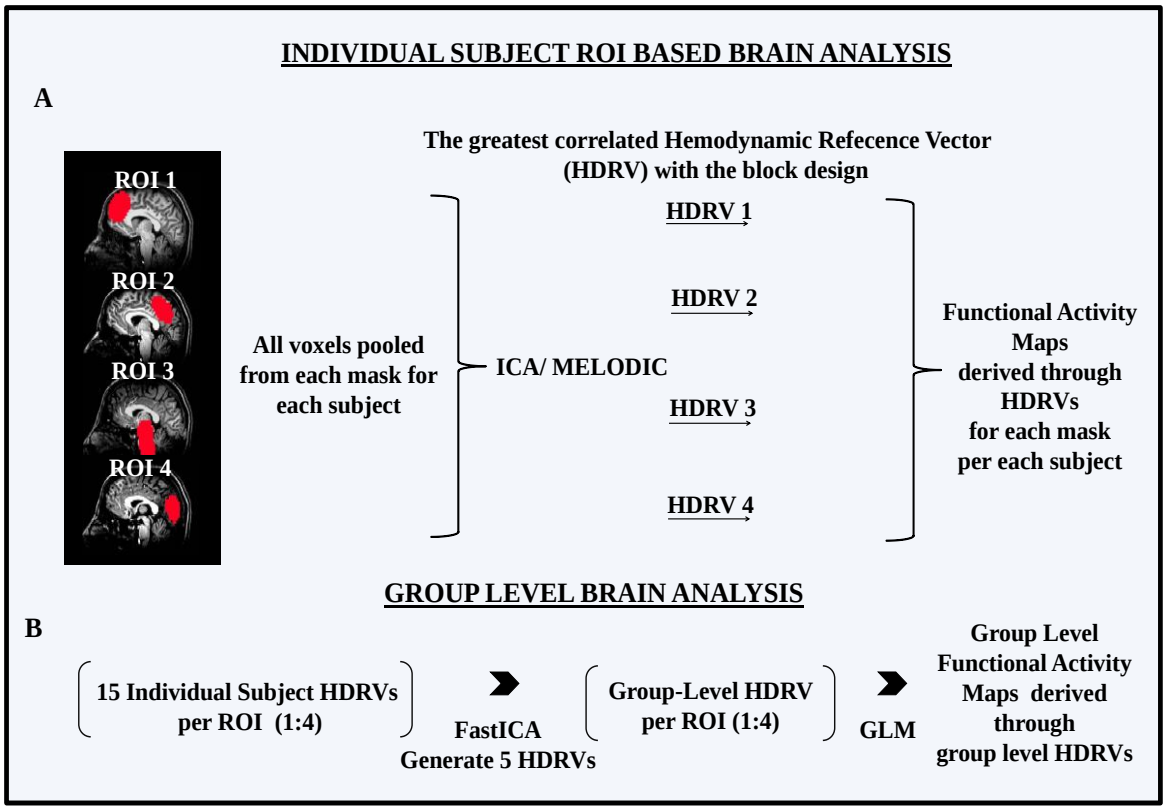

Figure 7.3 Summary of Individual Subject (7.3A) and Group Level steps (7.3B) for ROI based brain analysis.

7.3 Results

Data were analyzed individually for both ROI based brain analysis and global (whole) brain analysis. The functional activity maps for each ROI per subject were compared between methods. Figure 7.4 shows functional activity examples from three subjects that compares ROI based brain analysis versus global (whole) brain analysis. As can be

observed from Figure 7.4, ROI based brain analysis shows larger clusters of functional activity for each ROI than the results global (whole) brain.

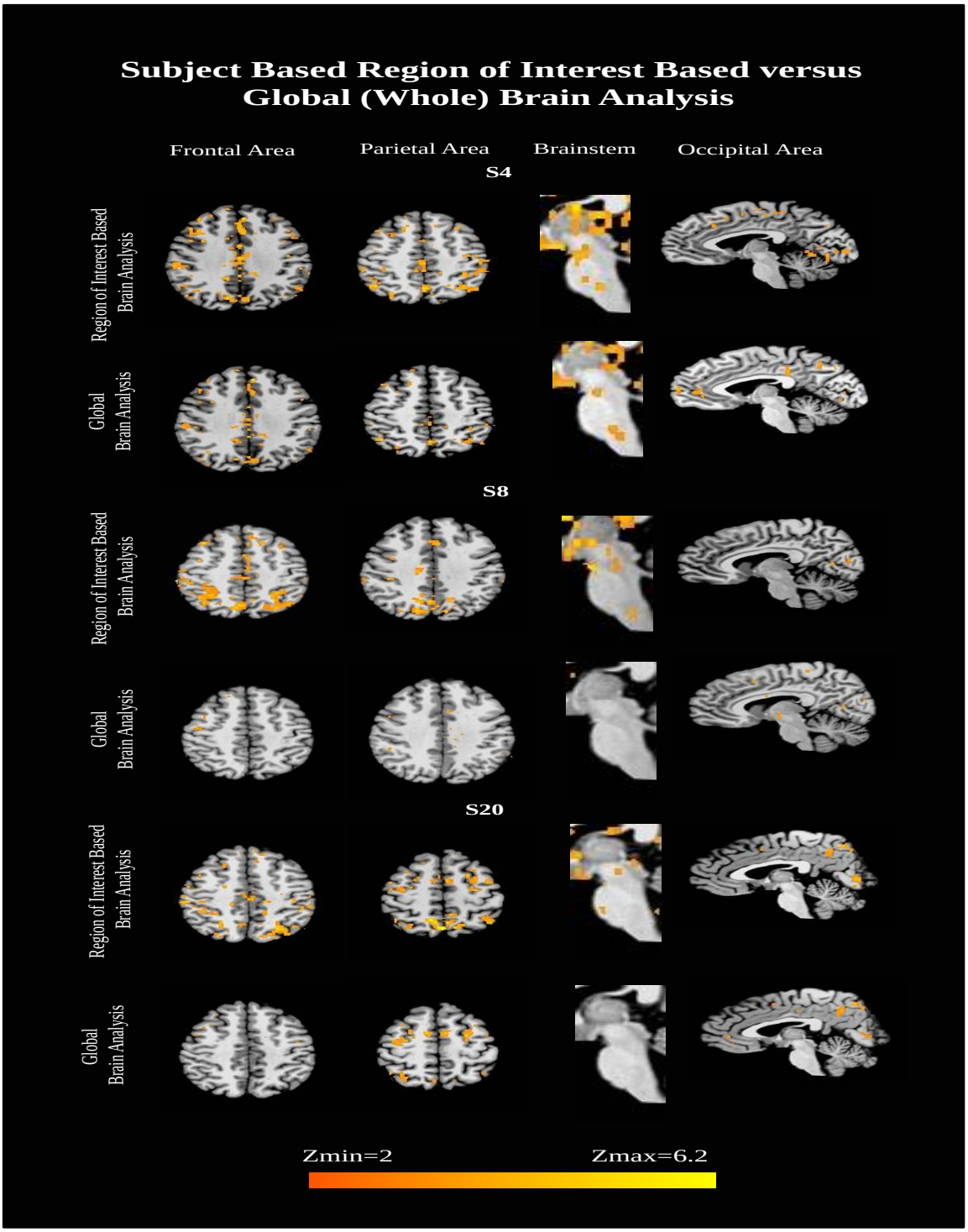

Figure 7.4 Example of functional activity comparison between ROI based analysis and global (whole) brain analysis for three subjects.

There were two approaches for quantification of the difference observed between these methods. First, to determine whether significant functional activitation differences existed between the results of ROI based analysis and the global (whole) brain analysis, the beta weights from general linear model were compared using a paired *t*-test of the fifteen indivudal subjects in a voxel-wise basis to create a statistical significance functional activity maps as shown in Figure 7.5. The statistical difference functional activity maps are displayed using the scaled T-value as the color overlay upon standardized location of significantly different areas of activation.

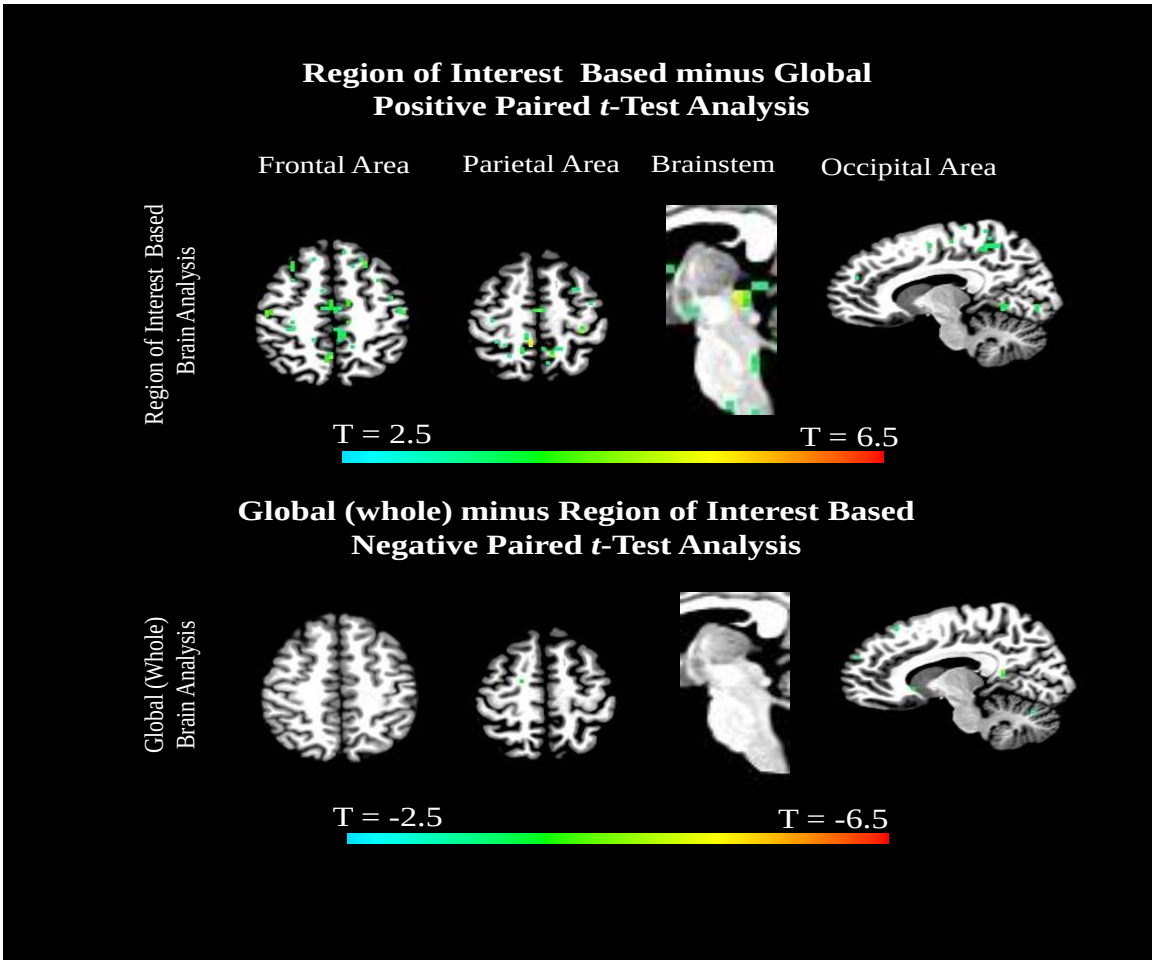

Figure 7.5 The paired t-tests using the beta weights from ROI based and global (whole) brain analysis.

Further analysis continued with calculation of maximum correlation and mean of the correlation values for all voxels from the ROI masks. Same subject-specific ROI masks were used for the global (whole) brain analysis's results to compare with the results of ROI based brain analysis. According to the results obtained, there were statistically significant difference for maximum correlation values between ROI based brain and global (whole) brain analysis. Figure 7.6 shows the comparison of maximum correlation values of fifteen subjects observed for ROI based and global (whole) brain analysis, including their p-values. Although, there was statistically significance in maximum correlation values, the mean of all voxels from the ROI masks did not show any statistically significant difference at individual subject level.

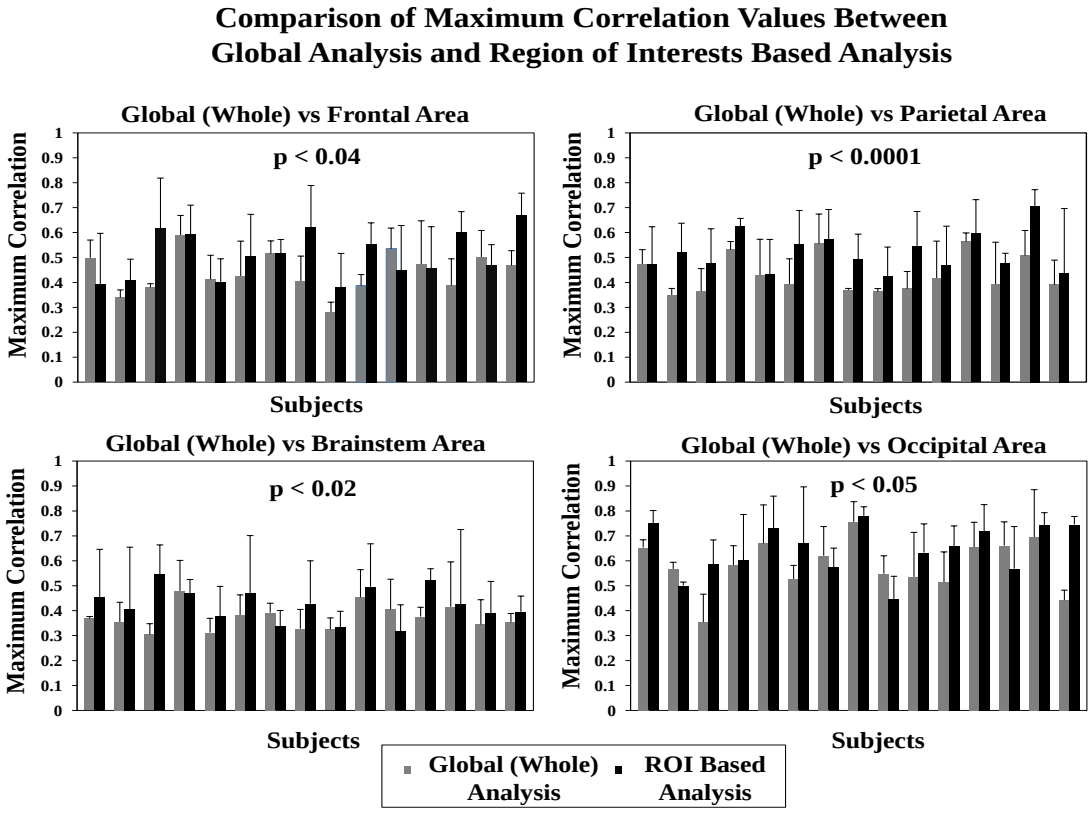

Figure 7.6 Comparison of maximum correlation values between global (whole) analysis and ROI based analysis.

After individual subject level results, group level results are obtained. Group level results are displayed in Figure 7.7 and Figure 7.8. Figure 7.7 shows group level hemodynamic reference vectors of each ROI and global (whole) obtained by using hierarchical ICA.

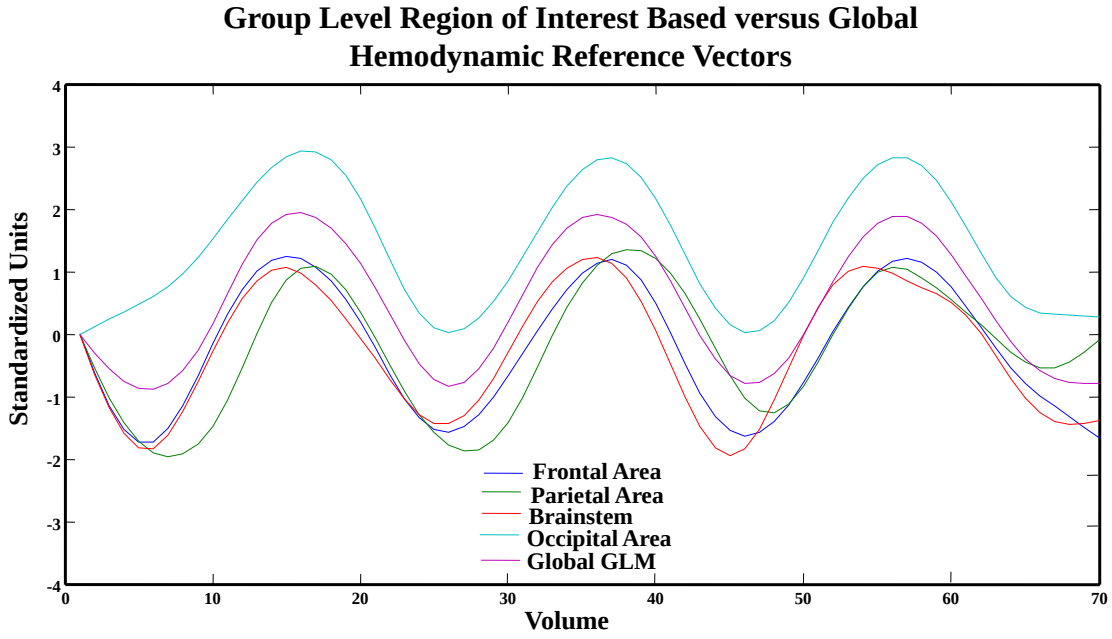

Figure 7.7 Group level hemodynamic reference vectors for ROI based analysis and global (whole) brain analysis. As can be seen from the figure, group level frontal and parietal signals carry similar trend which also shows a latency in contrast to group level brainstem signal. Interestingly, group levels signals from occipital ROI based analyis and global (whole) brain analysis shows similarity.

Figure 7.8 represents group level functional activity maps after regression of hemodynamic reference vectors, showin in Figure 7.7. Figure 7.8 shows that ROI based brain analysis is sensitive to detect functional connectivity between frontal-parietal areas and to show increase in the spatial extent of functional activity on both cortical and subcortical areas. Group level ROI based analysis results for frontal area did not display increase in the spatial extent of functional activity maps in comparison with global (whole) brain analysis, on the other hand, it showed functional connectivity with parietal

area. Group level ROI based analysis results for parietal area indicated both functional connectivity to the frontal area and increase in the spatial extent of functional activity in comparison with global (whole) brain analysis. Furthermore, group level ROI based results for brainstem indicated increase in spatial extent of functional activity. Interestingly, group level ROI based analysis and global (whole) results for occipital area did not represent any difference in comparison to global (whole) brain analysis, however, individual subject level results showed a difference with a $p < 0.05$.

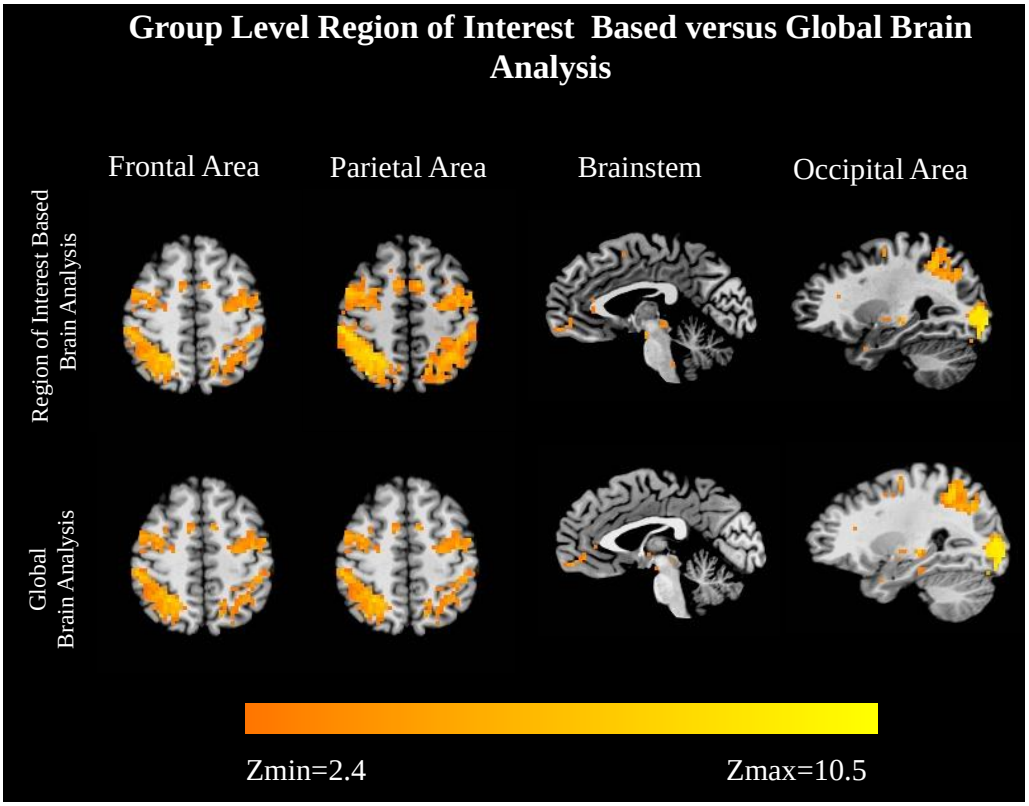

Figure 7.8 Images show group level functional activity for ROI-based analysis (upper images) and global (whole) brain analysis (lower images). Data were overlaid onto a standardized Talairach-Tournoux normalized image.

7.4 Discussion

7.4.1 Overview

This chapter of the dissertation uses a method called as ROI based analysis, whereas most fMRI methods are for global (whole) brain. The comparison between these two fMRI analysis approaches are done where ROI based analysis showed more sensitive results at individual subject and group levels for frontal, parietal, brainstem, and occipital areas.

7.4.2 Region of Interests (ROIs)

In here, frontal, parietal, brainstem and occipital area were selected as ROIs. As mentioned previously, primate investigations shows FEF [14] of frontal, LIP [15] of parietal, midbrain [18] of brainstem, and BA 17 [11] of occipital are some examples for cortical and subcortical areas involved in vergence system. Additionally, fMRI investigations on humans [31, 32] indicates similar areas which are recruited for vergence ocular movements. Based upon previous primate and human studies, ROIs of this investigation were included boundaries of the specific areas mentioned above. In future, masks with the range of ROI-specific coordinates will be targeted. Hence, finer-grained analyses might provide more sensitive exploration of how that cortical or subcortical ROI is correlated with the experimental paradigms.

7.4.3 ICA and ROI based Analysis

A combination of ROI with a standard ICA was documented by Keck and colleagues [269]. In their investigation, they showed that the combination of these methods can be very useful because 1- Specific ROIs created for fMRI data can define the involvement of the area to the task in both spatial and temporal levels, 2-ICA as a multivariate blind

source separation technique can derive coupled networks emerged from the ROIs beside demonstrating unexpected functional activations [269]. Thus, in this recent investigation, ROI based analysis with a ICA was used as a more sensitive method to exhibit a relationship between the areas of interest and the conducted experimental paradigm in comparison with global (whole) brain analysis.

7.4.4 Avoiding Inter-Subject Variability via ROI-Based Analysis

Inter-subject variability is a serious issue for fMRI imaging analysis methods. Problematic alignment of a functional activity could stem from both folding [270-272] and variations in sulci and gyri patterns [273-276]. Due to these problems, ROI based analysis derived from native space of each subject might provide less information loss and better functional activity localization related to anatomical landmarks [95]. ROI based analysis, therefore, can show increased sensitivity and functional resolution in comparison to global (whole) brain analysis because ROI based analysis focuses on specific brain regions incorporating anatomical differences across the subjects to the analysis [266, 277]. In this recent investigation, the masks for ROIs were drawn in native space of each subject, and then further steps were applied. Although, representation of the results were done by normalization of the fMRI data at both individual subject and group levels, a few studies demonstrated that spatial normalization had no significant effect on spatial localization of functional activity [278, 279].

7.4.5 Temporal Differentiation on Group Level Hemodynamic Reference Vectors and Group Level Functional Activity Maps

A hierarchical ICA processed to investigate group-level results of the fMRI data. This method and its application were discussed in the previous sections of the dissertation (see also Chapter 6). Group-level hemodynamic reference vectors (HDVRs) or can be called as temporal independent components (tICs) showed some differences which might due to the physiological characteristics of the areas of interests for ROI based analysis. A delayed latency is observed for group-level frontal-parietal tICs in comparison to group level tIC of brainstem. Interestingly, group-level tICs for both occipital region and global (whole) brain analysis showed similar signal patterns. Differences in temporal properties and/or neurovascular coupling might be the reasons why these variations occurred [77, 264]. For instance, vascular factors such as vascular compliance and vascular density might affect temporal features of the signals [217, 218]. A study by Diedrichsen and colleagues indicated that forty percent in the fMRI signal of brainstem might be due to the respiratory system [221]. As discussed in Chapter 6, subcortical areas like brainstem and cerebellum are surrounded by dense vasculature bed, therefore, the correlation between physiological characteristics of areas and the task might influence the BOLD activity [221]. This might be the reason why differentiation in the temporal features of the brainstem is observed in comparison to the other group level tICs of ROIs and the global (whole) brain analysis.

The functional spatial maps obtained from these signals showed shared pattern between the frontal-parietal regions for both methods applied on fMRI data. Alkan and colleagues observed similar results where the group-level tICs demonstrated similar

frontal-parietal signal shape and obtained frontal-parietal network as one separate component [87]. Robust frontal-parietal connectivity for both fMRI analysis methods could subject to shift of receptive fields within frontal-parietal areas [252, 253] and also attentional top-down feedback signals [280]. Group level ROI based analyses for brainstem, occipital areas, and global (whole) brain analysis showed also connectivity to the some other cortical areas.

Occipital area indicated large cluster of functional activity on precuneus of the parietal area, whereas brainstem pointed connectivity to the anterior cingulate of the frontal cortex for both analysis of this task-induced fMRI data. Tomasi and Volkow mapped brain networks from the 1000 Functional Connectomes project where the strongest functional connectivity density (hubs) were observed in ventral precuneus and in primary visual cortex (BA17/BA18) for resting state networks [281]. Same team also exhibited that ventral precuneus/posterior cingulate as one essential hubs out of four is correlated to the default mode, dorsal attention, visual and somatosensory cortical networks [282]. Hence, in this recent investigation, ROI based analysis on occipital area and global (whole) brain analysis indicates strong connectivity between precuneus and primary visual cortex (BA17/BA18) for a vergence dependent visual task. Furthermore, Tomasi and Volkow demonstrated subcortical regions have the weakest functional connectivity density at rest [281]. Based upon this outcome, this should explain why ROI based analysis of brainstem and global (whole) brain analysis did not show robust connectivity with other regions of the brain.

In here, main concern that might arise from how connectivity maps at rest can be linked to the task-induced fMRI investigation as in here. Mennes and colleagues showed

that task-induced BOLD activity and neural activity during rest shares common control mechanism in which task-related neural activity can be predicted via properties of resting state [81]. Therefore, it can be claimed that there exists an evidence of correlation between resting state and task-induced fMRI connectivity.

7.5 Conclusion

In this recent investigation, the comparison between ROI-based versus global (whole) brain analysis was done. Results showed that ROI-based analysis gives finer outcomes than the global (whole) brain analysis. However, it does not mean that global (whole) brain analysis is less efficient method than ROI-based analysis because 1-outside the ROIs, there might be other areas involved in experimental paradigms, 2- the functional activity observed can be triggered from an area which might not be the region of interest [277]. The conducted experiments and their outcomes can be depicted via both ROI based analysis and global (whole) brain analysis. Hence, implementation of both ROI-based analysis and global (whole) brain analysis on an fMRI data can be a powerful approach which can complete each other at inadequate points for explaining the results of fMRI data.

CHAPTER 8

CONCLUSIONS AND FUTURE DIRECTIONS

The main purpose of this dissertation is to quantify neural substrates of vergence system on healthy controls by using fMRI as an imaging modality. This approach is tested by 1- mapping functional activity, and 2- implementation of different signal processing methods.

In specific aim 1 (Chapter 3), the cortical and subcortical substrates of the vergence system are targeted. Then a comparison is done between the vergence and saccadic systems where differentiation and similarities are detected. This objective of the dissertation helped to understand how a large area of the brain is involved in stereoscopic vision. On the other hand, spatially existant locations of vergence related neurons and their functional activity were observed via fMRI as shown in primate studies.

Specific aim 2 (Chapter 4) of this dissertation used memory-guided vergence paradigm in comparison to the two other vergence-related experiments. This is the first investigation which used memory-guided vergence experiment in the field. Furthermore, because of the roles of posterior parahippocampal area (PPHA) on the memory function of the brain, this area was chosen as the region of interest. Therefore, the correlation between the memory and PPHA was demonstrated via memory-guided vergence experiment. Two other vergence experiments have shown no statistically significant correlation between memory function and PPHA.

Specific aim 3 of this dissertation (Chapter 5) shows interconnectivity across brain regions influenced by the higher cognitive demand like prediction. Granger-Causality Analysis as a signal processing method is used to study interconnectivity of the selected brain regions that are important for processing of vergence dependent visual tasks. Simple tracking and predictable tracking vergence tasks are compared to understand the impact of prediction onto the causal relationships between the regions of interests.

Specific aim 4 (Chapter 6) used spatial and temporal ICA to study the underlying sources for different oculomotor systems. Shared central processing is observed at spatial level between the saccade and vergence networks. Hierarchical ICA application at group level to define temporal properties of the underlying sources that showed signals from frontal and parietal areas shares similar patterns in contrast to the signal from the cerebellum. The group level signal from cerebellum has a delayed latency which might be due to the neuronal and/or neurovascular coupling differences. In conclusion, spatial and temporal ICA can be used as an efficient method to derive neural networks at both individual subject and group levels.

Finally, specific aim 5 (Chapter 7) of this dissertation is to compare two fMRI analysis methods 1- ROI based analysis, 2- global (whole) brain analysis by using a simple vergence experimental paradigm. For ROI based analysis, frontal, parietal, brainstem and occipital areas are selected as region of interests. The comparison between these methods showed that ROI based analysis might derive more sensitive results than the global (whole) brain analysis. Results showed that ROI based analysis can derive stronger functional activity networks like frontal-parietal, besides showing more robust

functional activity on subcortical regions, like the brainstem, than global (whole) brain analysis.

Overall, the aims of this dissertation are essential for understanding high level processing of vergence system on healthy controls. fMRI as an imaging modality is used to map functional neural sites of the vergence system. Moreover, fMRI data acquired via application of vergence based experimental paradigms are processed by different signal processing techniques. These different analysis methods can shed light on interconnectivity and underlying sources, and can provide functional activity maps that are more accurate than that of traditional analysis methods. Additionally, outcomes of quantifying of vergence movements at neural level via fMRI can also be used as a powerful tool to support primate and human behavioral eye movement investigations. Furthermore, conditions like traumatic brain injury (TBI) might trigger oculomotor dysfunctions [8]. Consequently, neural differentiation between healthy individuals, patients with neural dysfunctions, and other injuries may be evaluated via quantification of vergence movements through fMRI.

Future work includes the studies of adaptation mechanisms across oculomotor systems. The ability to adapt is critical to survival and it varies between individuals. The visual system makes use of adaptation processes to improve its functional efficiency and precision, most notably during eye movement [283]. For example, Alvarez and colleagues showed that the dynamics of vergence system are prone to manipulation [284]. In control theory, the vergence system has two components: the preprogrammed (transient) and the feedback (sustained) components. Speed of a vergence ocular movement depends on transient preprogrammed component. On the other hand, the role

of the feedback component is fine tuning [285, 286]. Consequently, transient components of faster systems like saccades and vergence step and sustaining components of slower movements like vergence ramp and smooth pursuit might be modified in a similar way. Quantification of the adaptive control via oculomotor systems can lead to understanding interactions among ocular systems. This behavioral investigation might also be carried at the neuronal level via fMRI to demonstrate if centralized and/or distinct neural substrates exist. Therefore, this might help not only to comprehend control mechanism of adaptation behind oculomotor systems, but also explain why a good adaptor for one system, can also be a good adaptor for another system.

REFERENCES

[1] D. Purves, *et al.*, *Neurosciences*, 4th ed. Sunderland: Sinauer, 2008.

[2] G. Paxinos and K. M. Jurgen, *The Human Nervous System*, 2nd ed.: Academic Press, 2004.

[3] R. E. Kandel, *et al.*, *Principles of Neural Science*, 4th ed.: McGraw-Hill Medical, 2000.

[4] *Simple Anatomy of the Retina*. Retrieved from: http://webvision.med.utah.edu/book/part-i-foundations/simple-anatomy-of-the-retina/

[5] D. Felleman and D. Van Essen, "Distributed hierarchical processing in the primate cerebral cortex.," *Cereb Cortex.* , vol. 1, pp. 1-47, 1991.

[6] *Sense Organs*. Retrieved from: http://www.arthursclipart.org/medical/senseorgans/page_03.htm

[7] *The Eye Muscles*. Retrieved from: http://www.eyecareforchildren.com/childseyes.html

[8] R. J. Leigh and S. D. Zee, *The Neurology of Eye Movements*, 4th ed.: Oxford University Press, USA, 2006.

[9] D. Milea, *et al.*, "Cortical mechanisms of saccade generation from execution to decision," *Ann N Y Acad Sci*, vol. 1039, pp. 232-238, Apr 2005.

[10] C. Pierrot-Deseilligny, *et al.*, "Eye movement control by the cerebral cortex," *Curr Opin Neurol*, vol. 17, pp. 17-25, Feb 2004.

[11] Poggio GF, *et al.*, "Stereoscopic mechanisms in monkey visual cortex: binocular correlation and disparity selectivity.," *J Neurosci*, vol. 8, pp. 4531-4550., 1988.

[12] T. Akao, *et al.*, "Visual and vergence eye movement-related responses of pursuit neurons in the caudal frontal eye fields to motion-in-depth stimuli," *Exp Brain Res*, vol. 164, pp. 92-108, Jul 2005.

[13] S. Kurkin, *et al.*, "Neurons in the caudal frontal eye fields of monkeys signal three-dimensional tracking.," *Ann N Y Acad Sci.*, vol. 1004, pp. 262-270, 2003.

[14] P. D. Gamlin and K. Yoon, "An area for vergence eye movement in primate frontal cortex," *Nature,* vol. 407, pp. 1003-1007, Oct 26 2000.

[15] J. Gnadt and L. Mays, "Neurons in monkey parietal area LIP are tuned for eye-movement parameters in three-dimensional space.," *J Neurophysiol,* vol. 73, pp. 280-297, 1995.

[16] A. Genovesio and S. Ferraina, "Integration of retinal disparity and fixation-distance related signals toward an egocentric coding of distance in the posterior parietal cortex of primates," *J Neurophysiol,* vol. 91, pp. 2670-2684, Jun 2004.

[17] B. G. Cumming and S. J. Judge, "Disparity-induced and blur-induced convergence eye movement and accommodation in the monkey," *J Neurophysiol,* vol. 55, pp. 896-914, May 1986.

[18] S. J. Judge and B. G. Cumming, "Neurons in the monkey midbrain with activity related to vergence eye movement and accommodation," *J Neurophysiol,* vol. 55, pp. 915-930, May 1986.

[19] L. E. Mays and J. D. Porter, "Neural control of vergence eye movements: activity of abducens and oculomotor neurons," *J Neurophysiol,* vol. 52, pp. 743-761, Oct 1984.

[20] Nitta T, *et al.,* "Involvement of the cerebellar dorsal vermis in vergence eye movements in monkeys.," *Cereb Cortex,* vol. 18, pp. 1042-1057, 2008.

[21] Nitta T, *et al.,* "Vergence eye movement signals in the cerebellar dorsal vermis.," *Cereb Cortex* vol. 171, pp. 173-176, 2008.

[22] M. Takagi, *et al.,* "Effects of lesions of the cerebellar oculomotor vermis on eye movements in primate: Binocular control.," *Progress in Brain Research,* vol. 142, pp. 19-33, 2003.

[23] H. Zhang and P. D. Gamlin, "Neurons in the posterior interposed nucleus of the cerebellum related to vergence and accommodation. I. Steady-state characteristics," *J Neurophysiol,* vol. 79, pp. 1255-1269, Mar 1998.

[24] P. D. Gamlin, *et al.,* "The role of cerebro-pontocerebellar pathways in the control of vergence eye movements.," *Eye,* vol. 10(Pt2), pp. 167-171, 1996.

[25] U. Buttner and W. Waespe, "Purkinje cell activity in the primate flocculus during optokinetic stimulation, smooth pursuit eye movements and VOR-suppression," *Exp Brain Res,* vol. 55, pp. 97-104, 1984.

[26] P. D. Gamlin, "Neural mechanisms for the control of vergence eye movements," *Ann N Y Acad Sci,* vol. 956, pp. 264-272, Apr 2002.

[27] H. Mizushima and T. Seki, "Midbrain hemorrhage presenting with oculomotor nerve palsy: case report," *Surg Neurol,* vol. 58, pp. 417-420, Dec 2002.

[28] H. Rambold, *et al.*, "Vergence deficits in pontine lesions.," *Neurology,* vol. 62, pp. 1850-1853, 2004.

[29] Rambold H, *et al.*, "Pontine lesions may cause selective deficits of "slow" vergence eye movements.," *Ann N Y Acad Sci.,* vol. 1039, pp. 567-570, 2005.

[30] H. Rambold, *et al.*, "Palsy of "fast" and "slow" vergence by pontine lesions," *Neurology,* vol. 64, pp. 338-340, Jan 25 2005.

[31] T. L. Alvarez, *et al.*, "Functional anatomy of predictive vergence and saccade eye movements in humans: a functional MRI investigation," *Vision Res,* vol. 50, pp. 2163-2175, Oct 12 2010.

[32] Y. Alkan, *et al.*, "Differentiation between vergence and saccadic functional activity within the human frontal eye fields and midbrain revealed through fMRI.," *PLoS One.,* vol. 6, 2011.

[33] B. R. Cottereau, *et al.*, "Disparity-tuned population responses from human visual cortex," *J Neurosci,* vol. 31, pp. 954-965, Jan 19 2011.

[34] A. T. Smith and M. B. Wall, "Sensitivity of human visual cortical areas to the stereoscopic depth of a moving stimulus," *J Vis,* vol. 8, pp. 1 1-12, 2008.

[35] S. Ogawa, *et al.*, "Oxygenation-sensitive contrast in magnetic resonance image of rodent brain at high magnetic fields.," *Magn Reson Med.* , vol. 14, pp. 68-78, 1990.

[36] K. K. Kwong, *et al.*, "Dynamic magnetic resonance imaging of human brain activity during primary sensory stimulation," *Proc Natl Acad Sci U S A,* vol. 89, pp. 5675-5679, Jun 15 1992.

[37] B. Biswal and J. Ulmer, "Blind source separation of multiple signal sources of fMRI data sets using independent component analysis.," *J Comput Assist Tomogr.,* vol. 23, pp. 265-271., 1999.

[38] V. Calhoun, *et al.*, "fMRI activation in a visual-perception task: network of areas detected using the general linear model and independent components analysis.," *Neuroimage.* , vol. 14, pp. 1080-1088, 2001.

[39] M. McKeown, *et al.*, "Analysis of fMRI data by blind separation into independent spatial components.," *Hum Brain Mapp.,* vol. 6, pp. 160-188, 1998.

[40] Y. Bababekova, *et al.*, "Font size and viewing distance of handheld smart phones," *Optom Vis Sci,* vol. 88, pp. 795-797, Jul 2011.

[41] D. M. Hoffman, *et al.*, "Vergence-accommodation conflicts hinder visual performance and cause visual fatigue," *J Vis,* vol. 8, pp. 33 1-30, 2008.

[42] P. A. Howarth, "Potential hazards of viewing 3-D stereoscopic television, cinema and computer games: a review," *Ophthalmic Physiol Opt,* vol. 31, pp. 111-122, Mar 2011.

[43] J. L. Semmlow, *et al.*, "Short-term adaptive control processes in vergence eye movements.," *Current Psychology of Cognition,* vol. 21, pp. 243–261., 2002.

[44] S. B. Hutton, "Cognitive control of saccadic eye movements," *Brain Cogn,* vol. 68, pp. 327-340, Dec 2008.

[45] K. Johnston and S. Everling, "Neurophysiology and neuroanatomy of reflexive and voluntary saccades in non-human primates," *Brain Cogn,* vol. 68, pp. 271-283, Dec 2008.

[46] R. Müri and T. Nyffeler, "Neurophysiology and neuroanatomy of reflexive and volitional saccades as revealed by lesion studies with neurological patients and transcranial magnetic stimulation (TMS)." *Brain Cogn.,* vol. 68, pp. 284-292, 2008.

[47] J. E. McDowell, *et al.*, "Neurophysiology and neuroanatomy of reflexive and volitional saccades: evidence from studies of humans," *Brain Cogn,* vol. 68, pp. 255-270, Dec 2008.

[48] Paus, "Location and function of the human frontal eye-field: a selective review.," *Neuropsychologia,* vol. 34, pp. 475-483, 1996.

[49] L. E. Mays, *et al.*, "Neural control of vergence eye movements: neurons encoding vergence velocity," *J Neurophysiol,* vol. 56, pp. 1007-1021, Oct 1986.

[50] Y. Zhang, *et al.*, "Antidromic identification of midbrain near response cells projecting to the oculomotor nucleus," *Exp Brain Res,* vol. 84, pp. 525-528, 1991.

[51] Y. Zhang, *et al.*, "Characteristics of near response cells projecting to the oculomotor nucleus," *J Neurophysiol,* vol. 67, pp. 944-960, Apr 1992.

[52] L. E. Mays, "Neural control of vergence eye movements: convergence and divergence neurons in midbrain," *J Neurophysiol,* vol. 51, pp. 1091-1108, May 1984.

[53] J. T. Enright, "Changes in vergence mediated by saccades," *J Physiol,* vol. 350, pp. 9-31, May 1984.

[54] A. N. Kumar, *et al.*, "Directional asymmetry during combined saccade-vergence movements," *J Neurophysiol,* vol. 93, pp. 2797-2808, May 2005.

[55] C. Busettini and L. Mays, "Saccade-vergence interactions in macaques. II. Vergence enhancement as the product of a local feedback vergence motor error and a weighted saccadic burst.," *J Neurophysiol,* vol. 94, pp. 2312-2330, 2005.

[56] D. S. Zee, *et al.*, "Saccade-vergence interactions in humans," *J Neurophysiol,* vol. 68, pp. 1624-1641, Nov 1992.

[57] A. F. van Leeuwen, *et al.*, "Dynamics of horizontal vergence movements: interaction with horizontal and vertical saccades and relation with monocular preferences," *Vision Res,* vol. 38, pp. 3943-3954, Dec 1998.

[58] C. Erkelens, *et al.*, "Ocular vergence under natural conditions. II. Gaze shifts between real targets differing in distance and direction.," *Proc R Soc Lond B Biol Sci.*, vol. 236, pp. 441-465, 1989.

[59] H. Collewijn, *et al.*, "Voluntary binocular gaze-shifts in the plane of regard: dynamics of version and vergence," *Vision Res,* vol. 35, pp. 3335-3358, Dec 1995.

[60] J. W. Bisley and M. E. Goldberg, "Attention, intention, and priority in the parietal lobe," *Annu Rev Neurosci,* vol. 33, pp. 1-21, 2010.

[61] T. M. Herrington and J. A. Assad, "Temporal sequence of attentional modulation in the lateral intraparietal area and middle temporal area during rapid covert shifts of attention," *J Neurosci,* vol. 30, pp. 3287-3296, Mar 3 2010.

[62] Y. Liu, *et al.*, "Intention and attention: different functional roles for LIPd and LIPv," *Nat Neurosci,* vol. 13, pp. 495-500, Apr 2010.

[63] S. Ferraina, *et al.*, "Reaching in depth: hand position dominates over binocular eye position in the rostral superior parietal lobule," *J Neurosci,* vol. 29, pp. 11461-11470, Sep 16 2009.

[64] R. Bhattacharyya, *et al.*, "Parietal reach region encodes reach depth using retinal disparity and vergence angle signals.," *J Neurophysiol.* , vol. 102, pp. 805-816, 2009.

[65] M. Xu-Wilson, *et al.*, "Cerebellar contributions to adaptive control of saccades in humans," *J Neurosci,* vol. 29, pp. 12930-12939, Oct 14 2009.

[66] Y. Kojima, *et al.*, "Changes in simple spike activity of some Purkinje cells in the oculomotor vermis during saccade adaptation are appropriate to participate in motor learning.," *J Neurosci,* vol. 30, pp. 3715-3727., 2010.

[67] P. C. van Broekhoven, *et al.*, "Cerebellar contributions to the processing of saccadic errors," *Cerebellum,* vol. 8, pp. 403-415, Sep 2009.

[68] T. L. Alvarez, *et al.*, "Vision therapy in adults with convergence insufficiency: clinical and functional magnetic resonance imaging measures," *Optom Vis Sci,* vol. 87, pp. E985-1002, Dec 2010.

[69] K. Ciuffreda and B. Tannen, *Eye Movement Basics For The Clinician*: Mosby, 1995.

[70] J. Semmlow, *et al.*, "Correction of saccade-induced midline errors in responses to pure disparity vergence stimuli. ," *Journal of Eye Movement,* vol. 2, pp. 1-13, 2009.

[71] J. Semmlow, *et al.*, "Saccadic Behavior during the response to Pure Disparity Vergence Stimuli I: General Properties," *Journal of Eye Movement Research,* vol. 1, pp. 1-11, 2008.

[72] O. A. Coubard and Z. Kapoula, "Saccades during symmetrical vergence," *Graefes Arch Clin Exp Ophthalmol,* vol. 246, pp. 521-536, Apr 2008.

[73] R. W. Cox, "AFNI: software for analysis and visualization of functional magnetic resonance neuroimages," *Comput Biomed Res,* vol. 29, pp. 162-73, Jun 1996.

[74] T. R. Oakes, *et al.*, "Comparison of fMRI motion correction software tools," *Neuroimage,* vol. 28, pp. 529-543, Nov 15 2005.

[75] J. Talairach and P. Tournoux, *Co-planar Stereotaxic Atlas of the Human Brain; Talairach J, Tournoux P*: New York: Thieme, 1988.

[76] S. S. Kannurpatti, *et al.*, "Increasing measurement accuracy of age-related BOLD signal change: minimizing vascular contributions by resting-state-fluctuation-of-amplitude scaling," *Hum Brain Mapp,* vol. 32, pp. 1125-1140, Jul 2011.

[77] S. S. Kannurpatti, *et al.*, "Neural and vascular variability and the fMRI-BOLD response in normal aging," *Magn Reson Imaging,* vol. 28, pp. 466-476, May 2010.

[78] F. G. Hillary, *et al.*, "Functional magnetic resonance imaging technology and traumatic brain injury rehabilitation: guidelines for methodological and conceptual pitfalls," *J Head Trauma Rehabil,* vol. 17, pp. 411-430, Oct 2002.

[79] F. G. Hillary and B. Biswal, "The influence of neuropathology on the FMRI signal: a measurement of brain or vein?," *Clin Neuropsychol,* vol. 21, pp. 58-72, Jan 2007.

[80] B. Biswal, *et al.*, "Cerebral blood flow is reduced in chronic fatigue syndrome as assessed by arterial spin labeling.," *J Neurol Sci.,* vol. 301, pp. 9-11, 2011.

[81] M. Mennes, *et al.*, "Inter-individual differences in resting-state functional connectivity predict task-induced BOLD activity," *Neuroimage,* vol. 50, pp. 1690-1701, May 1 2010.

[82] V. Calhoun, *et al.*, "Modulation of temporally coherent brain networks estimated using ICA at rest and during cognitive tasks.," *Hum Brain Mapp.,* vol. 29, pp. 828-838, 2008.

[83] M. Gavrilescu, *et al.*, "Functional connectivity estimation in fMRI data: influence of preprocessing and time course selection," *Hum Brain Mapp,* vol. 29, pp. 1040-1052, Sep 2008.

[84] G. S. Berns, *et al.*, "Continuous functional magnetic resonance imaging reveals dynamic nonlinearities of "dose-response" curves for finger opposition," *J Neurosci,* vol. 19, p. RC17, Jul 15 1999.

[85] J. H. Missimer, *et al.*, "Data-driven analyses of an fMRI study of a subject experiencing phosphenes," *J Magn Reson Imaging,* vol. 31, pp. 821-828, Apr 2010.

[86] S. Malinen, *et al.*, "Towards natural stimulation in fMRI--issues of data analysis.," *Neuroimage.,* vol. 35, pp. 131-139, 2007.

[87] Y. Alkan, *et al.*, "Segregation of frontoparietal and cerebellar components within saccade and vergence networks using hierarchical independent component analysis of fMRI.," *Vis Neurosci.,* vol. 28, pp. 247-261, 2011.

[88] Z. Yang, *et al.*, "Ranking and averaging independent component analysis by reproducibility (RAICAR)," *Hum Brain Mapp,* vol. 29, pp. 711-725, Jun 2008.

[89] G. E. Nybakken, *et al.*, "Test-retest precision of functional magnetic resonance imaging processed with independent component analysis," *Neuroradiology,* vol. 44, pp. 403-406, May 2002.

[90] M. A. Quigley, *et al.*, "Comparison of independent component analysis and conventional hypothesis-driven analysis for clinical functional MR image processing," *AJNR Am J Neuroradiol,* vol. 23, pp. 49-58, Jan 2002.

[91] C. F. Beckmann and S. M. Smith, "Probabilistic independent component analysis for functional magnetic resonance imaging," *IEEE Trans Med Imaging,* vol. 23, pp. 137-152, Feb 2004.

[92] N. K. Logothetis and B. A. Wandell, "Interpreting the BOLD signal," *Annu Rev Physiol,* vol. 66, pp. 735-769, 2004.

[93] D. Attwell and C. Iadecola, "The neural basis of functional brain imaging signals," *Trends Neurosci,* vol. 25, pp. 621-625, Dec 2002.

[94] C. Rosano, *et al.*, "Pursuit and saccadic eye movement subregions in human frontal eye field: a high-resolution fMRI investigation," *Cereb Cortex,* vol. 12, pp. 107-115, Feb 2002.

[95] M. H. Grosbras, *et al.*, "An anatomical landmark for the supplementary eye fields in human revealed with functional magnetic resonance imaging," *Cereb Cortex,* vol. 9, pp. 705-711, Oct-Nov 1999.

[96] C. Pierrot-Deseilligny, *et al.*, "The role of the human dorsolateral prefrontal cortex in ocular motor behavior," *Ann N Y Acad Sci,* vol. 1039, pp. 239-251, Apr 2005.

[97] B. Ward, "Simultaneous inference for FMRI Data," 2000.

[98] J. R. Binder, *et al.*, "Neural correlates of sensory and decision processes in auditory object identification," *Nat Neurosci,* vol. 7, pp. 295-301, Mar 2004.

[99] A. Schmid, *et al.*, "An fMRI study of anticipation and learning of smooth pursuit eye movements in humans," *Neuroreport,* vol. 12, pp. 1409-1414, May 25 2001.

[100] J. W. Lewis, *et al.*, "Distinct cortical pathways for processing tool versus animal sounds," *J Neurosci,* vol. 25, pp. 5148-5158, May 25 2005.

[101] D. C. Van Essen, *et al.*, "An integrated software suite for surface-based analyses of cerebral cortex," *J Am Med Inform Assoc,* vol. 8, pp. 443-459, Sep-Oct 2001.

[102] R. H. Wurtz, "Neuronal mechanisms of visual stability," *Vision Res,* vol. 48, pp. 2070-2089, Sep 2008.

[103] J. D. Schall and L. Boucher, "Executive control of gaze by the frontal lobes," *Cogn Affect Behav Neurosci,* vol. 7, pp. 396-412, Dec 2007.

[104] P. H. Schiller and E. J. Tehovnik, "Neural mechanisms underlying target selection with saccadic eye movements," *Prog Brain Res,* vol. 149, pp. 157-171, 2005.

[105] K. G. Thompson and N. P. Bichot, "A visual salience map in the primate frontal eye field," *Prog Brain Res,* vol. 147, pp. 251-262, 2005.

[106] H. Hasebe, *et al.*, "Human cortical areas activated in relation to vergence eye movements-a PET study," *Neuroimage,* vol. 10, pp. 200-208, Aug 1999.

[107] S. Ferraina, *et al.*, "Disparity sensitivity of frontal eye field neurons," *J Neurophysiol,* vol. 83, pp. 625-629, Jan 2000.

[108] K. Fukushima, *et al.*, "Coding of smooth eye movements in three-dimensional space by frontal cortex," *Nature,* vol. 419, pp. 157-162, Sep 12 2002.

[109] A. Serra, *et al.*, "Disorders of vergence eye movements," *Curr Opin Neurol,* vol. 24, pp. 32-37, Feb 2011.

[110] M. Vernet and Z. Kapoula, "Binocular motor coordination during saccades and fixations while reading: a magnitude and time analysis.," *J Vis.,* vol. 9, 2009.

[111] H. Collewijn, *et al.*, "Trajectories of the human binocular fixation point during conjugate and non-conjugate gaze-shifts," *Vision Res,* vol. 37, pp. 1049-1069, Apr 1997.

[112] C. R. Rosenthal, *et al.*, "Supplementary eye field contributions to the execution of saccades to remembered target locations," *Prog Brain Res,* vol. 171, pp. 419-423, 2008.

[113] S. Kastner, *et al.*, "Topographic maps in human frontal cortex revealed in memory-guided saccade and spatial working-memory tasks," *J Neurophysiol,* vol. 97, pp. 3494-3507, May 2007.

[114] P. S. Goldman-Rakic, "Architecture of the prefrontal cortex and the central executive," *Ann N Y Acad Sci,* vol. 769, pp. 71-83, Dec 15 1995.

[115] E. K. Miller and J. D. Cohen, "An integrative theory of prefrontal cortex function," *Annu Rev Neurosci,* vol. 24, pp. 167-202, 2001.

[116] D. Badre and A. Wagner, "Frontal lobe mechanisms that resolve proactive interference.," *Cereb Cortex.* , vol. 15, pp. 2003-2012, 2005.

[117] H. E. Schendan and C. E. Stern, "Where vision meets memory: prefrontal-posterior networks for visual object constancy during categorization and recognition," *Cereb Cortex,* vol. 18, pp. 1695-1711, Jul 2008.

[118] K. Velanova, *et al.*, "Maturational changes in anterior cingulate and frontoparietal recruitment support the development of error processing and inhibitory control," *Cereb Cortex,* vol. 18, pp. 2505-2522, Nov 2008.

[119] K. Johnston, *et al.*, "Top-down control-signal dynamics in anterior cingulate and prefrontal cortex neurons following task switching," *Neuron,* vol. 53, pp. 453-462, Feb 1 2007.

[120] F. Polli, *et al.*, "Rostral and dorsal anterior cingulate cortex make dissociable contributions during antisaccade error commission.," *Proc Natl Acad Sci U S A.* , vol. 102, pp. 15700-15705, 2005.

[121] T. Matsuda, *et al.*, "Functional MRI mapping of brain activation during visually guided saccades and antisaccades: cortical and subcortical networks," *Psychiatry Res,* vol. 131, pp. 147-155, Jul 30 2004.

[122] H. L. Dean, *et al.*, "Visual and saccade-related activity in macaque posterior cingulate cortex," *J Neurophysiol,* vol. 92, pp. 3056-3068, Nov 2004.

[123] H. L. Dean and M. L. Platt, "Allocentric spatial referencing of neuronal activity in macaque posterior cingulate cortex," *J Neurosci,* vol. 26, pp. 1117-1127, Jan 25 2006.

[124] C. R. Olson, *et al.*, "Single neurons in posterior cingulate cortex of behaving macaque: eye movement signals," *J Neurophysiol,* vol. 76, pp. 3285-3300, Nov 1996.

[125] D. J. Quinlan and J. C. Culham, "fMRI reveals a preference for near viewing in the human parieto-occipital cortex," *Neuroimage,* vol. 36, pp. 167-187, May 15 2007.

[126] H. O. Richter, *et al.*, "Functional neuroanatomy of the human near/far response to blur cues: eye-lens accommodation/vergence to point targets varying in depth," *Eur J Neurosci,* vol. 20, pp. 2722-2732, Nov 2004.

[127] T. Sander, *et al.*, "Vergence deficits in patients with cerebellar lesions," *Brain Cogn,* vol. 132, pp. 103-115, 2009.

[128] Baddeley AD and H. GJ, *Working memory. In: The psychology of learning and motivation*: San Diego: Academic., 1974.

[129] Courtney SM, *et al.*, "Object and Spatial Visual Working Memory Activate Separate Neural Systems in Human Cortex," *Cereb Cortex.*, vol. 6, pp. 39-49, 1996.

[130] Osaka Naoyuki, *et al.*, *The Cognitive Neuroscience of Working Memory* Oxford University Press, 2007.

[131] Brignani D, *et al.*, "The when and where of spatial storage in memory-guided saccades.," *Neuroimage. ,* vol. 52, pp. 1611-1620, 2010.

[132] O. Hikosaka and R. H. Wurtz, "Visual and oculomotor functions of monkey substantia nigra pars reticulata. III. Memory-contingent visual and saccade responses," *J Neurophysiol,* vol. 49, pp. 1268-1284, May 1983.

[133] M. A. Segraves and M. E. Goldberg, "Functional properties of corticotectal neurons in the monkey's frontal eye field," *J Neurophysiol,* vol. 58, pp. 1387-1419, Dec 1987.

[134] K. Ohtsuka, *et al.*, "Nonvisual eye position control in a patient with ocular lateropulsion," *Ophthalmologica,* vol. 197, pp. 85-89, 1988.

[135] K. Ohtsuka, *et al.*, "Accuracy of memory-guided saccades," *Ophthalmologica,* vol. 198, pp. 53-56, 1989.

[136] Q. Yang and Z. Kapoula, "Distinct control of initiation and metrics of memory-guided saccades and vergence by the FEF: a TMS study," *PLoS One,* vol. 6, p. e20322, 2011.

[137] R. Srimal and C. E. Curtis, "Persistent neural activity during the maintenance of spatial position in working memory," *Neuroimage,* vol. 39, pp. 455-468, Jan 1 2008.

[138] Koch G, *et al.*, "rTMS evidence of different delay and decision processes in a fronto-parietal neuronal network activated during spatial working memory.," *Neuroimage,* vol. 24, pp. 34-39., 2005.

[139] Courtney SM, *et al.*, "An area specialized for spatial working memory in human frontal cortex.," *Science,* vol. 279, pp. 1347-1351, 1998.

[140] C. E. Curtis and M. D'Esposito, "Persistent activity in the prefrontal cortex during working memory," *Trends Cogn Sci,* vol. 7, pp. 415-423, Sep 2003.

[141] M. D'Esposito, *et al.*, "Functional MRI studies of spatial and nonspatial working memory," *Brain Res Cogn Brain Res,* vol. 7, pp. 1-13, Jul 1998.

[142] D. C. Glahn, *et al.*, "Maintenance and manipulation in spatial working memory: dissociations in the prefrontal cortex," *Neuroimage,* vol. 17, pp. 201-213, Sep 2002.

[143] F. M. Mottaghy, *et al.*, "Modulation of the neuronal circuitry subserving working memory in healthy human subjects by repetitive transcranial magnetic stimulation," *Neurosci Lett,* vol. 280, pp. 167-170, Feb 25 2000.

[144] M. Oliveri, *et al.*, "Parieto-frontal interactions in visualobject and visual-spatial working memory: evidence from transcranial magnetic stimulation.," *Cereb. Cortex,* vol. 11, pp. 606-618, 2001.

[145] M. Petrides, "The role of the mid-dorsolateral prefrontal cortex in working memory," *Exp Brain Res,* vol. 133, pp. 44-54, Jul 2000.

[146] M. Petrides, *et al.*, "Functional activation of the human ventrolateral frontal cortex during mnemonic retrieval of verbal information," *Proc Natl Acad Sci U S A,* vol. 92, pp. 5803-5807, Jun 20 1995.

[147] J. B. Rowe, *et al.*, "The prefrontal cortex: response selection or maintenance within working memory?," *Science,* vol. 288, pp. 1656-1660, 2000.

[148] S. Funahashi, *et al.*, "Mnemonic coding of visual space in the monkey's dorsolateral prefrontal cortex," *J Neurophysiol,* vol. 61, pp. 331-349, Feb 1989.

[149] C. L. Colby, *et al.*, "Visual, presaccadic, and cognitive activation of single neurons in monkey lateral intraparietal area," *J Neurophysiol,* vol. 76, pp. 2841-2852, Nov 1996.

[150] L. G. Ungerleider, *et al.*, "A neural system for human visual working memory," *Proc Natl Acad Sci U S A,* vol. 95, pp. 883-890, Feb 3 1998.

[151] J. A. Sweeney, *et al.*, "Positron emission tomography study of voluntary saccadic eye movements and spatial working memory," *J Neurophysiol,* vol. 75, pp. 454-468, Jan 1996.

[152] C. Pierrot-Deseilligny, *et al.*, "Cortical control of memory-guided saccades in man," *Exp Brain Res,* vol. 83, pp. 607-617, 1991.

[153] M. V. Chafee and P. S. Goldman-Rakic, "Matching patterns of activity in primate prefrontal area 8a and parietal area 7ip neurons during a spatial working memory task," *J Neurophysiol,* vol. 79, pp. 2919-2940, Jun 1998.

[154] H. R. Friedman and P. S. Goldman-Rakic, "Coactivation of prefrontal cortex and inferior parietal cortex in working memory tasks revealed by 2DG functional mapping in the rhesus monkey," *J Neurosci,* vol. 14, pp. 2775-2788, May 1994.

[155] D. Luck, *et al.*, "The right parahippocampal gyrus contributes to the formation and maintenance of bound information in working memory," *Brain Cogn,* vol. 72, pp. 255-263, Mar 2010.

[156] Crane J. and M. B., "What went where? Impaired object-location learning in patients with right hippocampal lesions.," *Hippocampus,* vol. 15, pp. 216-231, 2005.

[157] V. D. Bohbot and S. Corkin, "Posterior parahippocampal place learning in H.M," *Hippocampus,* vol. 17, pp. 863-872, 2007.

[158] V. D. Bohbot, *et al.*, "Spatial memory deficits in patients with lesions to the right hippocampus and to the right parahippocampal cortex," *Neuropsychologia,* vol. 36, pp. 1217-1238, Nov 1998.

[159] V. D. Bohbot, *et al.*, "Memory deficits characterized by patterns of lesions to the hippocampus and parahippocampal cortex," *Ann N Y Acad Sci,* vol. 911, pp. 355-368, Jun 2000.

[160] V. D. Bohbot, *et al.*, "Rat spatial memory tasks adapted for humans: characterization in subjects with intact brain and subjects with selective medial temporal lobe thermal lesions," *Physiol Res,* vol. 51 Suppl 1, pp. S49-65, 2002.

[161] Prince SE, *et al.*, "Encoding and retrieving faces and places: distinguishing process- and stimulus-specific differences in brain activity.," *Neuropsychologia,* vol. 47, pp. 2282-2289, 2009.

[162] Schmidt D, *et al.*, "Visuospatial working memory and changes of the point of view in 3D space.," *Neuroimage,* vol. 36, pp. 955-968, 2007.

[163] B. D. Ward, "Analysis of Variance for FMRI Data," 1998.

[164] Kennedy DN, *et al.*, "Gyri of the human neocortex: an MRI-based analysis of volume and variance.," *Cereb Cortex. ,* vol. 8, pp. 372-384, 1998.

[165] Suzuki WA and A. DG., "Topographic organization of the reciprocal connections between the monkey entorhinal cortex and the perirhinal and parahippocampal cortices.," *J Neurosci.,* vol. 14, pp. 1856-1877., 1994.

[166] Murray EA and M. M., "Visual recognition in monkeys following rhinal cortical ablations combined with either amygdalectomy or hippocampectomy.," *J Neurosci.,* vol. 6, pp. 1991-2003., 1986.

[167] Zola-Morgan S, *et al.,* "Lesions of perirhinal and parahippocampal cortex that spare the amygdala and hippocampal formation produce severe memory impairment.," *J Neurosci.,* vol. 9, pp. 4355-4370., 1989.

[168] Gaffan D and M. EA., "Monkeys (Macaca fascicularis) with rhinal cortex ablations succeed in object discrimination learning despite 24-hr intertrial intervals and fail at matching to sample despite double sample presentations.," *Behav Neurosci.,* vol. 106, pp. 30-38, 1992.

[169] Suzuki WA, *et al.,* "Lesions of the perirhinal and parahippocampal cortices in the monkey produce long-lasting memory impairment in the visual and tactual modalities.," *J Neurosci.* , vol. 13, pp. 2430-2451, 1993.

[170] N. Sato and K. Nakamura, "Visual response properties of neurons in the parahippocampal cortex of monkeys," *J Neurophysiol,* vol. 90, pp. 876-886, Aug 2003.

[171] Jones EG and P. TP., "An anatomical study of converging sensory pathways within the cerebral cortex of the monkey.," *Brain.,* vol. 93, pp. 793-820., 1970.

[172] G. W. Van Hoesen, "The parahippocampal gyrus: New observations regarding its cortical connections in the monkey," *Trends in Neurosciences,* vol. 5, pp. 345-350, 1982.

[173] G. J. Blatt, *et al.,* "Parcellation of cortical afferents to three distinct sectors in the parahippocampal gyrus of the rhesus monkey: an anatomical and neurophysiological study," *J Comp Neurol,* vol. 466, pp. 161-179, Nov 10 2003.

[174] B. R. Postle, *et al.,* "Activity in human frontal cortex associated with spatial working memory and saccadic behavior," *J Cogn Neurosci,* vol. 12 Suppl 2, pp. 2-14, 2000.

[175] Naghavi HR and N. L., "Common fronto-parietal activity in attention, memory, and consciousness: shared demands on integration?," *Conscious Cogn.,* vol. 14, pp. 390-425, 2005.

[176] C. E. Curtis, "Prefrontal and parietal contributions to spatial working memory," *Neuroscience,* vol. 139, pp. 173-180, Apr 28 2006.

[177] E. Feredoes and B. R. Postle, "Prefrontal control of familiarity and recollection in working memory," *J Cogn Neurosci,* vol. 22, pp. 323-330, Feb 2010.

[178] B. J. Tamber-Rosenau, *et al.*, "Cortical mechanisms of cognitive control for shifting attention in vision and working memory," *J Cogn Neurosci*, vol. 23, pp. 2905-2919, Oct 2011.

[179] H. Oh and H. C. Leung, "Specific and nonspecific neural activity during selective processing of visual representations in working memory," *J Cogn Neurosci*, vol. 22, pp. 292-306, Feb 2010.

[180] M. A. Owen, *et al.*, "A specific role for the right parahippocampal gyrus in the retrieval of object-location: A positron emission tomography study," *Journal of Cognitive Neuroscience*, vol. 8, pp. 588-602, 1996.

[181] Z. Saad, *et al.*, "Analysis and use of FMRI response delays.," *Hum Brain Mapp.* , vol. 13, pp. 74-93, 2001.

[182] Z. S. Saad, *et al.*, "Estimation of FMRI response delays," *Neuroimage*, vol. 18, pp. 494-504, Feb 2003.

[183] V. Calhoun, *et al.*, "A method for making group inferences from functional MRI data using independent component analysis.," *Hum Brain Mapp.*, vol. 14, pp. 140-151, 2001.

[184] V. D. Calhoun, *et al.*, "A review of group ICA for fMRI data and ICA for joint inference of imaging, genetic, and ERP data," *Neuroimage*, vol. 45, pp. S163-172, Mar 2009.

[185] C. W. J. Granger, "Investigating Causal Relations by Econometric Models and Cross-Spectral Methods.," *Econometrica*, vol. 37, pp. 424-438, 1969.

[186] Goebel R., *et al.*, "Investigating directed cortical interactions in time-resolved fMRI data using vector autoregressive modeling and Granger causality mapping," *Magn Reson Imaging.*, vol. 21, pp. 1251-1261., 2003.

[187] Roebroeck A., *et al.*, "Mapping directed influence over the brain using Granger causality and fMRI.," *Neuroimage.*, vol. 25, pp. 230-242, 2005.

[188] A. T. Sack, *et al.*, "Dynamic premotor-to-parietal interactions during spatial imagery," *J Neurosci*, vol. 28, pp. 8417-8429, Aug 20 2008.

[189] T. A. de Graaf, *et al.*, "Brain network dynamics underlying visuospatial judgment: an FMRI connectivity study," *J Cogn Neurosci*, vol. 22, pp. 2012-2026, Sep 2010.

[190] T. A. de Graaf, *et al.*, "FMRI effective connectivity and TMS chronometry: complementary accounts of causality in the visuospatial judgment network," *PLoS One*, vol. 4, p. e8307, 2009.

[191] B. B. Biswal, *et al.*, "Task-dependent individual differences in prefrontal connectivity," *Cereb Cortex,* vol. 20, pp. 2188-2197, Sep 2010.

[192] Rypma B. and Prabhakaran V., "When less is more and when more is more: The mediating roles of capacity and speed in brain-behavior efficiency.," *Intelligence.,* vol. 37, pp. 207-222, 2009.

[193] Abler B., *et al.*, "Investigating directed influences between activated brain areas in a motor-response task using fMRI.," *Magn Reson Imaging. ,* vol. 24, pp. 181-185, 2006.

[194] N. Bien, *et al.*, "The brain's intention to imitate: the neurobiology of intentional versus automatic imitation," *Cereb Cortex,* vol. 19, pp. 2338-2351, Oct 2009.

[195] S. Graham, *et al.*, "Role of medial cortical, hippocampal and striatal interactions during cognitive set-shifting," *Neuroimage,* vol. 45, pp. 1359-1367, May 1 2009.

[196] J. Talairach and P. Tournoux, *Co-Planar Stereotaxic Atlas of the Human Brain*. New York: Thieme, 1988.

[197] G. Poggio, *et al.*, "Stereoscopic mechanisms in monkey visual cortex: binocular correlation and disparity selectivity.," *J Neurosci,* vol. 8, pp. 4531-4550., 1988.

[198] G. E. Poggio, "Mechanisms of stereopsis in monkey visual cortex," *Cereb Cortex,* vol. 5, pp. 193-204, May-Jun 1995.

[199] L. Petit and J. Haxby, "Functional anatomy of pursuit eye movements in humans as revealed by fMRI.," *J Neurophysiol.,* vol. 82, pp. 463-471, 1999.

[200] M. Taira, *et al.*, "Parietal neurons represent surface orientation from the gradient of binocular disparity.," *J Neurophysiol,* vol. 83, pp. 3140-3146., 2000.

[201] H. Rambold, *et al.*, "Pontine lesions may cause selective deficits of "slow" vergence eye movements.," *Ann N Y Acad Sci.,* vol. 1039, pp. 567-570, 2005.

[202] T. Nitta, *et al.*, "Involvement of the cerebellar dorsal vermis in vergence eye movements in monkeys.," *Cereb Cortex,* vol. 18, pp. 1042-1057, 2008.

[203] E. A. Jeff B. Cromwell, *Multivariate Tests for Time Series Models*: Sage Publications, 1994.

[204] G. Schwartz, "Estimating the dimension of a model.," *The Annals of Statistics,* vol. 5, pp. 461-464, 1978.

[205] A. K. Seth, "Causal connectivity of evolved neural networks during behavior," *Network,* vol. 16, pp. 35-54, Mar 2005.

[206] E. Kowler and R. M. Steinman, "The effect of expectations on slow oculomotor control. I. Periodic target steps," *Vision Res,* vol. 19, pp. 619-632, 1979.

[207] G. R. Barnes and P. T. Asselman, "The mechanism of prediction in human smooth pursuit eye movements," *J Physiol,* vol. 439, pp. 439-461, Aug 1991.

[208] S. Ron, *et al.*, "Applying a model of saccadic prediction to patients' saccadic eye movements," *Brain Behav Evol,* vol. 33, pp. 179-182, 1989.

[209] C. Rashbass and G. Westheimer, "Disjunctive eye movements," *J Physiol,* vol. 159, pp. 339-360, Dec 1961.

[210] V. V. Krishnan, *et al.*, "An analysis of latencies and prediction in the fusional vergence system," *Am J Optom Arch Am Acad Optom,* vol. 50, pp. 933-939, Dec 1973.

[211] T. L. Alvarez, *et al.*, "Comparison of disparity vergence system responses to predictable and non-predictable stimulations," *Current Psychology of Cognition,* vol. 21, pp. 343-375, 2002.

[212] A. N. Kumar, *et al.*, "Properties of anticipatory vergence responses," *Invest Ophthalmol Vis Sci,* vol. 43, pp. 2626-2632, Aug 2002.

[213] T. J. Buschman and E. K. Miller, "Top-down versus bottom-up control of attention in the prefrontal and posterior parietal cortices," *Science,* vol. 315, pp. 1860-1862, Mar 30 2007.

[214] S. L. Bressler, *et al.*, "Top-down control of human visual cortex by frontal and parietal cortex in anticipatory visual spatial attention," *J Neurosci,* vol. 28, pp. 10056-10061, Oct 1 2008.

[215] Handwerker DA., *et al.*, "Variation of BOLD hemodynamic responses across subjects and brain regions and their effects on statistical analyses.," *Neuroimage,* vol. 21, pp. 1639-1651., 2004.

[216] R. B. Buxton, *Introduction to Functional Magnetic Resonance Imaging: Principles and Techniques.* New York.: Cambridge Univ. Press,, 2002.

[217] R. V. Harrison, *et al.*, "Blood capillary distribution correlates with hemodynamic-based functional imaging in cerebral cortex," *Cereb Cortex,* vol. 12, pp. 225-233, Mar 2002.

[218] C. Iadecola, "Intrinsic signals and functional brain mapping: caution, blood vessels at work.," *Cereb Cortex.*, vol. 12, pp. 223-224., 2002.

[219] S. A. Huettel and G. McCarthy, "Regional differences in the refractory period of the hemodynamic response: an event-related fMRI study," *Neuroimage,* vol. 14, pp. 967-976, Nov 2001.

[220] C. Windischberger, *et al.*, "Consistency of inter-trial activation using single-trial fMRI: assessment of regional differences.," *Brain Res Cogn Brain Res.*, vol. 13, pp. 129-138., 2002.

[221] J. Diedrichsen, *et al.*, "Advances in functional imaging of the human cerebellum," *Curr Opin Neurol,* vol. 23, pp. 382-387, Aug 2010.

[222] J. M. Levin, *et al.*, "Influence of baseline hematocrit and hemodilution on BOLD fMRI activation," *Magn Reson Imaging,* vol. 19, pp. 1055-1062, Oct 2001.

[223] A. T. Lee, *et al.*, "Discrimination of large venous vessels in time-course spiral blood-oxygen-level-dependent magnetic-resonance functional neuroimaging," *Magn Reson Med,* vol. 33, pp. 745-754, Jun 1995.

[224] Zonta M., *et al.*, "Neuron-to-astrocyte signaling is central to the dynamic control of brain microcirculation.," *Nat Neurosci.*, vol. 6, pp. 43-50, 2003.

[225] J. Semmlow, *et al.*, "Short-term Adaptive Control Processes in Vergence Eye Movements," *Current Psychology of Cognition,* vol. 21, pp. 243-261, 2002.

[226] K. A. Dyckman, *et al.*, "An effect of context on saccade-related behavior and brain activity," *Neuroimage,* vol. 36, pp. 774-784, Jul 1 2007.

[227] P. A. Bandettini, *et al.*, "Time course EPI of human brain function during task activation," *Magn Reson Med,* vol. 25, pp. 390-397, Jun 1992.

[228] G. Varoquaux, *et al.*, "A group model for stable multi-subject ICA on fMRI datasets," *Neuroimage,* vol. 51, pp. 288-299, May 15 2010.

[229] G. Hung, *et al.*, "Identification of accommodative vergence contribution to the near response using response variance.," *Invest Ophthalmol Vis Sci.* , vol. 24, pp. 772-777, 1983.

[230] Y. Y. Lee, *et al.*, "Sustained convergence induced changes in phoria and divergence dynamics," *Vision Res,* vol. 49, pp. 2960-2972, Dec 2009.

[231] E. Kim, *et al.*, "The relationship between phoria and the ratio of convergence peak velocity to divergence peak velocity.," *Invest Ophthalmol Vis Sci.,* vol. 51, pp. 4017-4027, 2010.

[232] T. L. Alvarez, *et al.*, "Short-term predictive changes in the dynamics of disparity vergence eye movements," *J Vis,* vol. 5, pp. 640-649, 2005.

[233] P. Comon, "Independent component analysis, A new concept?," *Signal Processing,* vol. 36, pp. 287-314, 1994.

[234] A. Hyvarian, *et al.*, *Independent Component Analysis.* New York: John Wiley & Sons., 2001.

[235] V. Schmithorst and R. Brown, "Empirical validation of the triple-code model of numerical processing for complex math operations using functional MRI and group Independent Component Analysis of the mental addition and subtraction of fractions.," *Neuroimage.,* vol. 22, pp. 1414-1420., 2004.

[236] F. Esposito, *et al.,* "Independent component analysis of fMRI group studies by self-organizing clustering," *Neuroimage,* vol. 25, pp. 193-205, Mar 2005.

[237] V. Perlbarg, *et al.*, "CORSICA: correction of structured noise in fMRI by automatic identification of ICA components," *Magn Reson Imaging,* vol. 25, pp. 35-46, Jan 2007.

[238] Y. Guo and G. Pagnoni, "A unified framework for group independent component analysis for multi-subject fMRI data," *Neuroimage,* vol. 42, pp. 1078-1093, Sep 1 2008.

[239] J. Sui, *et al.*, "A CCA+ICA based model for multi-task brain imaging data fusion and its application to schizophrenia," *Neuroimage,* vol. 51, pp. 123-134, May 15 2010.

[240] E. Seifritz, *et al.*, "Spatiotemporal pattern of neural processing in the human auditory cortex," *Science,* vol. 297, pp. 1706-1708, Sep 6 2002.

[241] J. Himberg, *et al.*, "Validating the independent components of neuroimaging time series via clustering and visualization," *Neuroimage,* vol. 22, pp. 1214-1222, Jul 2004.

[242] Y. O. Li, *et al.*, "Estimating the number of independent components for functional magnetic resonance imaging data," *Hum Brain Mapp,* vol. 28, pp. 1251-1266, Nov 2007.

[243] V. Kiviniemi, *et al.*, "Functional segmentation of the brain cortex using high model order group PICA.," *Hum Brain Mapp.*, vol. 30, pp. 3865-3886., 2009.

[244] E. Oja and Z. Yuan, "The fastICA algorithm revisited: convergence analysis," *IEEE Trans Neural Netw,* vol. 17, pp. 1370-1381, Nov 2006.

[245] J. R. Duhamel, *et al.*, "The updating of the representation of visual space in parietal cortex by intended eye movements," *Science,* vol. 255, pp. 90-92, Jan 3 1992.

[246] A. P. Batista, *et al.*, "Reach plans in eye-centered coordinates," *Science,* vol. 285, pp. 257-260, Jul 9 1999.

[247] M. Kusunoki and M. E. Goldberg, "The time course of perisaccadic receptive field shifts in the lateral intraparietal area of the monkey," *J Neurophysiol,* vol. 89, pp. 1519-1527, Mar 2003.

[248] M. M. Umeno and M. E. Goldberg, "Spatial processing in the monkey frontal eye field. I. Predictive visual responses," *J Neurophysiol,* vol. 78, pp. 1373-1383, Sep 1997.

[249] M. A. Sommer and R. H. Wurtz, "Influence of the thalamus on spatial visual processing in frontal cortex," *Nature,* vol. 444, pp. 374-377, Nov 16 2006.

[250] M. M. Umeno and M. E. Goldberg, "Spatial processing in the monkey frontal eye field. II. Memory responses," *J Neurophysiol,* vol. 86, pp. 2344-2352, Nov 2001.

[251] W. P. Medendorp, *et al.*, "Gaze-centered updating of visual space in human parietal cortex," *J Neurosci,* vol. 23, pp. 6209-6214, Jul 16 2003.

[252] E. P. Merriam, *et al.*, "Spatial updating in human parietal cortex," *Neuron,* vol. 39, pp. 361-373, Jul 17 2003.

[253] E. P. Merriam, *et al.*, "Remapping in human visual cortex," *J Neurophysiol,* vol. 97, pp. 1738-1755, Feb 2007.

[254] G. Westheimer, "Eye movement responses to a horizontally moving visual stimulus," *AMA Arch Ophthalmol,* vol. 52, pp. 932-941, Dec 1954.

[255] D. S. Zee, *et al.*, "Ocular motor abnormalities in hereditary cerebellar ataxia," *Brain,* vol. 99, pp. 207-234, Jun 1976.

[256] L. M. Optican and D. A. Robinson, "Cerebellar-dependent adaptive control of primate saccadic system," *J Neurophysiol,* vol. 44, pp. 1058-1076, Dec 1980.

[257] C. Quaia, *et al.*, "Model of the control of saccades by superior colliculus and cerebellum," *J Neurophysiol*, vol. 82, pp. 999-1018, Aug 1999.

[258] H. Chen-Harris, *et al.*, "Adaptive control of saccades via internal feedback," *J Neurosci*, vol. 28, pp. 2804-2813, Mar 12 2008.

[259] M. Desmurget, *et al.*, "Functional adaptation of reactive saccades in humans: a PET study," *Exp Brain Res*, vol. 132, pp. 243-259, May 2000.

[260] T. Ohyama, *et al.*, "Learning-induced plasticity in deep cerebellar nucleus," *J Neurosci*, vol. 26, pp. 12656-12663, Dec 6 2006.

[261] F. Shutoh, *et al.*, "Memory trace of motor learning shifts transsynaptically from cerebellar cortex to nuclei for consolidation," *Neuroscience*, vol. 139, pp. 767-777, May 12 2006.

[262] W. T. Thach, "On the mechanism of cerebellar contributions to cognition," *Cerebellum*, vol. 6, pp. 163-167, 2007.

[263] V. Ethier, *et al.*, "Spontaneous recovery of motor memory during saccade adaptation," *J Neurophysiol*, vol. 99, pp. 2577-2583, May 2008.

[264] B. Biswal, *et al.*, "Hemodynamic scaling of fMRI-BOLD signal: validation of low-frequency spectral amplitude as a scalability factor.," *Magn Reson Imaging.*, vol. 25, pp. 1358-1369, 2007.

[265] R. A. Poldrack, "Region of interest analysis for fMRI," *Soc Cogn Affect Neurosci*, vol. 2, pp. 67-70, Mar 2007.

[266] A. Nieto-Castanon, *et al.*, "Region of interest based analysis of functional imaging data," *Neuroimage*, vol. 19, pp. 1303-1316, Aug 2003.

[267] Dinstein I, *et al.*, "Executed and Observed Movements Have Different Distributed Representations in Human aIPS," *J Neurosci.*, vol. 28, pp. 11231-11239., 2008.

[268] R. F. Schwarzlose, *et al.*, "The distribution of category and location information across object-selective regions in human visual cortex," *Proc Natl Acad Sci U S A*, vol. 105, pp. 4447-4452, Mar 18 2008.

[269] R. I. Keck, *et al.*, "Region of interest based independent component analysis," in *ICONIP'06 Proceedings of the 13 international conference on Neural Information Processing - Volume Part I*, 2006, pp. 1048-1057

[270] N. Geschwind and W. Levitsky, "Human brain: left-right asymmetries in temporal speech region," *Science,* vol. 161, pp. 186-187, Jul 12 1968.

[271] H. Juch, *et al.*, "Anatomical variability of the lateral frontal lobe surface: implication for intersubject variability in language neuroimaging," *Neuroimage,* vol. 24, pp. 504-514, Jan 15 2005.

[272] F. Tomaiuolo, *et al.*, "Morphology, morphometry and probability mapping of the pars opercularis of the inferior frontal gyrus: an in vivo MRI analysis," *Eur J Neurosci,* vol. 11, pp. 3033-3046, Sep 1999.

[273] K. Amunts, *et al.*, "Broca's region revisited: cytoarchitecture and intersubject variability," *J Comp Neurol,* vol. 412, pp. 319-341, Sep 20 1999.

[274] B. Fischl, *et al.*, "Cortical folding patterns and predicting cytoarchitecture," *Cereb Cortex,* vol. 18, pp. 1973-1980, Aug 2008.

[275] G. Rajkowska and P. Goldman-Rakic, "Cytoarchitectonic definition of prefrontal areas in the normal human cortex: I. Remapping of areas 9 and 46 using quantitative criteria.," *Cereb Cortex.,* vol. 5, pp. 307-322, 1995.

[276] G. Rajkowska and P. S. Goldman-Rakic, "Cytoarchitectonic definition of prefrontal areas in the normal human cortex: II. Variability in locations of areas 9 and 46 and relationship to the Talairach Coordinate System," *Cereb Cortex,* vol. 5, pp. 323-337, Jul-Aug 1995.

[277] A. Nieto-Castanon and E. Fedorenko, "Subject-specific functional localizers increase sensitivity and functional resolution of multi-subject analyses," *Neuroimage,* Jul 8 2012.

[278] K. Swallow, *et al.*, "Reliability of functional localization using fMRI.," *Neuroimage.,* vol. 20, pp. 1561-1577., 2003.

[279] A. Miki, *et al.*, "Reproducibility of visual activation in functional MR imaging and effects of postprocessing," *AJNR Am J Neuroradiol,* vol. 21, pp. 910-915, May 2000.

[280] S. Kastner and L. G. Ungerleider, "Mechanisms of visual attention in the human cortex," *Annu Rev Neurosci,* vol. 23, pp. 315-341, 2000.

[281] D. Tomasi and N. D. Volkow, "Functional connectivity hubs in the human brain," *Neuroimage,* vol. 57, pp. 908-917, Aug 1 2011.

[282] D. Tomasi and N. Volkow, "Association between functional connectivity hubs and brain networks.," *Cereb Cortex.,* vol. 21, pp. 2003-2013, 2011.

[283] E. H. Kim, *et al.*, "Short-term adaptations of the dynamic disparity vergence and phoria systems," *Exp Brain Res*, vol. 212, pp. 267-278, Jul 2011.

[284] T. L. Alvarez, *et al.*, "Short-term predictive changes in the dynamics of disparity vergence eye movements.," *Journal of Vision*, vol. 5, pp. 640-649, 2005.

[285] G. K. Hung, *et al.*, "A dual-mode dynamic model of the vergence eye movement system," *IEEE Trans Biomed Eng*, vol. 33, pp. 1021-1028, Nov 1986.

[286] J. L. Semmlow, *et al.*, "Quantitative assessment of disparity vergence components.," *Investigative Ophthalmology Visual Science*, vol. 27, pp. 558-564, 1986.